THE MAGNITUDE OF THE TROPOSPHERIC RESPONSE TO SOLAR VARIABILITY

by

Neill Simon Cooper

Atmospheric Physics Group

Imperial College

LONDON

A thesis submitted for the degree of Doctor of Philosophy

at the University of London

May, 1981

ABSTRACT

The possible effect of solar variability on atmospheric tides and planetary waves is considered. Each may be sensitive to middle atmosphere variations, and in this way solar variability could affect the troposphere.

Tides in the atmosphere are principally due to ozone absorption of Ultra-Violet (UV) radiation and water vapour absorption of visible radiation. The semi-diurnal (12 hour) tide is mainly due to the former forcing. So changes in the solar UV output will result in changes in the semi-diurnal tide.

If, as has been suggested by Heath and Thekaekara (1977), the solar UV output increases by 20% from sunspot minimum to sunspot maximum, then the semi-diurnal tide would significantly increase in amplitude. However, from tropical data the semi-diurnal tide is found not to vary over the sunspot cycle. From this it is concluded that the solar UV output varies by, at most, a couple of percent over the sunspot cycle.

The diurnal (24 hour) tide has only a small component due to ozone absorption of UV. As the remaining forcings are tropospheric, and vary negligibly over the sunspot cycle, the diurnal tide should vary insignificantly with solar activity. However, it is found to decrease significantly from sunspot maximum to sunspot minimum. This variation remains unexplained.

It has been suggested by Bates (1977) and Geller and Alpert (1980) that planetary waves are sensitive to solar activity, due to alterations in the middle atmosphere winds. Using a quasi-geostrophic wave model it is found that wave number 2 is insensitive to middle atmosphere wind changes. However, observational studies have suggested that it is this wave which is most sensitive to solar variability. It is shown that neglecting radiative cooling results in gross overestimation of the sensitivity of wave number 1 to middle atmosphere wind changes. It is also found that the effect of changes in these winds, not necessarily in response to solar activity, is to produce perturbation waves which have vertical phase lines at the ground.

The LORD answered Job:

"Have you entered the storehouses of snow
or seen the storehouses of the hail?
What is the way to the place where the
lightning is dispersed,
or the place where the east winds are
scattered over the earth?
Does the rain have a father?
Who fathers the drops of dew?
From whose womb comes the ice?
Who gives birth to the frost from the
heavens?
Who endowed the heart with wisdom,
or gave understanding to the heart?
Who has the wisdom to count the clouds?
Who can tip over the water jars of
the heavens?"

CONTENTS

INTRODUCTION

Though the study of sun-weather relationships has a long history, recently there has been a growth of interest. There is an abundance of papers claiming to show an observed tropospheric response to solar variability. However, meteorologists are sceptical and solar activity is not included in their prognostic models. This, the proponents of sun-weather connections claim, results in inaccurate forecasts. But there is as yet no way that solar activity could be included in meteorological models, for there is no generally accepted theory which predicts tropospheric changes of the observed magnitude in response to solar variability. This also casts doubt on the observations, for they are not supported by any theory.

This thesis concentrates on one particular theory, that the troposphere is noticeably affected by solar variability due to alterations in the middle atmosphere. The idea that tropospheric waves may be altered by solar variability, due to changes in the middle atmosphere affecting their vertical propagation, was first suggested by Hines (1974). In the model of Bates (1977), planetary waves in the troposphere are sensitive to middle atmosphere zonal wind changes. However, this result is contrary to that of Geller and Alpert (1980), who found that the effect of zonal wind alterations on planetary waves is negligible more than three scale heights below the zonal wind change.

The effect of solar variability on atmospheric tides has previously received scant attention. This may be because atmospheric tides do not affect the weather. However, as the semi-diurnal tide

is predominantly forced by ozone absorbing solar Ultra-Violet radiation, it is a useful tool for investigating any possible middle-atmospheric response to solar variability.

Before the effect of solar variability on the atmosphere can be considered, the variations in solar output need to be assessed. This is done in Chapter 1, where upper estimates for the variations in Ultra-Violet and total radiation output over the sunspot cycle and solar rotation period are considered. The effects that such variations would have on the middle atmosphere, in particular ozone concentrations and the zonal wind, are described in Chapter 2.

Of the many suggested mechanisms by which solar variability may affect the troposphere, a few are outlined in Chapter 3. It is also shown therein that for solar variability to be important it must affect the troposphere via an amplification mechanism, whereby small changes in the total solar energy output result in proportionately much larger changes in the troposphere.

The nucleus of this study is in Chapters 4 and 5. In Chapter 4 the effect of solar variability on atmospheric tides is considered. Theoretical values for the effect of a 20% change in solar Ultra-Violet output (Section 4.5.1) are compared with those observed (Section 4.5.2). As well as this, a new simple model of tides is presented (Section 4.3). It qualitatively predicts the main seasonal and latitudinal variations in the diurnal, semi-diurnal and ter-diurnal tides.

The effects of solar variability on planetary waves, due to changes in the middle atmosphere, are analysed in Chapter 5. The

forcing due to ozone absorbing Ultra-Violet radiation is shown, in Section 5.2.1, to be negligible. The zonal wind alterations used here are more realistic, and smaller, than those of Bates (1977) and Geller and Alpert (1980). The effect of radiative (Newtonian) cooling on the sensitivity of the waves to wind changes is considered. As the theory predicts changes which are inconsistent with the observations, the latter are also considered. In Section 5.4.1, the observations of Parker (1976), of the sunspot cycle variation in surface pressure, are briefly discussed. The observations of King et al. (1977), of large variations in 500 mb height over the solar rotation period of 27.5 days, are considered in more detail in Section 5.4.2.

The principle conclusions of this study are given in the final Sections of Chapters 4 and 5.

CHAPTER 1

THE SUN

1.1. Introduction

The Sun is a very normal star, neither large nor small, neither bright nor dim, neither young nor old, neither hot nor cold. It is located in one of the spiral arms of a medium sized, middle aged Galaxy. However, to our world the Sun is vitally significant. Without its light and energy there would be no life on earth and no atmospheric motions, for the temperature would be close to absolute zero.

We are interested here in the Sun's energy output and its possible changes so as to evaluate the effect such changes may have on the atmosphere. Compared to "variable stars" the Sun is constant, but it does have transient features. These features, such as sunspots and solar flares, are collectively referred to as "solar activity".

Sunspots are areas of low surface temperature and hence emit less radiation than their surrounds, while the largest flares release up to 10^{26} Watts. Even so, these effects will only change the total solar output by, at the largest estimates, a fraction of a percent. However, certain parts of the solar output, such as X-ray radiation and high energy particles, are highly variable. The effect of solar activity on these and other solar emissions, are now considered.

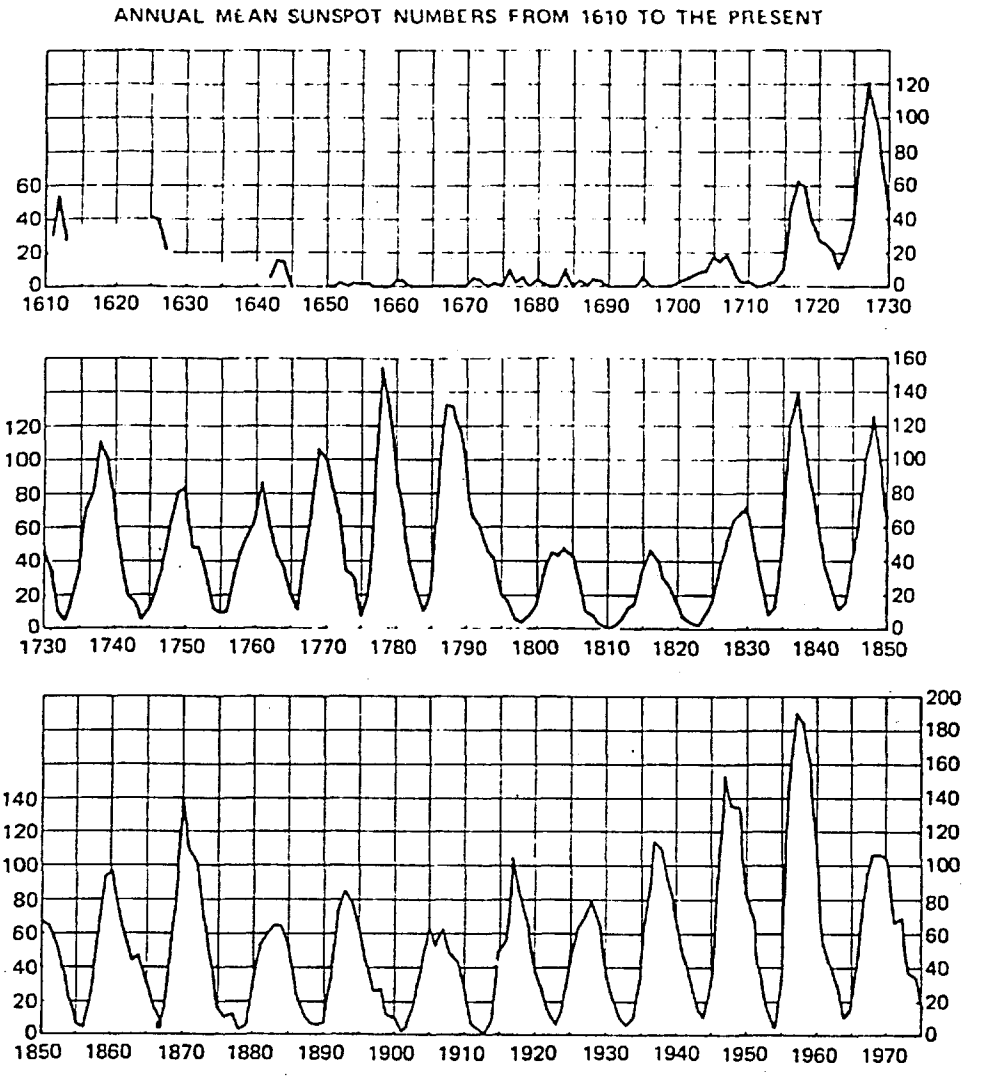

Figure 1.1 The annual mean sunspot number, A.D. 1700 - 1975. From Eddy (1977)

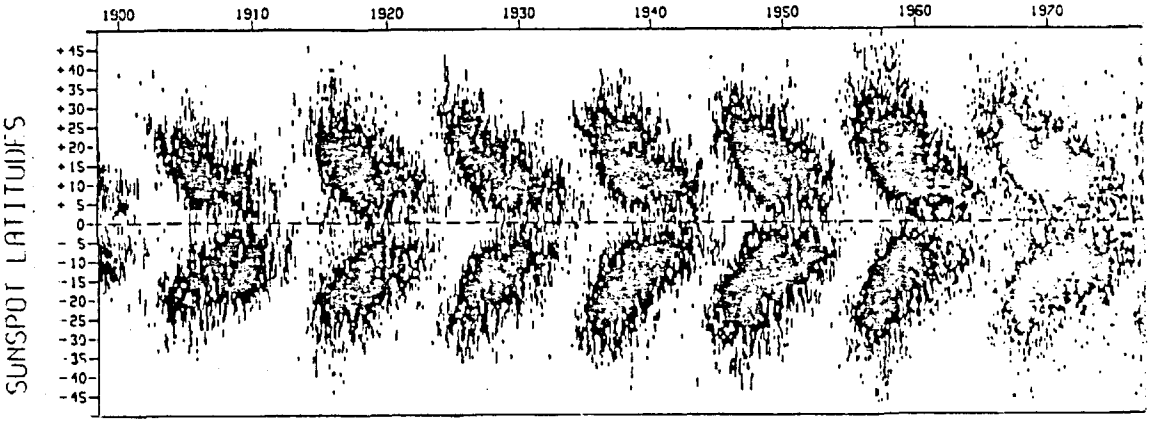

Figure 1.2 Solar butterfly diagram, A.D. 1898 - 1976. After Yallop and Hohenkert (1980).

1.2. Solar Activity

The only solar activity observable with the unaided eye is very large sunspots. The Chinese recorded 112 sunspots between 28 B.C. and 1638 A.D., without the aid of telescopes. In 1610 astronomy was revolutionised by the invention of the telescope. This was an epoch of high sunspot activity, so when astronomers pointed their new instrument at the Sun, they observed many sunspots.

By observing a sunspot group over a period of a few days it is clear that the Sun rotates with a synodic (observed from the earth) period of about 27 days. Other important, but less obvious, characteristics available from sunspot data were not noticed until more than two centuries later. It was in 1843 that Schwabe announced that he thought there was a 10 year cycle in the number of sunspots. This result was not generally accepted until Wolf, using observations since the time of Galileo, found the period to be 11.1 years. This quasi-periodic behaviour in the sunspot number is clearly seen in Figure 1.1 which also shows the "Maunder Minimum" of very few observations of sunspots between 1650 and 1700.

Variations in amplitude from one solar cycle to the next can be seen from Figure 1.1. The period is not constant but has varied between 7 and 17 years. Only a quarter of the well documented cycles (since 1750) have periods differing from 11.0 years (the average) by less than 6 months. So the sunspot cycle is only quasi-periodic. This introduced difficulties in evaluating and modelling the variations in solar output over the sunspot cycle.

As well as the number of spots varying during the sunspot

cycle, Carrington (1858) observed that their latitude also changes. The first spots in a new cycle appear between solar latitudes 20° and 35°. When the number of spots is largest ("Sunspot Maximum") they form between 5° and 30°, while at the end of the sunspot cycle spots develop below 15° latitude. This is shown in Figure 1.2, from Yallop and Hohenkert (1980), where the latitude of spots is plotted against time. From this diagram it can be seen that there is an overlap between sunspot cycles of a couple of years, during which time both the first spots of the new cycle and the last spots of the old cycle are simultaneously present.

Sunspots (and solar activity in general) tend to congregate together in groups which are "centres of activity". The Wolf sunspot number (R) used in Figure 1.1, is calculated from both the number of individual spots (f) and the number of groups (g) by the formula

$$R = k(10g + f)$$

The k factor is to standardise the observing station. The formula is somewhat arbitrary but is still the primary measure of solar activity.

Closely associated with sunspots are solar flares, which are sudden, short lived increases in intensity. The frequency of these features, which are best observed in the Hydrogen Alpha light, is proportional to the sunspot number. Small flares last for only a few minutes but the brightest flares are observable for several hours.

Flares are only rarely observable in visible light, and so they have little effect on the intensity of solar emission of

visible (and Ultra Violet) radiation. However they have a dominating influence on solar cosmic ray and X-ray radiation. So these emissions vary with the sunspot cycle as the number of flares does.

The other main signs of solar activity are faculae (bright areas near sunspots which are visible in white light) and prominances (gaseous sheets in the chromosphere, also called filaments). Faculae, being bright areas, emit more visible radiation than the surrounding surface. Apart from this, the effect of faculae and prominances on solar emission is unknown.

1.3. Solar Rotation

The first sunspot observations by telescope revealed that the Sun rotated with a period of about one lunar month. What was not realised was that the Sun does not rotate as a rigid body. The phenomenon of "differential rotation" (i.e. material at different solar latitudes rotating with different angular velocities) was first noticed by Carrington (1863). The synodic period of rotation varies from about 27 days, at the solar equator, to over 40 days, at the poles. By analysing 56 years of sunspot data, Newton and Nunn (1951) derived an expression relating the synodic period (t) for recurrent sunspots to solar latitude (B):-

$$t = 26.87 + 5.93 \sin^2 B \qquad (1.1)$$

A consequence of differential rotation is that, as the average latitude of sunspots varies over the sunspot cycle, the average rotation rate of sunspots also varies. This is seen in Figure 1.3 where the synodic period at the average latitude of sunspots for 1943-1977 is plotted. The sunspot distribution is from Fracastoro and Marocchi (1978) and Newton and Nunn's formula

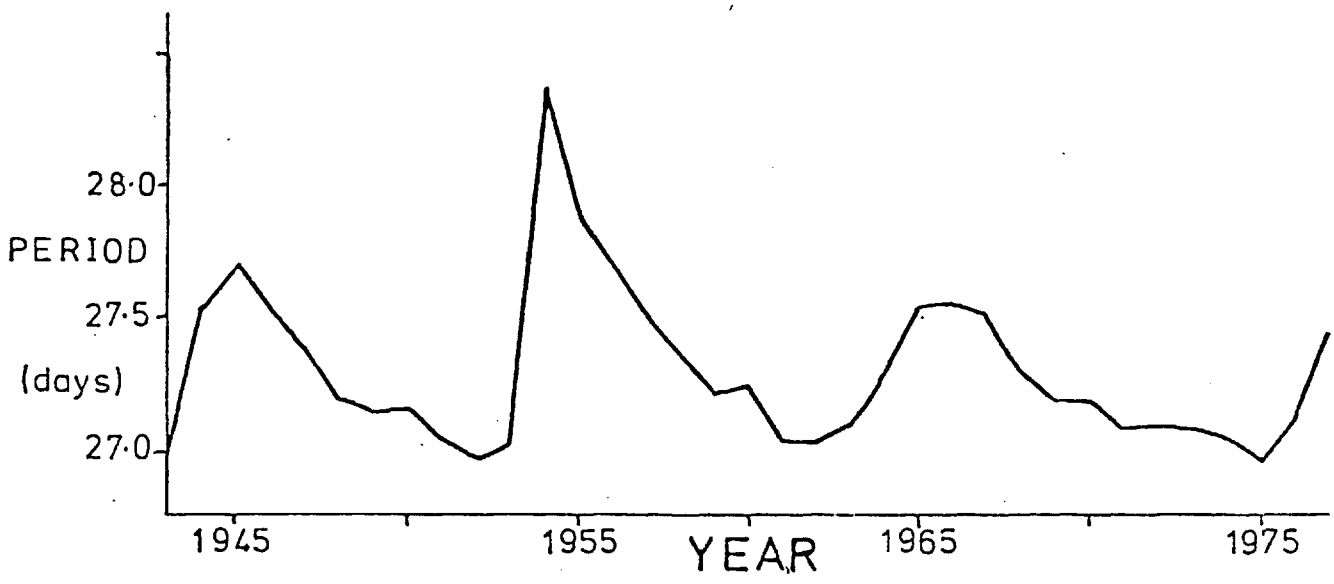

Figure 1.3 The variation of the synodic period at the mean sunspot latitude, 1943-1977. Sunspot data from Fracastro and Marocchi (1978), using the formula of Newton and Nunn (1951).

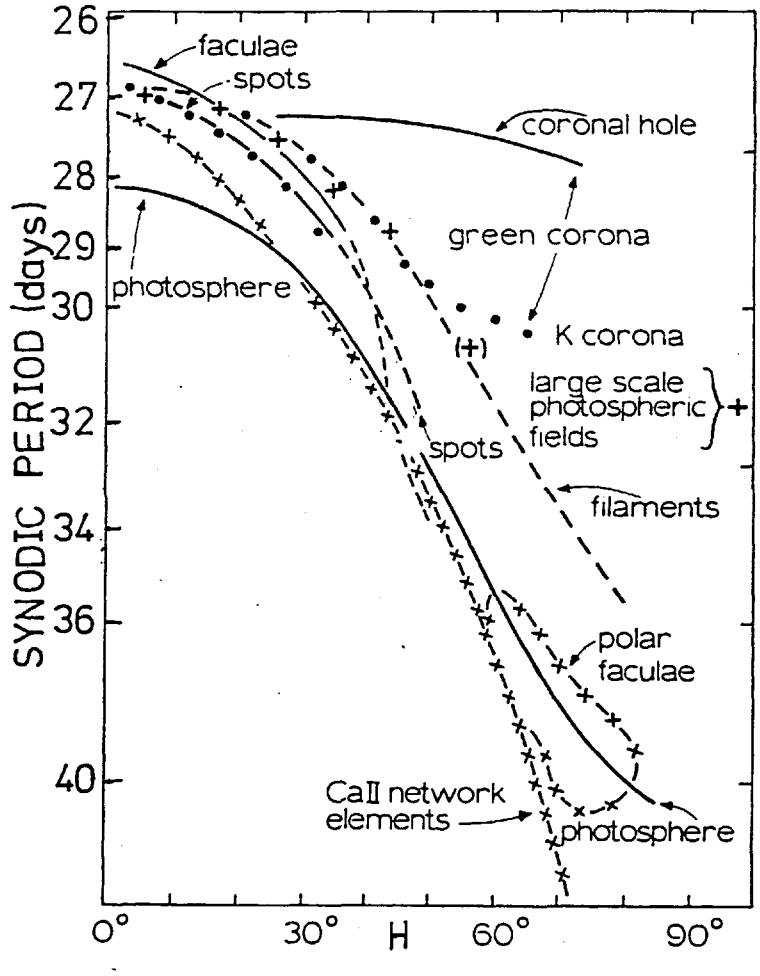

Figure 1.4 Variation of the synodic period with Solar latitude (H), and solar parameter considered. After van Tend and Zwaan (1976)

(1.1) is used to calculate the synodic period at the average latitude.

By using formula 1.1, however, one of many formulae which slightly, yet significantly, differ has been chosen. The difference is not due to the use of the form $t = a + b \sin^2 B$, for this is generally accepted as being a suitable representation of solar rotation for sunspot latitudes ($B < 40^\circ$), but rather in the actual values of a and b taken. Results differing by one or two percent are obtained if non-recurrent spots, small spots or all spots are considered instead of recurrent spots. Similarly slightly different results are obtained if faculae, filaments, coronal holes or the corona are used.

Instead of observing a "tracer", which is a feature on the solar surface and so may have a velocity relative to the local fluid, direct measurements of velocity can be made by analysing the Doppler shift of spectral lines. Using this method Howard and Harvey (1970) found that

$$t = 28.18 + 3.83 \sin^2 B \qquad (1.2)$$

which for the equator is almost 5% higher than equation 1.1. They also found day to day variations of the order of 5%.

A third technique for measuring solar rotation rates has been suggested by Rhodes et al. (1979). The method is based on the fact that waves in a moving medium are Doppler shifted. In this case the frequency of surface pressure waves on the Sun (p-modes) are affected by solar rotation. By considering the two dimensional power spectra (in horizontal and temporal wave number) at any point, the doppler shift can be estimated, and hence the rotational

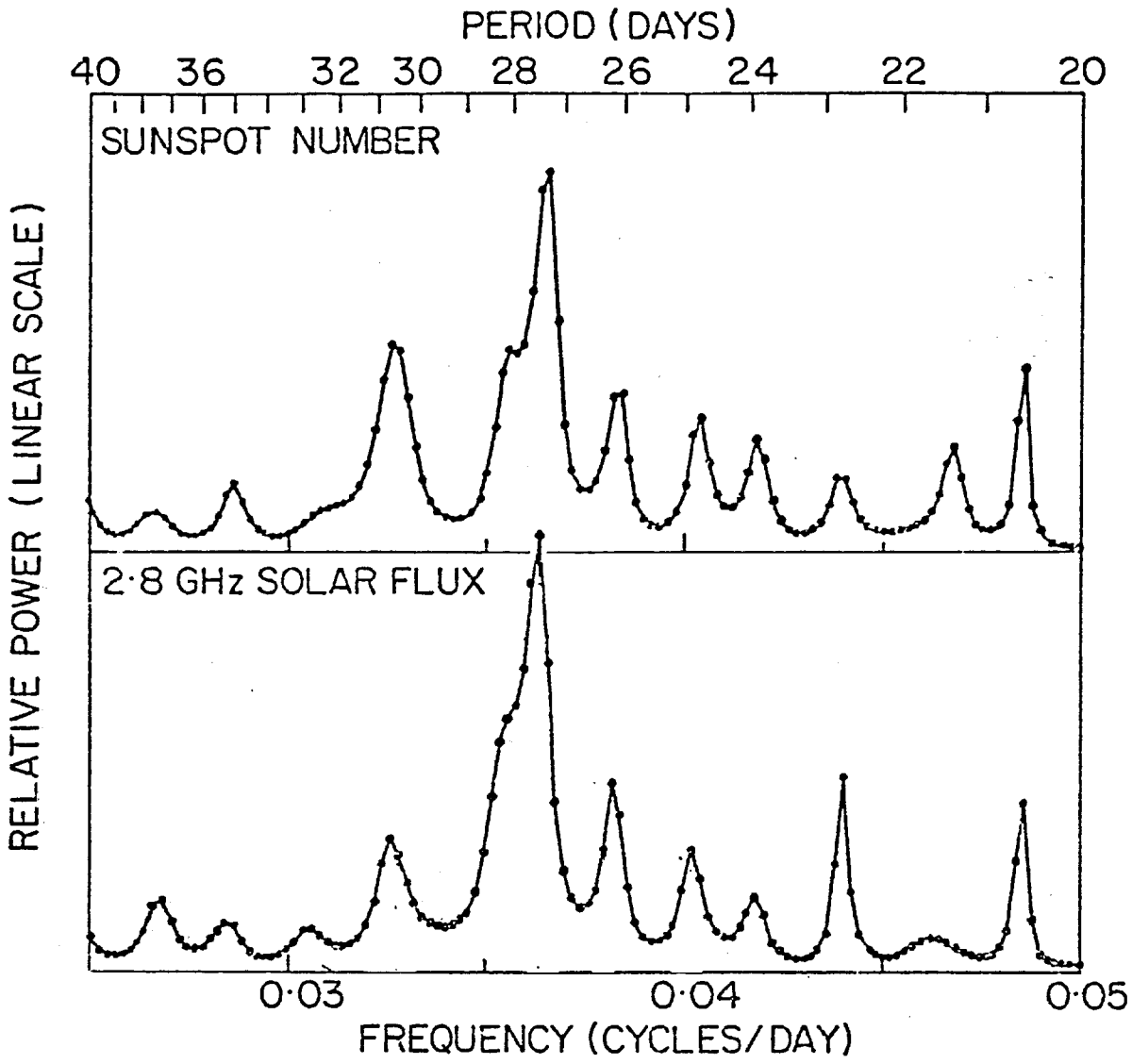

POWER SPECTRA OF DAILY VALUES, 1963-1972

Figure 1.5 Power spectra of daily values of sunspot number and 2.8GHz solar flux, 1963-1972. After King et al (1977).

velocity. P-modes are used because they have very distinctive power spectra with well defined lines. This method may become a viable alternative to tracer and spectroscopic Doppler shift measurements.

As well as depending on the method used the rotation rate also varies from year to year. Livingston and Duvall (1979), analysing spectroscopic Doppler shifts, calculated that the equatorial rotation rate rose by 3.7(± 0.7)% between 1966 and 1978. For the same period it was found that the polar rotation rate varied with the sunspot cycle, being about 8% lower at sunspot maximum than at sunspot minimum. The Sun's rotation rate also depends on altitude as well as on latitude, phase of sunspot cycle and observational method used. Slightly different observations, illustrating this variability, are shown in Figure 1.4.

For investigating possible tropospheric responses to solar rotation a single value for the rotation period would be useful, though alternatively a "key date" method is possible. This period can be obtained by evaluating the power spectrum of a solar property, as in King et al. (1977). They obtained a slightly different result for 10.7 cm flux (27.51 ± 0.15 days) compared to that for sunspots (27.37 ± 0.14 days) for 1963 to 1972 (see Figure 1.5). Their result for sunspots compares well with the value of 27.33 for the mean rotation rate of spots (weighted by area) for the same period. Another value that can be used is the rotation period of the Interplanetary Magnetic Field. Like the values in Figure 1.3 this is in fact variable rather than a single value.

All of these are attempts to approximate the actual period of

interest which is that in the solar output. Like the solar rotation rate this may vary with wavelength observed - assuming, that is, that there is any significant variation.

1.4. Solar Output

The Sun produces vast amounts of energy, and energetic particles, because of nuclear fusion reactions in its core. This energy is predominantly emitted as electromagnetic radiation with wavelengths between 3000Å and 20000Å. Only a minute proportion of the total energy emitted is at those wavelengths (Radio, X-ray and far Ultra-Violet) where the output greatly varies. Of predominant interest in this work will be the Ultra-Violet radiation which contributes 1% to the total energy output from the Sun and, it has been claimed, varies significantly. It is absorbed in the stratosphere by ozone and this is considered in Section 2.2.

1.4.1. Average Solar Output

The amount of energy received by a unit area in a unit time, from the Sun at a distance of one astronomical unit (average earth-sun distance) is called the "solar constant", S. It was not until 1969 that continuous measurements of S from above the terrestrial atmosphere were made (from Mariners VI and VII). Using these, and other recent observations, Fröhlich (1977) calculated an average value of

$$S = 1373(\pm 20)\ Wm^{-2}$$

The distribution of this energy with wavelength is shown in Figure 1.6 using data from Allen (1973). Assuming that the Sun is a perfect black body radiator (which is true for visible wavelengths) then, using Wien's displacement law, the peak in the spectrum at

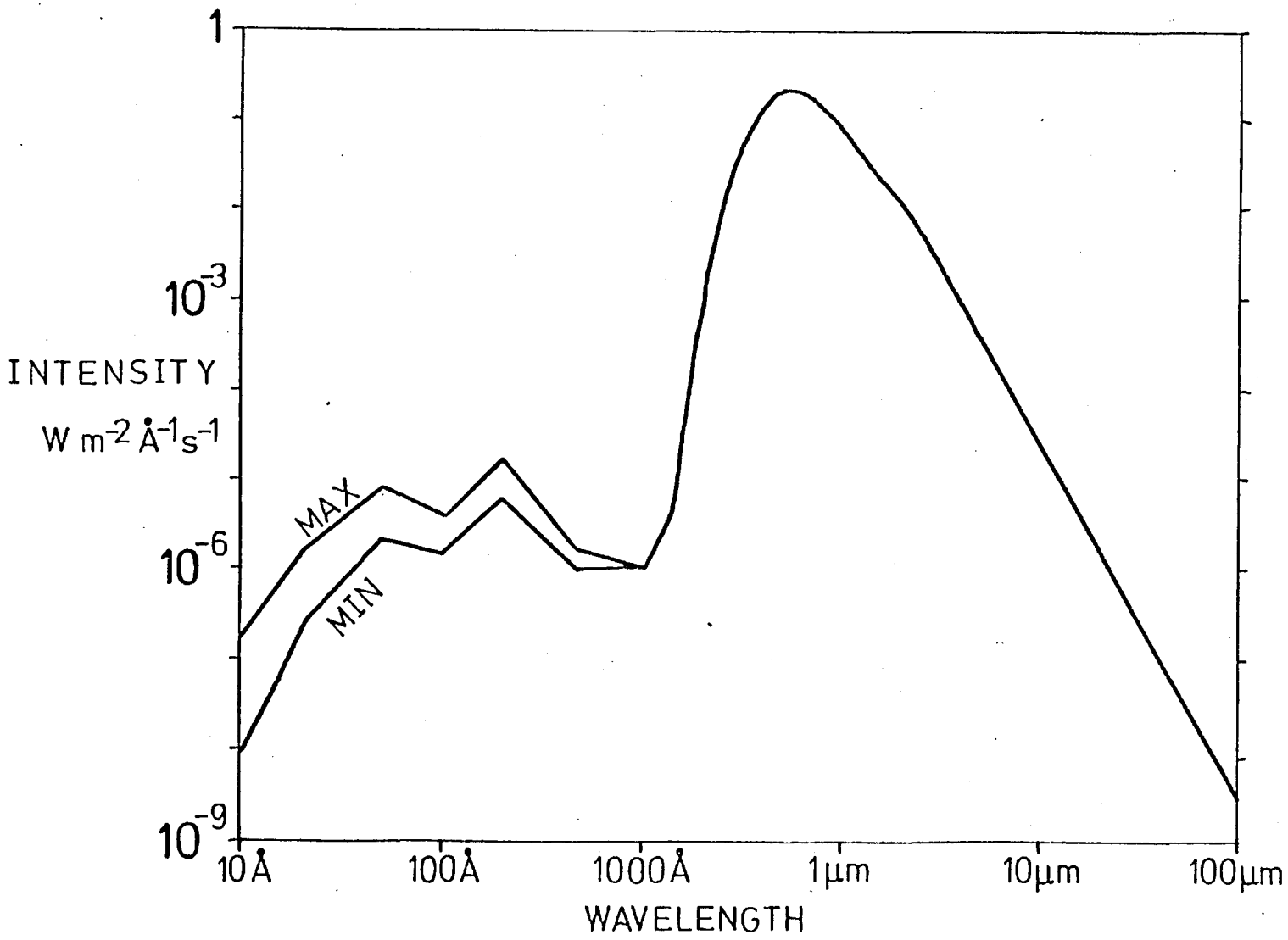

Figure 1.6 The Solar Spectrum. "MAX" is at sunspot maximum, "MIN" at sunspot minimum. Values from Allen (1973)

4600Å implies a solar surface temperature of 6300K (slightly higher than observed). When there is no solar activity the solar spectrum is close to that of a black body for all wavelengths longer than 3000Å. Below this, there is a wealth of emission lines and emission continua, formed at temperatures of between 8000K and 4000K. However if the spectrum (Figure 1.6) is analysed with greater resolution then it is found that absorption and emission lines are superimposed on the continuum at all wavelengths, though the continuum is less apparent at lower wavelengths.

1.4.2. Effect of Solar Rotation

Regions of solar activity can persist for several rotations of the Sun. Vitinskij (1969) has also suggested that there are "prefered longitudes" at which activity will occur. If sunspots do alter the solar output then this effect will vary with rotation, so creating an apparent cycle of about 27 days. (The total output of the Sun will not have this cycle, but the output seen from the earth will.) This effect can be seen in Figure 1.5 (note also that subsidiary peaks in the two graphs coincide, reinforcing the dependence of solar 10.7 cm radiation on sunspot number).

Sunspots, being relatively cool, emit less radiation than the average solar surface; faculae, being warm, emit more. Sunspots and faculae occur together, so the two effects will tend to balance one another. Using typical values for the total area and mean temperature of sunspots and faculae, their combined effect on the solar output can be evaluated. This was done by Foukal et al. (1977) using data from 1969, a time of maximum solar activity. They calculated that sunspots would decrease the solar output by not more

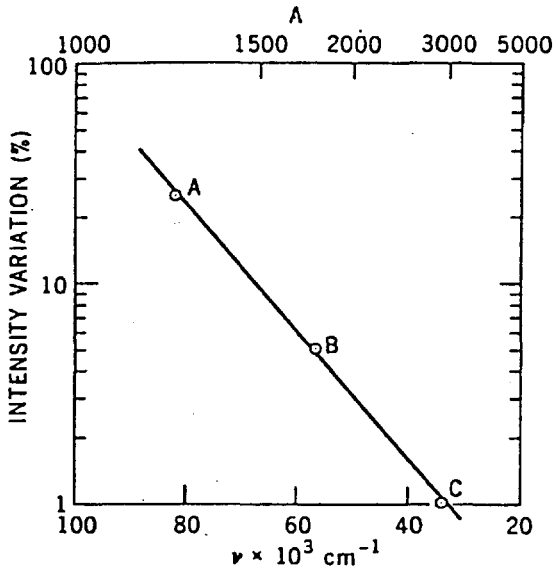

Figure 1.7 (right) Variation in UV solar spectral irradiance per solar rotation. $100(E_{max}-E_{min})/E_{min}$, observed with three sensors on Nimbus 3 near solar maximum. (From Heath, 1973)

Figure 1.8 (below) Measurements of the solar constant as function of date. Horizontal line is the mean value, least-squares linear regression fit to 1966-1969 data is also shown. From Fröhlich (1977)

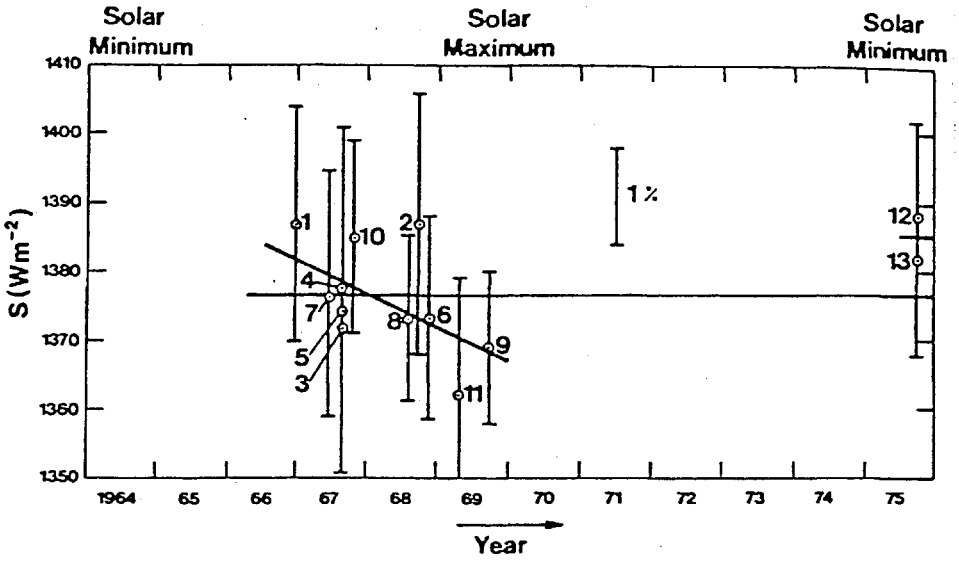

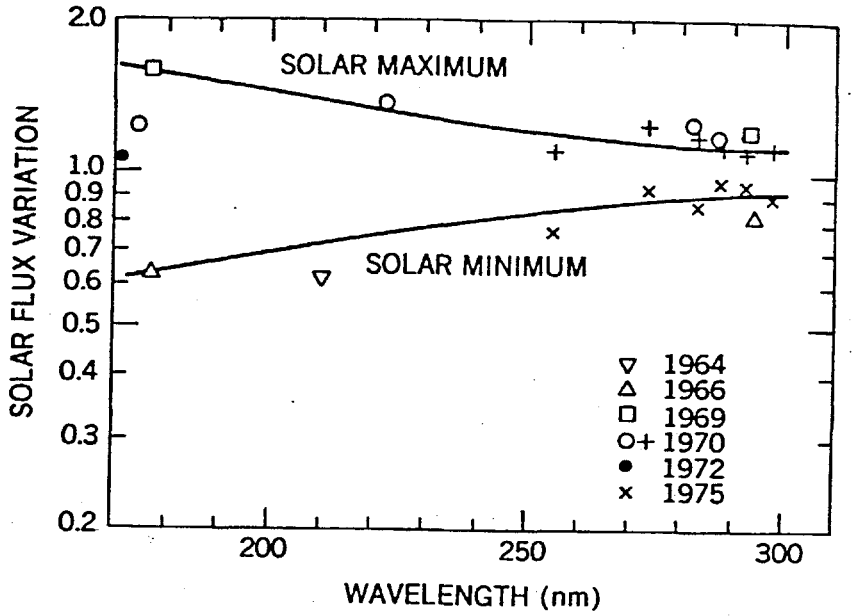

Figure 1.9 Variations in solar spectral irradiance apparently related to the sunspot cycle, based on observations from 1964 to 1975. From Heath and Thekaekara (1977)

than 0.05% while faculae would have a maximum effect of +0.4%. This they compared with the Mariner VI and VII observations of the total solar irradiance between 2000Å and 500000Å (99.99% of S). They found no observable evidence for sunspots or faculae affecting the solar constant, with an upper limit, due to experimental uncertainty, of 0.03%. So any change in the solar constant, greater than 0.03%, over the sunspot cycle or during solar rotation, cannot be due directly to the temperature of sunspots and faculae.

There is a variation in the 10.7 cm flux because of rotation. This is because at this wavelength, as well as there being the quiet Sun contribution to solar output, there is also a component, called the S-component, whose intensity is related to sunspot areas. Whether Ultra-Violet radiation also varies with rotation is the subject of debate. Heath (1973) claims that it does, slightly (1%) near visible wavelengths but greatly at extreme Ultra-Violet wavelengths, as shown in Figure 1.7.

The effect that such a variation, as outlined above, would have on ozone, tides and planetary waves, is described later (in Chapters 2, 4 and 5 respectively). In those calculations the amount of variability used is that given by Heath, and is considered as an upper limit of the actual variability.

1.4.3. Effect of Sunspot Cycle

As extra terrestrial observations of solar irradiance have been made for little over a decade, it is difficult to deduce whether the solar constant varies with the sunspot cycle. As the number of sunspots varies there is, a fortiori, a change in the solar output. But as shown by Foukal et al. (1977) this effect is

no more than 0.03%.

Though satellite measurements are more accurate than surface ones, the instruments used suffer from severe degradation, so any variation with a time scale of years cannot be easily separated from instrumental effects. Figure 1.8 is taken from Fröhlich (1977) and includes balloon and rocket as well as satellite observations. It indicates that there may be a cyclic variation in S of amplitude 1.5% with a minimum at sunspot maximum. However, an alternative interpretation of the data is that S was constant. Until more reliable and continuous measurements, over at least one sunspot cycle, have been made, this problem cannot be resolved.

There are similar problems with measurements of the solar flux in particular spectral bands. Heath and Thekaekara (1977) have claimed that the solar flux at 1750Å is about a factor of 2.5 greater at solar maximum than at solar minimum, while at 3000Å the variability is about 18% (see Figure 1.9). However, in a footnote to their paper, Simon (1977) questions the values at about 2000Å and suggests that the results are too high. Smith and Gottlieb (1974) state "there is no solar cycle effect longwavewards of 1500Å", but provide no observations to support this claim.

It is known that the sunspot cycle has important effects on some parts of the solar output. An extreme case of this is solar particles, which are primarily released by flares, the frequency of which is governed by the sunspot cycle. However, this and the other cases of solar output modulated by the sunspot cycle, occur in energetically insignificant portions of the output.

For later calculations it will normally be assumed that the only variability that need be taken into account is in the Ultra-Violet ($\lambda < 3500$Å), where the values obtained by Heath and Thekaekara (Figure 1.9) will be used. It is clear from the above discussion that this model does not necessarily represent the true behaviour but will be useful in predicting the maximum expected tropospheric response to solar variability.

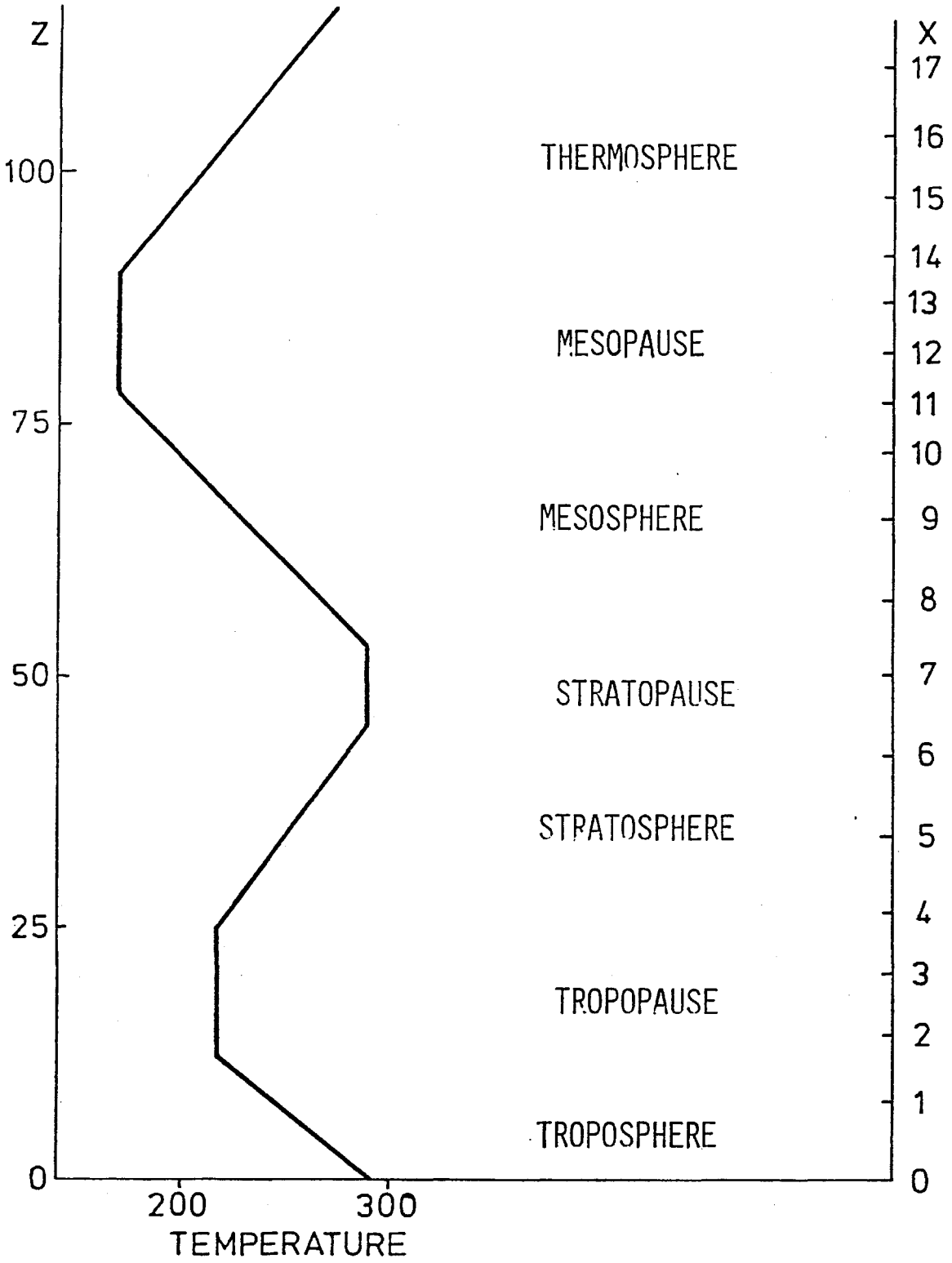

Figure 2.1 Variation of the mid-latitude temperature with height. Also given are the names used to describe different regions of the atmosphere. z is the height in kilometres, while X is in scale heights.

CHAPTER 2

THE ATMOSPHERE

2.1. General

On the earth, atmospheric motion is due entirely to solar heating. An immediate consequence of this is that variations in solar output will affect the atmosphere. The vertical variation of temperature, shown in Figure 2.1, is determined by absorption of solar radiation. This is most noticeable at the stratopause, where the warm temperature is due to ozone absorbing Ultra-Violet radiation. In the troposphere, the gradient of temperature is shallower than would occur in radiative equilibrium for in that case the atmosphere would be unstable.

The nomenclature used to describe the various levels in the atmosphere is shown in Figure 2.1. The region between the tropopause and the mesopause is referred to as "The Middle Atmosphere". We will consider what effect changes in the middle atmosphere, such as those which solar variability may cause, would have on the troposphere.

The only effect of solar variability on the middle atmosphere considered here is that in Ultra-Violet radiation (UV). If, as suggested by Heath and Thekaekara (1977), UV greatly varies with solar activity, then more radiation will be absorbed by ozone at solar maximum than at solar minimum. This would warm up the stratopause and probably also affect the mean zonal winds, which are related to the latitudinal temperature gradient.

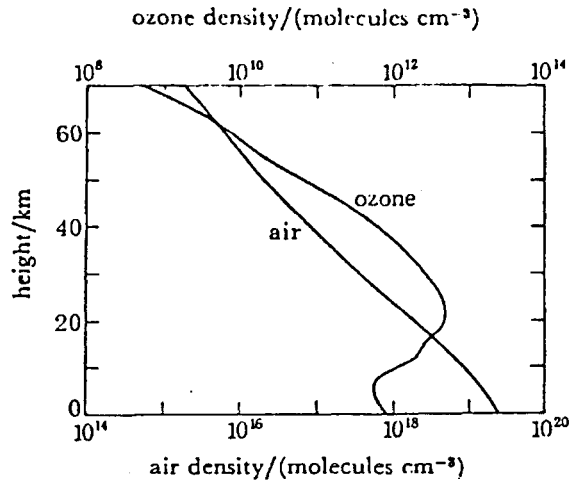

Figure 2.2 The density of air and ozone in mid-latitudes as a function of altitude. Note that the density scales differ by a factor of 10^6 so that curves intersect at 1 part in 10^6 of ozone. From Thrush (1980).

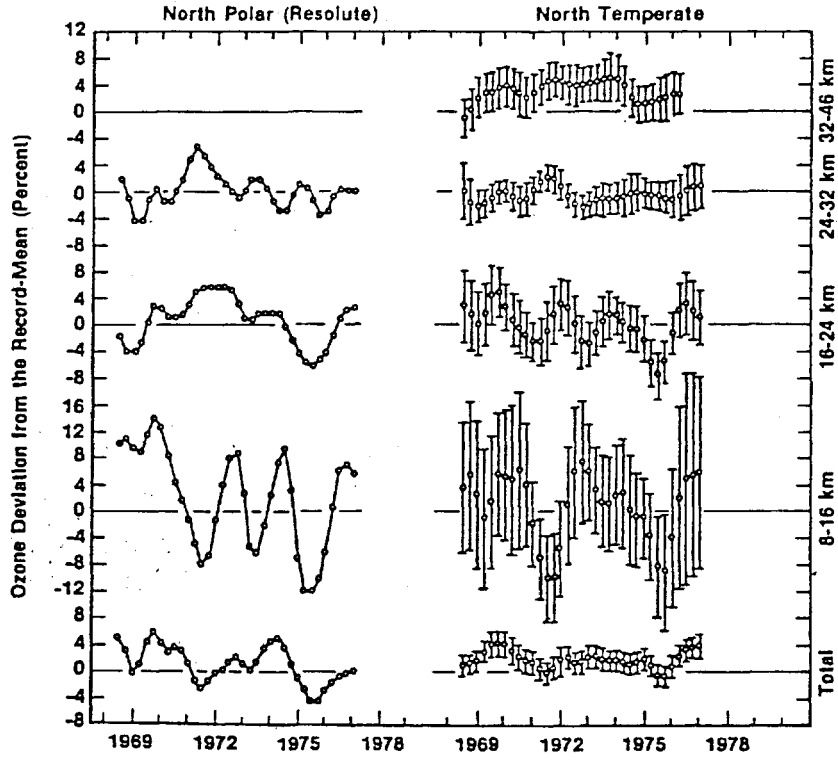

Figure 2.3 Estimated ozone variations in North Polar and north temperatelatitudes based on ozonesonde measurements in 8-16,16-24 and 24-32 km layers, Umkehr measurements in the 32-46 km layer, and total-ozone measurements. A 1-2-1 smoothing has been applied twice to the ozone values at seasonal intervals. The vertical bars extend two standard deviations on either side of the mean. Tick marks are in summer. From Angell and Korshover (1979)

2.2. The Ozone Layer

For the reasons given above, ozone has a very important effect on the stratosphere. However, its greatest concentration is only 3 parts per million while it is densest (10^{13} molecules per cc) at 25 km (see Figure 2.2). As ozone absorbs UV effectively, concentrations of only 10^{11} molecules per cc absorbing significantly, the maximum heating, at about 50 km, is above the maximum ozone concentration. The "ozone layer", defined as the region where heating due to ozone absorption is important, is between about 30 and 60 km.

The ozone layer absorbs about 20 Wm^{-2} of UV, and 10 Wm^{-2} of visible radiation when the sun is at the zenith. As the heating is mainly due to UV, changes in it will alter the stratopause temperature and also the photo-chemical equilibrium, and hence ozone concentrations. Callis and Nealy (1978) and Penner and Chang (1978) predict the effect of large changes in UV. Angell and Korshover (1978, 1979) show the observed changes in ozone concentration and stratospheric temperature from year to year.

The ozone layer may also be altered by other aspects of solar variability. Dütch (1979) considers the effect of solar proton events, modulation of NO_x production by galactic cosmic rays and auroral electrons. The effects are slight, and are ignored here.

To model its effect, UV variations need to be parameterised. The results of Callis and Nealy (1978) used here have a 20% sunspot cycle variation between 2100Å and 3070Å, and a 50% variation between 1750Å and 2100Å. The results of Penner and Chang (1978) involve changes of 35% below 2600Å, 0% above 3400Å and a linear

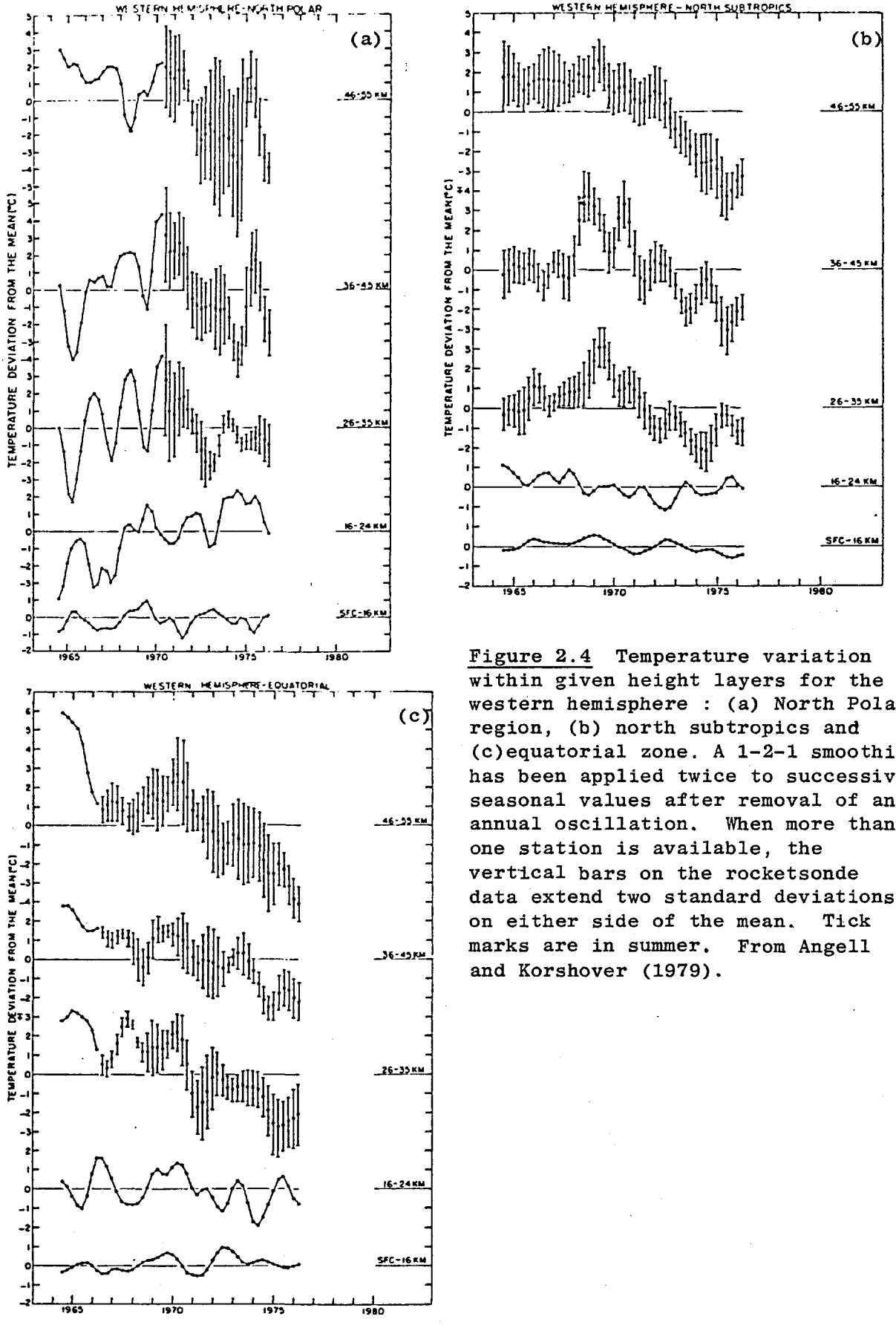

Figure 2.4 Temperature variation within given height layers for the western hemisphere : (a) North Polar region, (b) north subtropics and (c)equatorial zone. A 1-2-1 smoothing has been applied twice to successive seasonal values after removal of an annual oscillation. When more than one station is available, the vertical bars on the rocketsonde data extend two standard deviations on either side of the mean. Tick marks are in summer. From Angell and Korshover (1979).

interpolation in between. The models show that an increase in UV intensity results in the ozone concentration being increased by about 10% below 35 km. However, higher than this temperature feedback, due to the temperature dependence of reactions involving ozone, becomes important. Near the stratopause increased UV results in decreases in ozone of up to 20%. (This is illustrated in Figure 4.19.) Concurrent temperature changes have a maximum near the stratopause of 15°C.

These values are larger than observed. Angell and Korshover (1979) found the ozone concentrations for altitudes below the stratopause at different locations. There is no clear sunspot cycle variation at any level, nor in the total ozone, at North Polar and northern temperate latitudes (see Figure 2.3). This is to be compared with the theoretical decrease of about 10% from 1969 (sunspot maximum) to 1975 (sunspot minimum).

Similarly Angell and Korshover (1978) sought a solar cycle effect in stratospheric temperature. They divided the hemisphere into three latitude regions. A solar cycle effect was most apparent in the North subtropical region, where the stratospheric temperature was 2 to 4° higher at sunspot maximum than at sunspot minimum, (see Figure 2.4). The data for the polar region was very noisy and no significant variation is apparent, while in the tropics the most noticeable feature is a cooling trend. As only one sunspot cycle is considered the localised, sub-tropical, variations may not be caused by solar variations. Penner and Chang (1978) calculate the effect of UV variations on stratospheric temperature to be about ±3°C. While this agrees with Angell and Korshover's

sub-tropical observations, it is larger than their tropical observations.

So the sunspot cycle effect on both ozone and stratospheric temperature is overestimated by Penner and Chang, and even more so by Callis and Nealy (1978). This may be due to an overestimation of sunspot cycle variations in UV, a conclusion reached in Chapter 4 from an analysis of tidal variation.

Perturbations in the middle atmosphere temperature profile result in zonal wind changes, through the thermal wind relationship:

$$\frac{\partial u}{\partial z} = \frac{-g}{af} \frac{\partial}{\partial \theta} (\ln T)$$

So if the sub-tropical stratosphere is warmest at sunspot maximum, while the polar and equatorial regions are unaffected, then the mid-latitude westerlies will be strongest at sunspot maximum. Assuming a maximum warming of $3^{o}C$ at 40 km, decreasing linearly to $0^{o}C$ at 15 km and 90 km, and assuming the wind is unaltered below 15km, the mesospheric jet will be strengthened by 6.5 ms^{-1} and raised by 0.65 km.

These values are very similar to those predicted by Schoeberl and Strobel (1978b), who use a quasi-geostropheric middle atmosphere model to find the effect of ozone and solar variations on the middle atmosphere. They predict that the mesospheric jet should increase in strength by about 7 ms^{-1}, and rise 1 km, for each 10% increase in S. As almost all of the heating in their model was due to UV being absorbed by ozone, the results are equivalent to a change in UV of 10% with no variation at other wavelengths. They also predict a temperature rise of $6^{o}C$, per 10% increase in UV, at

the stratopause, larger than the result of Penner and Chang (1978), but smaller than that predicted by Callis and Nealy (1978).

From the above, if there is a ± 10% variation in the solar UV output over the sunspot cycle, then the mesospheric jet should vary in strength by ± 7 ms^{-1} (10%) and in height by ± 1 km (the mean height is about 60 km). Observations of the winds at this height have been made, from rocketsondes, for the last 20 years. Nastrom and Belmont (1980) analyse these, searching for a solar cycle effect. However, the response they find is in the semi-annual cycle. At a height of 60 km the semi-annual cycle has an amplitude of ~20 ms^{-1}. They find the solar cycle effect on this is ± 3·5 ± 1·7 ms^{-1}. They make no reference to any similar effect on the mean wind, or on the annual cycle. One can but assume that they found none.

In Section 5.3.2, the above zonal wind changes are used to investigate the effect of UV variability on tropospherically forced planetary waves.

CHAPTER 3

MECHANISMS

There have been numerous reports of tropospheric responses to solar variability. In contrast to this, there is a dearth of suggestions of realistic mechanisms whereby (slight) solar variability may noticeably affect the troposphere. Those mechanisms which at present receive the widest interest are described below.

3.1. Direct Calculations

The simplest model for predicting the global average temperature is to assume radiative equilibrium, so

$$\text{Energy absorbed} = \text{Energy emitted}$$

$$\pi R^2 (1-\bar{a}) S = 4\pi R^2 \bar{\varepsilon} \sigma \bar{T}^4$$

where S is the solar constant (1370 Wm^{-2})

$\bar{a}$ is a global albedo (~ 0.3)

$\bar{\varepsilon}$ is a global emissivity (~ 0.9)

$\bar{T}$ is a global temperature

σ is Stefans constant (5.7×10^{-8} Wm^{-2} K^{-4})

and R is the earth's radius

This zero-dimensional model assumes that the albedo and emissivity are constant over the earth. This is not true, but from the mean values given above $\bar{T} \simeq 261K$, so the model gives reasonable results. Now also assume that if the solar constant, and hence $\bar{T}$, changes, $\bar{a}$ and $\bar{\varepsilon}$ are unaffected (so there is no albedo, or emissivity, feedback). Then

$$\frac{dS}{d\bar{T}} = \frac{4S}{\bar{T}}$$

So a change in the solar constant of 0.1% (an upper estimate for

the variation over the sunspot cycle, see Section 1.4.3) would imply a mean global temperature change of 0.1°C. Refinements of the model lead to greater sensitivity. Manabe and Wetherald (1967) assuming radiative-convective equilibrium, found that the tropospheric response was 0.2°C, double that for the simplest model. This simple model also does not include the fact that variations in solar output depend on wavelength.

As the total mass of air in the atmosphere is constant, it is not easy to calculate how pressure will depend on energy input. Green (1979) evaluated the response to a sinusoidal variation in the solar constant of amplitude ΔS and period ω as follows. The excess heat input per unit mass is

$$\Delta Q = \frac{(1-\bar{a})\, e^{i\omega t}}{4 \rho_0 H} \Delta S .$$

which induces a heating, over a depth h

$$\frac{dT}{dt} = \frac{\Delta Q}{c_p}$$

and hence a pressure change

$$\delta p = -gh\delta\rho = -gh\rho_0 \frac{\Delta Q}{c_p \omega} = \frac{-(1-\bar{a})\, e^{i\omega t}\, \Delta S\, gh}{4 c_p H \omega}$$

This method implies a surface pressure oscillation of 0.04 mb in response to an oscillation of 0.1% in S. This is much less than the observations of 4 mb for the 27.5 day period (King et al., 1976) and of 2 mb for the sunspot cycle (Parker, 1976). The above argument was for a static atmosphere. In atmospheric waves, Kinetic Energy ($\frac{1}{2}\rho v^2$) is conserved, and hence wave amplitude is proportional to $(\rho / \rho_s)^{\frac{1}{2}}$ where ρ_s is the density of air at the source of the

waves. This factor, only significantly different from 1 for stratospherically forced waves, is therefore included into the expression for δp to parameterise dynamics. Hence including dynamics only slightly alters the results, so some sort of "amplification mechanism" is needed to explain the observations.

3.2. Feedback Mechanisms

A change in the global mean temperature may cause a change in the global mean albedo. This will result in feedback, since a decrease in albedo increases the total solar energy absorbed and hence the temperature. If an increase in temperature causes a decrease in albedo, then the feedback is positive, and the effect of solar variability is amplified. While if albedo increases with temperature, then there is negative feedback and the effect of solar variability is diminished.

In one-dimensional models the albedo is normally assumed to only depend on temperature via the total ice-cover. This automatically results in positive feedback as the albedo decreases when ice melts, which occurs as the temperature rises. Changes in cloud cover are neglected as they cannot be adequately parameterised in a one-dimensional model. However, Vallis (1980) has shown that these changes are very important. In global circulation models predicting the albedo is very difficult. In the atmosphere the albedo as well as depending on temperature is also dependent upon the humidity which in turn is determined by the past history of the air parcel. So the model, to be at all accurate, has to be very complicated. No such model has yet been used to investigate the possibility of albedo feedback in response to solar variability.

As well as being theoretically untested, the hypothesis that positive albedo feedback amplifies the tropospheric response to solar variability is also observationally untested. For the albedo, global or local, is very difficult to observe accurately. Ellis and Vonder Haar (1976) give a global mean value of 0.32 ± 0.02. No solar cycle variation has been isolated from the large background noise.

Being untested, and not producing any predictions (except from very simple, unrealistic models) the hypothesis that albedo feedback is an amplification mechanism is at present redundant.

3.3. Mechanisms Involving Ozone

Ozone, it has been claimed, varies with changes in the solar output (see Section 2.2). The possible tropospheric consequences of this variation, and that in Ultra-Violet radiation, is now considered.

3.3.1. Chappuis Band Absorption

As well as absorbing almost all the incident Ultra-Violet radiation, ozone also mildly absorbs at visible wavelengths, in the Chappuis Band. So changes in the total ozone concentrations will alter the amount of visible radiation absorbed, and hence also the amount that reaches the ground. As the Chappuis Band absorption is slight, it is a linear function of the total ozone. Angione et al. (1976) calculated that changes in ozone cause a 0.5% variation in the total radiant energy reaching the troposphere. However, they overestimated the change in ozone. Using a figure of 10% for the change in total ozone (see Section 2.2), a value of 0.1% is arrived at for the change in visible radiation. This is similar to

the suggested value for ΔS. While this effect may be important, it is not in itself an amplification mechanism.

3.3.2. Atmospheric Tides

Green (1979) suggested that observations of King et al. (1977), of planetary wave variations, may be due to changes in the tides, for isobaric surfaces are plotted at fixed universal time, while the tides are functions of local time. The effect is small, but not insignificant. At sea level the tides have amplitides of about 1 mb near the equator falling to about 0.2 mb at 50^{o}N/S. At the same latitudes planetary waves have amplitudes of 2 mb and 10 mb respectively. As most reports of solar induced changes in planetary waves are for high latitudes, the phenomena observed cannot be due solely to changes in the tides.

However, both the diurnal (24 hour) and the semi-diurnal (12 hour) atmospheric tides have significant components forced by ozone absorption of Ultra-Violet radiation. So changes in the UV flux will result in concurrent tidal variations. Due to the semi-diurnal tide being highly sensitive to the UV flux, observations of the tide can be used to estimate the variation in UV over the sunspot cycle. This is done in Chapter 4, where both the theory and observations are given.

3.3.3. Planetary Waves

Bates (1977) and Geller and Alpert (1980) showed that changes in the middle atmosphere zonal winds affect planetary waves. If such changes occur in response to solar variability, then an "amplification mechanism" would have been identified. This possibility is considered further in Chapter 5.

3.4. Other Mechanisms

The two mechanisms considered in later chapters have been outlined above (Sections 3.3.2 and 3.3.3). There was not time to consider other mechanisms that have been suggested. Some of these mechanisms are now described.

3.4.1. Thunderstorms

Brooks (1934) noted that there was, in some places, a strong correlation between the sunspot number and thunderstorm frequency. Around this result, Markson (1978) constructed a theory. The explanation of the observations is based on the strong solar-cycle effect in the ionosphere. This, it is postulated, will affect the electrical properties of the troposphere and in particular the frequency of thunderstorms. This is a reasonable explanation of Brooks' results which were based on reports of lightning and thunder, electrical properties. Markson then suggests that changing the electrical structure of a storm will change its dynamical structure by altering the cloud micro-physics, such as coalescence rates. This is much less plausible for the micro-physics is governed by the macro-physics, rather than vice-versa (Green, 1979). The reason for this is the enormous amount of Kinetic and Available Potential Energy in a thunderstorm. The amount of electrical energy, though large, is minute in comparison.

Another flaw in Markson's theory is that the more recent observations of Klejmenova (1967) are not in agreement with those of Brooks (1934).

3.4.2. Cirrus, Nacreous and Noctilucent Cloud

Roberts and Olson (1973) observed intensification of trough development shortly after geomagnetic storms. To explain this they suggest that cirrus cloud formation is increased at this time.

Geomagnetic storms are caused by solar flares which emit large numbers of highly energetic solar corpuscles. These deposit their energy, both directly and by secondary processes, in the atmosphere. If they have a significant effect as low down as 30 mb, then at that level atmospheric ions would be formed. These would act as condensation nuclei for Cirrus cloud formation. Roberts and Olson estimate the temperature perturbation to be 1 to 2°C. This would then change the static stability and make it easier for troughs to intensify. However, the ion production rate due to these high energy particles is much larger in the stratosphere than in the troposphere (Johnson and Imhof , 1975). So a similar process may affect Nacreous and Noctilucent clouds, though very little is known about their physics. Herman and Goldberg (1948, p.243) suggest that this will alter the albedo, perhaps significantly. However, as these clouds occur at high latitudes , a slight change in the albedo will have a negligible effect on the total radiation received by the earth.

3.4.3. Stratospheric Carbon Dioxide

As well as possibly affecting Nacreous and Noctilucent clouds, the ionisation due to high-energy particles, referred to in the previous section, may also affect carbon dioxide concentrations (Sekihara, 1979). This is because the reaction between CO_2 and O^+ ions is very fast. Changing carbon dioxide concentrations will

affect the cooling rate at tropopause level, and hence the temperature there. This will alter the stability of air masses at this level, and will modulate the frequency of trough development at high latitudes.

Schuurmans and Oort (1969) observed a temperature drop of 1.8 ($\pm$ 0.6)^{o}C in tropopause temperatures a day after solar flares, while Roberts and Olson (1973) noted an intensification of troughs.

CHAPTER 4

ATMOSPHERIC TIDES

4.1. Historical Introduction

Since time immemorial it has been known that the oceans rise and fall twice a day. That these tides are in some way related to lunar motion was first suggested 2,300 years ago by an explorer-mariner called Pytheas. During the subsequent 2,000 years many theories were proposed as to how the moon caused tides. The basis of the currently accepted theory is provided by Newton's Three Laws of Motion (Newton, 1687). One corollary of this theory is that tides are forced by the gravitational pull of the moon and sun. Newton (1687) realised that his theory would apply to the atmosphere as well as to the oceans, but he thought that atmospheric tides would be too small to be observed.

That the oceanic tide is related to the moon can be inferred from its period being close to 12.5 hours. The atmospheric tide repeatedly peaks at the same time of day and hence is sun synchronous. This regularity of the tide is most apparent at the equator, where the tide is larger and ambient pressure variations smaller, than at extra-tropical latitudes. So when Humboldt took a barometer with him to South America in 1799, he observed that the two daily maxima in pressure, at about 10.00 a.m. and 10.00 p.m., were so regular as to serve as a clock. These observations cannot be explained by Newton's gravitational theory, which predicts that the lunar forced tide would be largest in the atmosphere as well as in the ocean.

At the same time as Humboldt was sailing to South America,

Laplace was developing his tidal theory in Méchanique Céleste (Laplace, 1799). While Newton had considered a static equilibrium tide on a non-rotating earth, Laplace included the effect of the earth's rotation, which introduces dynamics into the theory. He found that in the ideal case of a uniformly deep ocean there are infinitely many free modes of oscillation, some of which could resonantly interact with solar or lunar forced tidal oscillation. However, Laplace's theory has very limited applications to the oceans, as they have (irregular) boundaries and also are of non-uniform depth.

Like Newton before him, Laplace considered the implications of his theory for atmospheric tides. As the atmosphere has no lateral boundaries, Laplace's tidal theory is appropriate, once the compressibility of air is taken into account. By considering an atmosphere with constant scale height, H, Laplace deduced that the atmospheric tidal motions can be inferred from the results for an ocean depth $h = \gamma H$ (where γ, the ratio of the specific heat of air at constant pressure to that at constant volume, equals 1.4). When forced modes are considered, h is an eigenvalue of the Laplace Tidal Equation, and for any given frequency there is an infinite set of "equivalent depths", $\{h_n\}$, each associated with a different latitude variation, given by the Hough Function $\Theta_n(\theta)$.

Laplace knew that the solar atmospheric tides were much larger than the lunar ones, and so he concluded that the solar components were due to thermal forcing. However, he thought that there was little hope of constructing a theory to describe thermally forced tides. As well as introducing mathematical difficulties, ascribing

the solar component to thermal forcing introduces another problem, succinctly described by Thomson (later Lord Kelvin):

> "The cause of the semi-diurnal variation of barometric pressure cannot be the gravitational tide-generating influence of the sun, because if it were there would be a much larger lunar influence of the same kind, while in reality the lunar barometric tide is insensible or nearly so. It seems, therefore, certain that the semi-diurnal variation of the barometer is due to temperature. Now, the diurnal term, in the harmonic analysis of the variation of temperature, is undoubtably much larger in all, or nearly all, places than the semi-diurnal. It is then very remarkable that the semi-diurnal term of the barometric effect of the variation of temperature should be greater, and so much greater as it is, than the diurnal." (Thomson, 1882)

He then proceeds to suggest a resonance theory in which it is postulated that one of the modes of free oscillation has a period very close to 12 hours, and hence the forcing would resonantly interact with this free mode. It was shown by Pekeris (1937) that this theory would be valid if the atmosphere above 80 km were cool ($\sim$ 200 K). The first measurements of the temperature at this level were made from rockets in the early 1950's. They showed that above 100 km the atmosphere is hot, hence resonance does not occur and Kelvin's theory is incorrect.

Heating due to direct atmospheric absorption of solar radiation by ozone and water vapour forces tidal motion. Using these two components of the forcing, Butler and Small (1963) calculated values for the semi-diurnal (12 hour) and ter-diurnal (8 hour) surface pressure oscillations that agreed with the observations. The reason why the semi-diurnal tide dominates the diurnal (24 hour) is that

forcing at all levels contributes towards its amplitude at the ground, while the amplitude of the diurnal tide decays exponentially away from the forcing.

4.2. Observations

In the analysis of observations the tides are assumed to be synonymous with the average diurnal variations with periods of 24, 12 and 8 hours, and hence they are obtained by Fourier analysis of hourly average values. (The "hourly average" is the mean value at a particular hour, averaged over many days.) The global distribution can then be expressed in terms of spherical harmonics and directly compared with the theory. As data is Fourier analysed to evaluate both tides (this chapter) and planetary waves (next chapter) a description of the technique is now given.

4.2.1. Fourier Analysis of One-Dimensional Data

The simplest, and the commonest, situation in which Fourier analysis is required is with one-dimensional data (e.g. pressure as a function of time, 500 mb height as a function of longitude). The technique can be illustrated by the following example:-

Let $\bar{p}(i)$ be the hourly annual average pressure, where $i = 0,1..23$ corresponds to 00Z, 01Z,..23Z. The Fourier coefficients A_n and B_n are defined by

$$\bar{p}(i) = A_0 + \sum_{r=1}^{12} \left(A_r \cos \frac{2\pi r i}{24} + B_r \sin \frac{2\pi r i}{24} \right) \qquad (4.1)$$

Using orthogonality properties it can be shown that for $m > 0$

$$A_m = \frac{2}{24} \sum_{i=0}^{23} \bar{p}(i) \cos \frac{2\pi m i}{24} \qquad (4.2a)$$

$$B_m = \frac{2}{24} \sum_{i=0}^{23} \bar{p}(i) \sin \frac{2\pi m i}{24} \qquad (4.2b)$$

This method has assumed that $\bar{p}(t)$ is periodic, while in general $\bar{p}(24)$ is not equal to $\bar{p}(0)$. The simplest way of accounting for this difference is to remove a linear trend. There is no a-priori reason for selecting a linear trend, but it is the easiest model to analyse.

A "corrected" pressure, $\bar{p}'(i)$ is used, where

$$\bar{p}'(i) = \bar{p}(i) - \left(\frac{i-12}{12}\right) d\bar{p} \tag{4.3}$$

and

$$d\bar{p} = \bar{p}(24) - \bar{p}(0) \tag{4.4}$$

The Fourier coefficients of $\bar{p}'$, A_n' and B_n', can be calculated as before.

$$A_m' = A_m + \frac{d\bar{p}}{24} \tag{4.5a}$$

$$B_m' = B_m + \frac{d\bar{p}}{24} \cot \frac{m\pi}{24} \tag{4.5b}$$

These corrections to the yearly average tides are small even in the extreme situation of there being a 50 mb difference between the surface pressure at the start and end of the year. For then $dp = 0.14$ mb and $B_m' - B_m = 0.04, 0.02$ mb for $m = 1, 2$. The data analysed here is for India, where the diurnal and semi-diurnal tides have amplitudes of about 0.6 mb and 1.1 mb, and Britain, where they are about 0.1 mb and 0.3 mb. So the corrections needed will be less than 10%, except for the British diurnal tide, and this large only if a low pressure system passes over the station at New Year. Often only one of $\bar{p}(0)$ and $\bar{p}(24)$ is tabulated, in which case no correction can be made.

Another cause of error in the Fourier analysis is due to the inaccuracy of the values used. The instantaneous pressure can be measured to an accuracy of 1 mb, so the annual averages are accurate to 0.003 mb. However, in the Indian data used they were only quoted to the nearest 0.1 mb. From this data, how precisely can the tides be calculated?

In this case there are 24 values $\bar{p}(i)$ each having a random error V_i. So $\bar{p}(i) = P(i) + V_i$, where P(i) is the actual hourly average surface pressure. Let the mean value of V be E(V), then the variance, $\mathrm{Var}(V) = E(V^2) - [E(V)]^2$. Consider a particular Fourier coefficient, the sine component of wave number m, then from equation 4.2b it can be seen that

$$E(A_m) = \frac{2}{24} \sum_{i=0}^{23} E(P(i)) \sin \frac{2\pi m i}{24} \qquad (4.6)$$

Now, as V is independent of i, $\sum_{i=0}^{23} E(V) \sin \frac{2\pi m i}{24} = 0$

Also
$$E(A_m^2) = \left(\frac{2}{24}\right)^2 \sum_{i=0}^{23} \sum_{j=0}^{23} E\left[(P(i)+V_i)(P(j)+V_j)\right. \times \sin \frac{2\pi m i}{24} \times \sin \frac{2\pi m j}{24} \qquad (4.7)$$

By considering the cases of $i = j$ and $i \neq j$ separately, the right hand side of 4.7 can be evaluated, giving

$$E(A_m^2) = [E(A_m)]^2 + \frac{2}{24}\left\{E(V^2) - [E(V)]^2\right\} \qquad (4.8)$$

And so

$$\mathrm{Var}(A_m) = \frac{2}{24} \mathrm{Var}(V) \qquad (4.9)$$

With readings quoted to the nearest 0.1 mb, $\mathrm{Var}(V) = \frac{1}{1200}$ mb^2, equation 4.9 gives that $\mathrm{Var}(A_m) = \left(\frac{1\text{mb}}{120}\right)^2$. Hence the standard

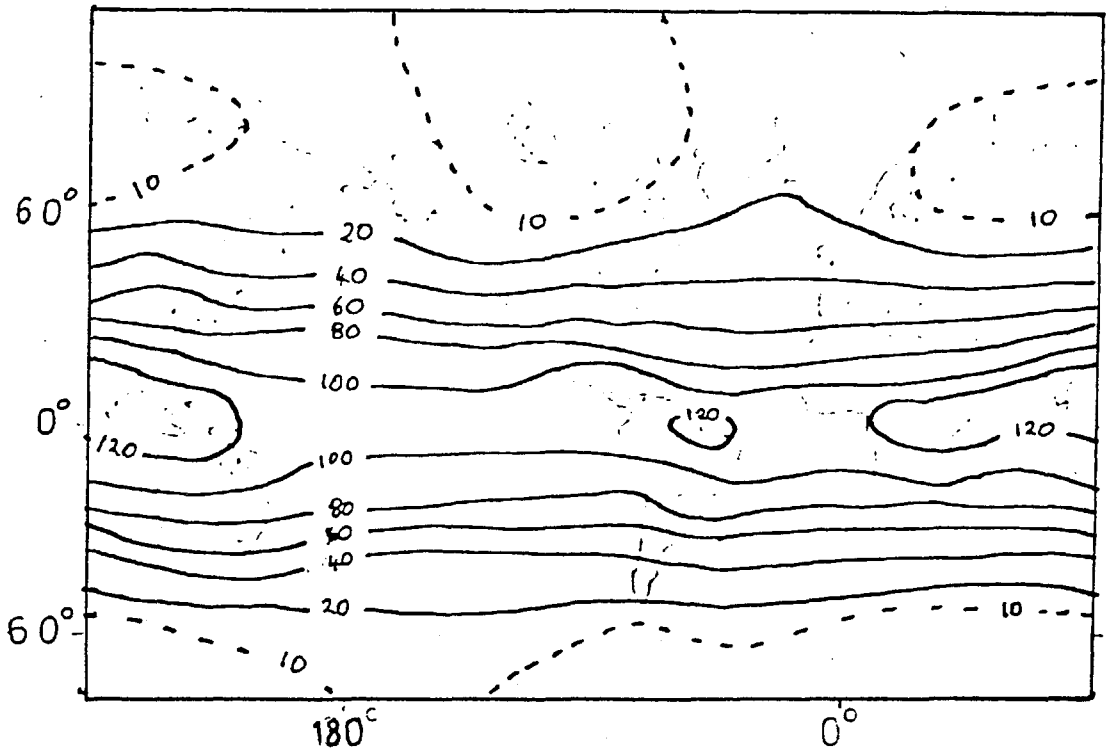

Figure 4.1 World maps of the semidiurnal tide showing: (a)-above- Amplitude (10^{-2} mb) and (b)-below-Phase. After Haurwitz (1956)

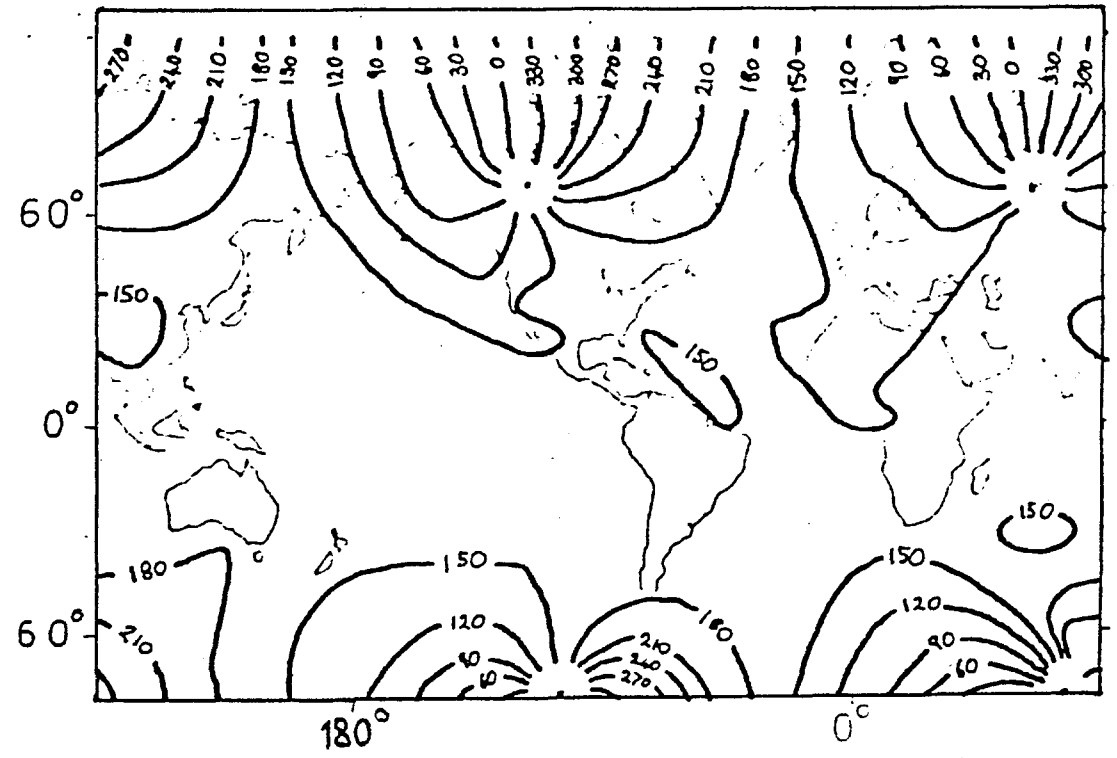

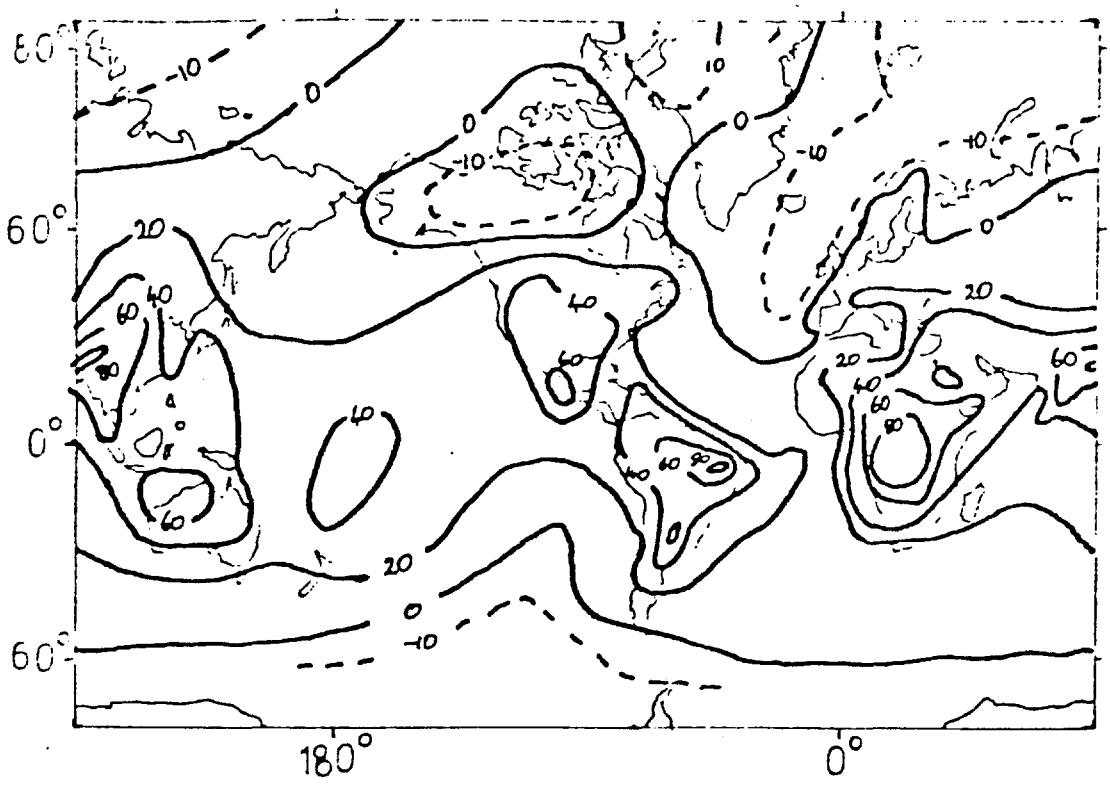

Figure 4.2 World maps of the diurnal tide showing equilines of: (a)-above- the sine and (b)-below- the cosine component in 10^{-2} mm of mercury. After Haurwitz (1965)

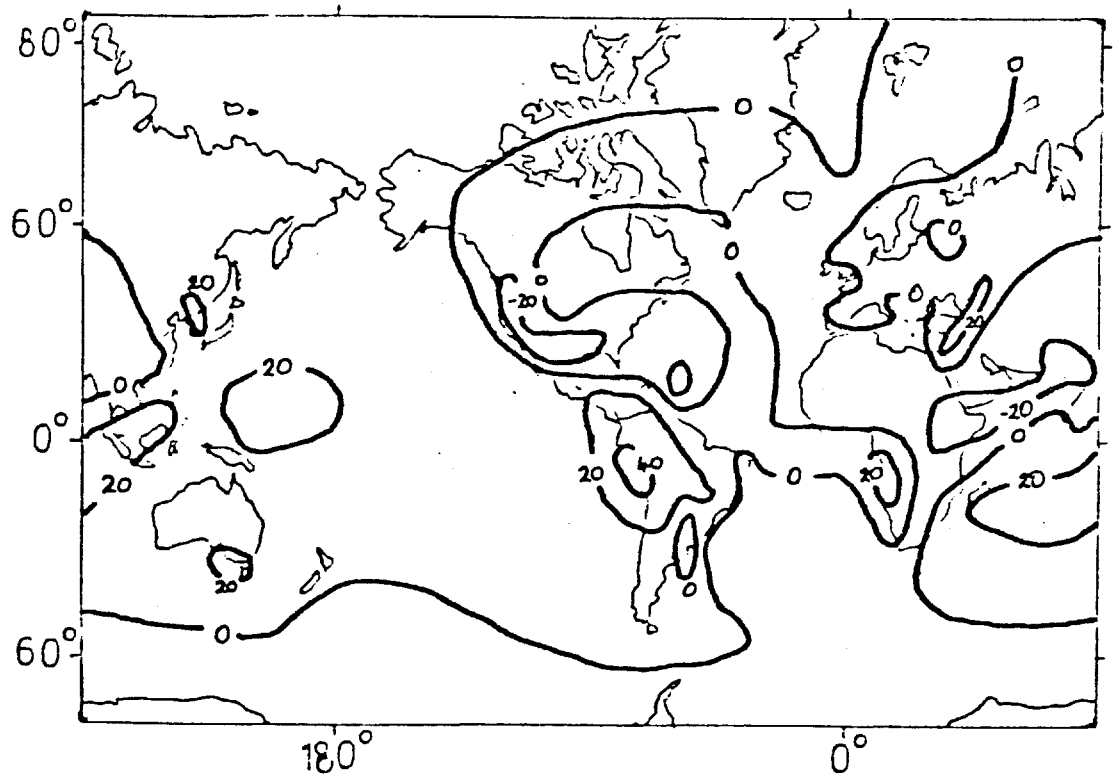

deviation of the error is about 0.01 mb, and the result of the tidal analysis can be expressed accurate to one more order of magnitude than the observations are quoted. So the error due to rounding is of the same order of magnitude as the maximum possible error due to variations between 00Z on January 1st and 24Z on December 31st.

4.2.2. Global Harmonic Analysis

By Fourier analysing the hourly annual average pressure at a station, the amplitude and the phase of the tides can be evaluated. Comparing several years' results shows that the semi-diurnal tide is almost constant, while the diurnal tide fluctuates between years. The errors in these mean tides can be reduced by averaging over several years of data. Compiling such averages, Haurwitz (1956 and 1965) plotted maps of the worldwide distribution of the annual average semi-diurnal and diurnal tides. These maps are reproduced here as Figures 4.1 and 4.2. From them it can be seen that the semi-diurnal tide has very little longitudinal variations, whereas the diurnal tide, dominated by orography and the land/sea pattern, depends on longitude as well as latitude.

The tides can be expressed as a linear sum of components whose latitudinal (θ), longitudinal (ϕ) and temporal (t) dependences have been separated. The tidal theory given in Section 4.4 shows that the canonical form for expressing the θ dependence of tides is in terms of Hough Functions, $\Theta_n^{\sigma,s}(\theta)$, which are eigenfunctions of the Laplace Tidal Equation. The longitudinal and temporal dependences are taken to be sinusoidal, so the diurnal variation of the surface pressure can be decomposed into its tidal components thus:

$$\bar{p}(i) = \sum_{\sigma=1}^{12} \sum_{s=-\infty}^{\infty} \sum_{n=0}^{\infty} A_n^{\sigma,s} \Theta_n^{\sigma,s}(\theta) \sin(\sigma t_G + s\phi + \varepsilon_n^{\sigma,s}) \qquad (4.10)$$

	Diurnal			Semi-Diurnal	
n	Amp($A_n^{1,1}$)	Phase($\varepsilon_n^{1,1}$)	n	Amp ($A_n^{2,2}$)	Phase($\varepsilon_n^{2,2}$)
-6	.124(.128)	1704(1708)	2	1.094(1.133)	0942(0940)
-4	.236(.246)	1704(1708)	3	.051 (.065)	0006(0034)
-2	.442(.458)	0516(0516)	4	.153 (.182)	0932(0934)
1	.273(.283)	0504(0504)	6	.059 (.072)	0928(0932)

Table 4.1 Amplitude (mb) and phase (time of maximum) of the main diurnal and semi-diurnal tidal components. Annual means, with equinoctal means (March, April, September, October) in brackets. (After Haurwitz and Cowley, 1973)

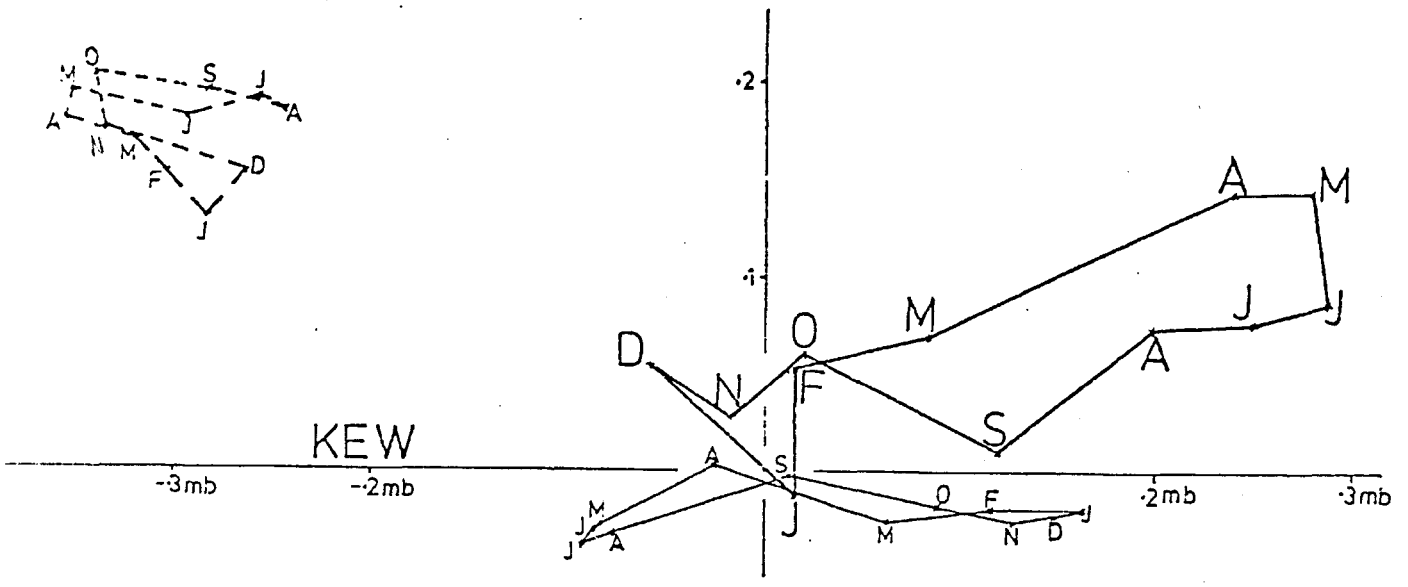

Figure 4.3 Annual variation of the Diurnal(thick line), semi-diurnal (dashed line) and ter-diurnal (thin line) surface pressure tides at Kew, (51°N,0°W)

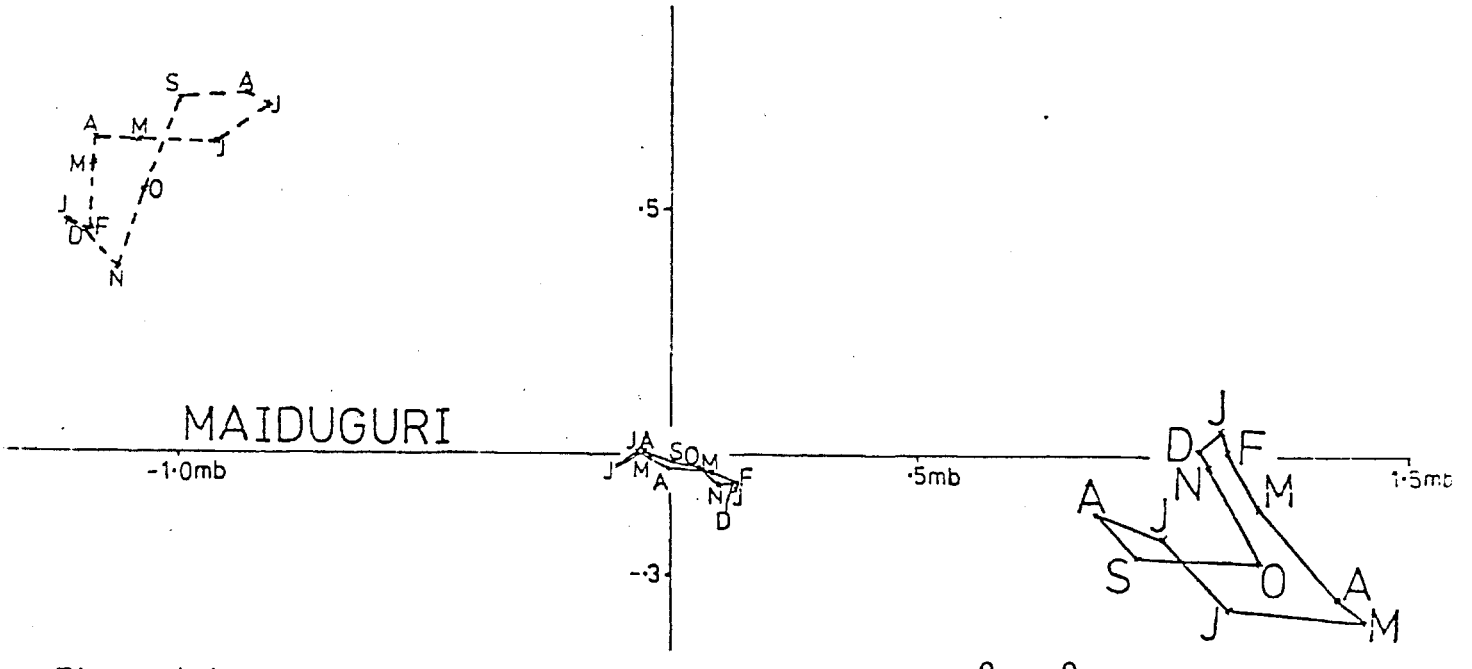

Figure 4.4 As Figure 4.3 but for Maiduguri, Nigeria (12°N,13°E)

where Greenwich Mean Time, $t_G = t_i - \phi$, and the local time $t_i = \frac{2\pi i}{24}$.

A method for evaluating $A_n^{\sigma,s}$ and $\varepsilon_n^{\sigma,s}$ is given by Haurwitz and Cowley (1973). Their tabulation of the main components, when $\sigma = s = 1$, and $\sigma = s = 2$, is reproduced here (Table 4.1). These results are for modes which are "stationary" relative to the Sun, hence their dependence on longitude and time can be expressed by a single variable, the local time (t_i), and $\sigma = s$. As the semi-diurnal tide, expressed in terms of local time, has little longitudinal variation, Table 4.1 lists all its important components. However, this is not the case for the diurnal tide which, having large longitudinal variations, has important modes which "travel" relative to the Sun. One of the significant "travelling" modes ($s = 0$) is stationary in the atmosphere, but the others (when $s \neq 0,1$) propagate relative to longitude as well as local time. Ozone heating, which only slightly depends on longitude, cannot force such large "travelling" components. They are due to orography and longitudinal variations in water vapour heating.

An alternative method of expressing the latitudinal variation of the tides is as a single expression. This form, used in all the early work on tidal observations, is based on the expansion

$$\bar{p}(i) = \sum_{s=-\infty}^{\infty} S^s(\theta) \sin(s\tau_i + \varepsilon^s) \qquad (4.11)$$

Chapman and Lindzen (1970) list values for $s = 1, 2$ and 3.

$$S^1(\theta) = \cdot 593 \cos^3\theta \text{ mb} \quad , \quad \varepsilon^1 = 12^\circ \qquad (4.12)$$

$$S^2(\theta) = 1 \cdot 16 \cos^3\theta \text{ mb} \quad , \quad \varepsilon^2 = 158^\circ \qquad (4.13)$$

$$S^3(\theta) = \cdot 563 \cos^3\theta \sin\theta \text{ mb} \quad , \quad \varepsilon^3 = \begin{cases} 175^\circ \text{ July} \\ 335^\circ \text{ January} \end{cases} \qquad (4.14)$$

From equation 4.14 it can be seen that the ter-diurnal tide changes phase by 180° between summer and winter, and also between hemispheres (shown by the sin θ term).

The diurnal and semi-diurnal, as well as the ter-diurnal, tides show systematic seasonal variations as can be seen from Figures 4.3 and 4.4. The former shows the monthly average tide at Kew (51°N, 0°W) for 1871-1926 (data from Mitchell, 1930), while the latter is for Maiduguri (12°N, 13°E) for 8 years (data from Giwa, 1972). At both stations there is clearly an annual cycle in the ter-diurnal tide, with a phase change of about 150° between summer and winter. Apparent in the semi-diurnal tide is

1. a semi-annual cycle in amplitude, with maxima shortly after the equinoxes and minima at the solstices, and
2. an annual cycle in phase, being latest in July and earliest in November, the difference being 25 minutes at Kew and 45 minutes at Maiduguri.

The diurnal patterns show no similarities, concurring with the deduction from Figure 4.1 that this tide varies greatly with geography.

A very simple model of tides, which assumes that the amplitude of the tides are proportional to Fourier components of solar heating is now presented.

4.3. Simple Model

It was shown by Butler and Small (1963) that the primary forcing of atmospheric tides is due to absorption of solar radiation by water vapour and ozone. Consideration of how the Fourier components of this heating varies with the seasons will give some

indication of how the tides vary during the year.

In this model the Sun's elevation is used to parametrise solar heating of the atmosphere, using the relationship

$$\sin E = \sin \delta \sin \theta + \cos \delta \cos \theta \cos H \tag{4.15}$$

where E is the solar elevation

θ is the latitude

and H is the local hour angle

The declination, δ, is equal to the latitude at which the sun is overhead. It is defined by the equation

$$\sin \delta = \sin 23.5^{\circ} \sin t_y$$

where t_y, the time of the year is 0 at the March equinox, $\frac{\pi}{2}$ at the summer solstice. H_o, the time of sunset (E = 0), is defined by equation 4.15 as

$$\cos H_o = - \tan \delta \tan \theta \tag{4.16}$$

The amount of energy incident on horizontal ground is proportional to sin E, so, if reflection and scattering are ignored,

$$\begin{aligned} Q(H) &= Q_o (\sin \delta \sin \theta + \cos \delta \cos \theta \cos H) \quad |H| \leq H_o \\ &= \begin{cases} Q_o \cos \delta \cos \theta (\cos H - \cos H_o) & |H| \leq H_o \\ 0 & |H| \geq H_o \end{cases} \end{aligned} \tag{4.17}$$

Where Q_o, the constant of proportionality, is the amount of energy absorbed by the atmosphere when the sun is at zenith (directly overhead). As Q is an even function of H, the Fourier sine components are all zero. Defining the cosine components by

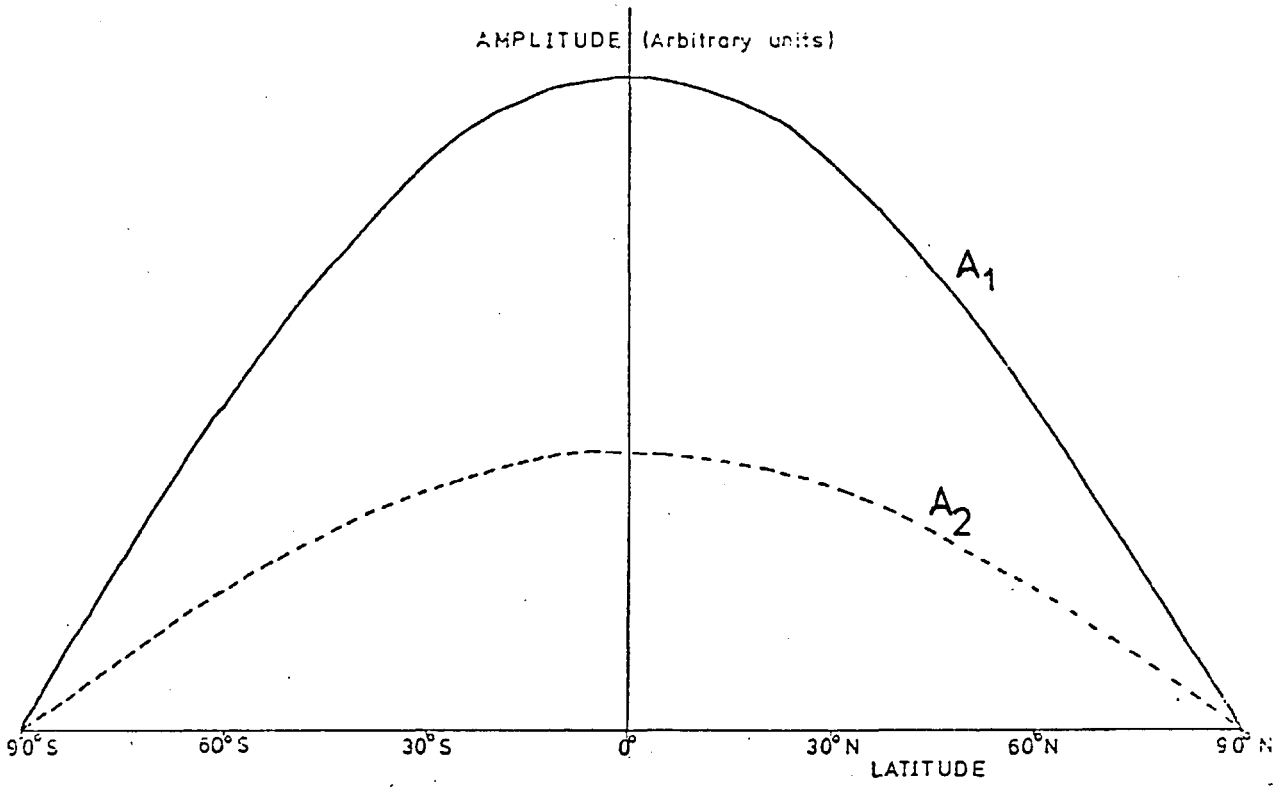

Figure 4.5 Variation of the diurnal (A_1) and semi-diurnal (A_2) heating with latitude at an equinox. The ter-diurnal component (A_3) is identically zero.

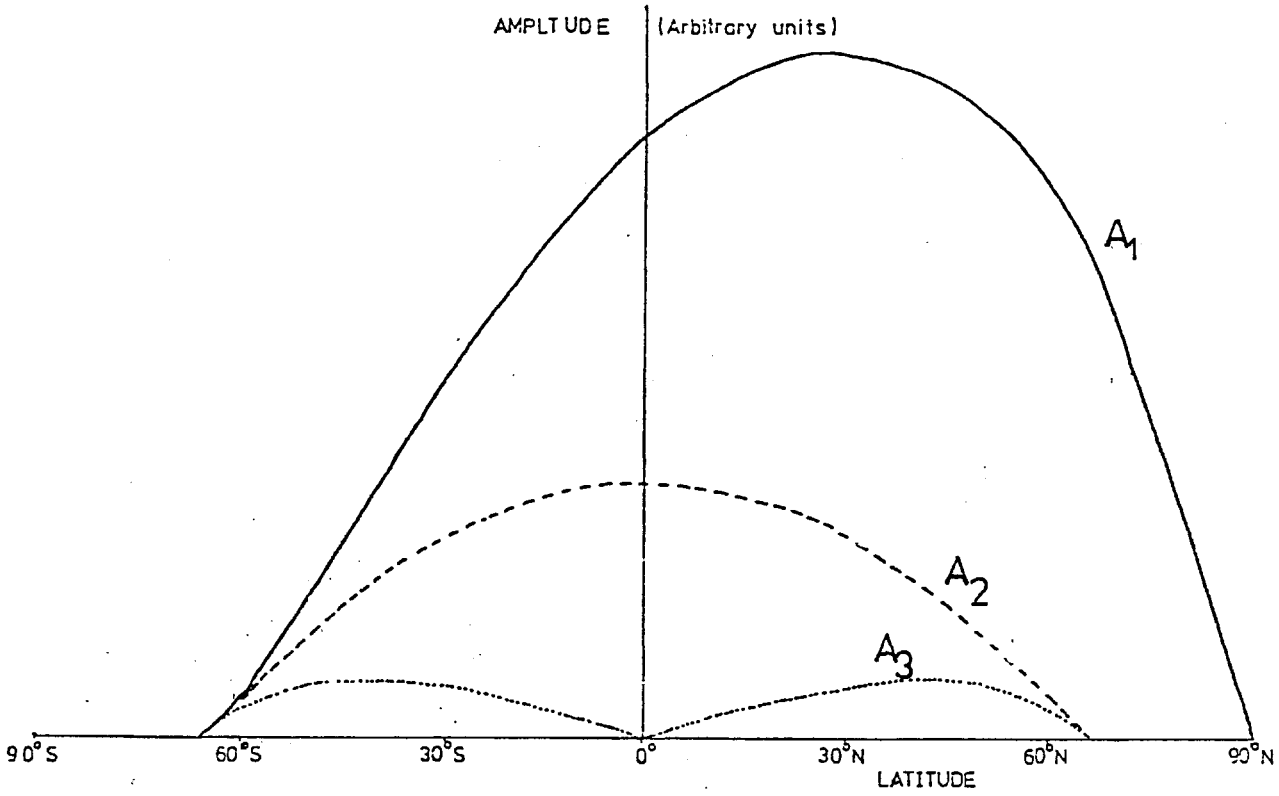

Figure 4.6 As Figure 4.5 but for the June solstice.

$$Q(H) = \tfrac{1}{2}A_0 + \sum_{n=1}^{\infty} A_n \cos nH \qquad (4.18)$$

Then
$$A_n = \frac{2}{\pi}\int_0^{H_0} Q(H)\cos nH\, dH \qquad (4.19)$$

The A_n's of interest here are

$$A_1 = \frac{Q_0}{\pi}\cos\delta\cos\theta\,(H_0 - \sin H_0 \cos H_0) \qquad (4.20)$$

$$A_2 = \frac{2Q_0}{3\pi}\cos\delta\cos\theta\,\sin^3 H_0 \qquad (4.21)$$

$$A_3 = \frac{2Q_0}{3\pi}\cos\delta\cos\theta\,\sin^3 H_0 \cos H_0 \qquad (4.22)$$

The only other situation to be resolved is what happens near the poles, when $|\tan\delta\tan\theta| > 1$ and hence H_0 does not exist? There are two cases to consider:-

(a) $\tan\delta\tan\theta > 1$ ("land of the midnight sun")

Then $A_1 = \cos\delta\cos\theta \cdot Q_0$

$A_n = 0$ for all $n \geqslant 2$.

(b) $\tan\delta\tan\theta < -1$ (sun always below the horizon)

$A_n = 0$ for all n.

Using these results with Equations 4.20 to 4.22, the tidal forcing can be estimated for any latitude and time of year. The situations at an equinox ($t_y = 0$ or π) and at a solstice ($t_y = \frac{\pi}{2}$ or $\frac{3\pi}{2}$) are illustrated in Figures 4.5 and 4.6 respectively. The following properties are readily observable:

(i) A_1 is largest at midsummer and smallest at midwinter, in extratropical latitudes, while at the equator it has two maxima, at the equinoxes.

(ii) A_2 is a maximum at the equinoxes and a minimum at the

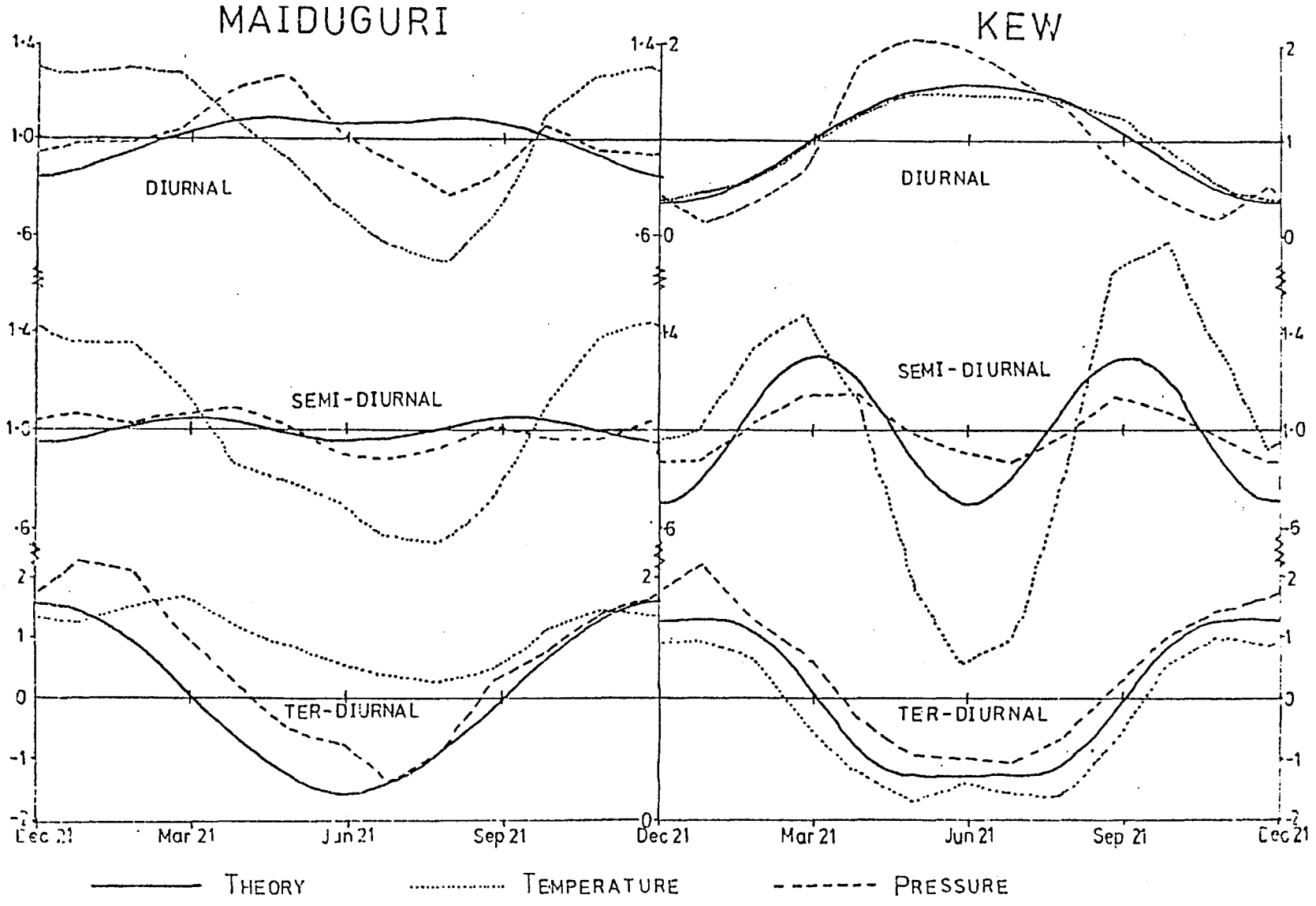

Figure 4.7 Comparison of the seasonal variations in the temperature and surface pressure tides at Kew and Maiduguri with the simple model. Each curve is normalised to have a mean absolute value of 1. Observed values for Kew from Mitchell (1930) and for Maiduguri from Giwa (1972).

solstices, for all latitudes.

(iii) There is a 180^{o} phase difference in A_3 between the Northern and Southern Hemispheres, and between summer and winter in the same Hemisphere.

A comparison between this theory and the observations of diurnal variations of pressure and temperature at Kew and Maiduguri is shown in Figure 4.7. The simple theory predicts seasonal changes in the Fourier coefficients of the diurnal temperature variation. At Kew it does so very well, apart from underestimating the changes in the semi-diurnal tide, while at Maiduguri it is a complete failure. This is because the theoretical seasonal changes are smaller nearer the equator (except for the ter-diurnal component), so other effects, such as cloud cover, have greater significance. However, the semi- and ter-diurnal variations in pressure are also close to the theoretical results. This is because these tides are predominantly due to the absorption of Ultra-Violet radiation (UV) by ozone on a global scale, so local and tropospheric variations are unimportant.

This simple theory gives good qualitative results, but a more complete, quantitative theory of tides is needed to investigate the effects of solar and ozonospheric variations on tides; this is described in the next Section.

4.4. Complex Theory

4.4.1. Approximations

The theory now outlined is based on that of Pekeris (1937), elucidated by Chapman and Lindzen (1970). Many approximations are used, these are:

(a) The atmosphere behaves like a perfect gas; which is true to within 0.2% below 100 km.

(b) The atmosphere is "thin", so if the earth's radius is a, and z is a typical height above the surface, then z/a is negligible compared to 1. This implies that g is assumed to be constant, when in fact it is 2% less at 100 km than it is at the ground.

(c) Hydrostatic equilibrium is assumed (vertical velocities not affecting pressure).

(d) The earth is assumed to be a perfect sphere. This implies that not only is ellipticity ignored, but so is topography. Hence tides travelling relative to the Sun cannot be modelled as there is no longitudinal variation.

(e) Dissipation, such as that due to viscosity and infra-red radiative transfer are ignored.

(f) The equations are linearised, and assumed to be in a steady state.

(g) The tides are assumed to be in an otherwise static atmosphere. This implies that in the basic state temperature, density and pressure are all independent of latitude and longitude.

(h) Gravitational tidal effects are neglected, though this introduces errors of up to 4%.

The hydrostatic approximation (c) can be shown to be valid by a posteriori checks. Chapman and Lindzen (1970) conclude that although the approximations (d) to (g) introduce errors, "the approximate theory does quite well in predicting solar thermotidal oscillations in surface pressure." Later work, (Lindzen and Hong, 1974, Walterscheid and Venkateswaran, 1979, Walterscheid et al., 1980) has investigated the effect of zonal winds on the tides and

found that it is a significant cause of the discrepancy between theory and observation.

4.4.2. Equations

The motion is described by the Navier-Stokes equations for a compressible gas. The atmosphere is assumed to be in local thermodynamic equilibrium. The equations of a motionless basic state are:-

Horizontal momentum and continuity $$u_0 = v_0 = w_0 = 0 \qquad (4.23a,b,c)$$

Gas Law $$p_0 = \rho_0 R T_0 \qquad (4.23d)$$

Hydrostatic $$\frac{1}{\rho_0}\frac{dp_0}{dz} = -g \qquad (4.23e)$$

Where u is westerly velocity

v is southerly velocity

w is vertical velocity

p is pressure

ρ is density

z is height in metres

T is the temperature

R is the gas constant for air

and the subscript o denotes the basic state

From 4.23 d and e

$$\frac{d}{dz}(\ln p_0) = -\left(\frac{g}{RT_0}\right) = \frac{-1}{H} \qquad (4.24)$$

H has the dimensions of length and is called the "scale height", for in an isothermal atmosphere the pressure decreases by a factor of e over a depth of one scale height. In the non-isothermal case, by

defining $$x = \int_0^z \frac{dz}{H} \tag{4.25}$$

then $$\rho_0(x) = \rho_0(0)\, e^{-x} \tag{4.26}$$

and also $$\rho_0 = p_0/gH \tag{4.27}$$

The linearised tidal equations are:-

Horizontal Momentum

$$\frac{\partial u'}{\partial t} - 2\omega v' \sin\theta = \frac{-1}{a\cos\theta}\,\frac{\partial}{\partial\phi}\left(\frac{p'}{\rho_0}\right) \tag{4.28a}$$

$$\frac{\partial v'}{\partial t} + 2\omega u' \sin\theta = \frac{-1}{a}\,\frac{\partial}{\partial\theta}\left(\frac{p'}{\rho_0}\right) \tag{4.28b}$$

Continuity

$$\frac{\partial \rho'}{\partial t} + \frac{d\rho_0}{dz} w' + \rho_0\left(\frac{1}{a\cos\theta}\,\frac{\partial u'}{\partial\phi} + \frac{1}{a\cos\theta}\,\frac{\partial}{\partial\theta}(v'\cos\theta) + \frac{\partial w}{\partial z}\right) = 0 \tag{4.28c}$$

Hydrostatic

$$\frac{\partial p'}{\partial z} = -\rho' g \tag{4.28d}$$

Gas Law

$$\frac{p'}{p_0} = \frac{\rho'}{\rho_0} + \frac{T'}{T_0} \tag{4.28e}$$

and the thermal energy equation

$$\frac{\partial T'}{\partial t} + \frac{dT_0}{dz} w' = \frac{1}{c_v} J' + (\gamma - 1)\,\frac{T_0}{\rho_0}\left(\frac{\partial \rho'}{\partial t} + \frac{d\rho_0}{dz} w'\right) \tag{4.28f}$$

Where ω is earth's rotation rate

J is the thermotidal heating of unit mass in unit time.

$\kappa = (\gamma - 1)/\gamma = \frac{2}{7}$

and the prime denotes the perturbation from the basic state.

In considering tidal motion, sinusoidal variation in time and longitude is assumed, while in the latitudinal direction the components are Hough Functions, so any property A can be expressed as

$$A = A_o + \sum_n \sum_s \sum_\sigma \hat{A}_n^{\sigma,s}(z)\, \Theta_n^{\sigma,s}(\theta)\, \exp[i(\sigma t + s\phi)] \qquad (4.29)$$

where A_o is the basic state. The superscripts (σ and s) and subscripts (n) will be dropped in future, except when this leads to ambiguity.

The main dependent variable used in the calculation is $\hat{G}$, the divergence ($\hat{X}$) corrected for diabatic heating. It is defined as

$$\hat{G} \equiv \hat{X} - \frac{\hat{J}}{c_p T_o} = \frac{-1}{\gamma p_o} \frac{D\hat{p}}{Dt} \qquad (4.30)$$

It can be shown (Chapman and Lindzen, 1970) that

$$\frac{\left[H(z)\frac{d^2\hat{G}(z)}{dz^2} + \left\{\frac{dH(z)}{dz} - 1\right\}\frac{d\hat{G}(z)}{dz}\right]}{\left[\left\{\frac{dH(z)}{dz} + \kappa\right\}\hat{G}(z) - \frac{\kappa \hat{J}(z)}{\gamma g H(z)}\right]} = \frac{g F_\theta[\Theta(\theta)]}{4a^2\omega^2\Theta(\theta)} \qquad (4.31)$$

where

$$F_\theta \equiv \frac{1}{\cos\theta}\frac{\partial}{\partial\theta}\left(\frac{\cos\theta}{f^2-\sin^2\theta}\frac{\partial}{\partial\theta}\right) - \frac{1}{f^2-\sin^2\theta}\left(\frac{s}{f}\frac{f^2+\sin^2\theta}{f^2-\sin^2\theta} + \frac{s^2}{\cos^2\theta}\right) \qquad (4.32)$$

The left hand side of Equation 4.31 is a function of z only, while the right hand side is a function of Θ only. Hence both are equal to a (separation) coefficient, denoted by -1/h, and Equation 4.31 can be separated into two equations. First the Θ equation is considered. As it was first derived by Laplace, it is also called

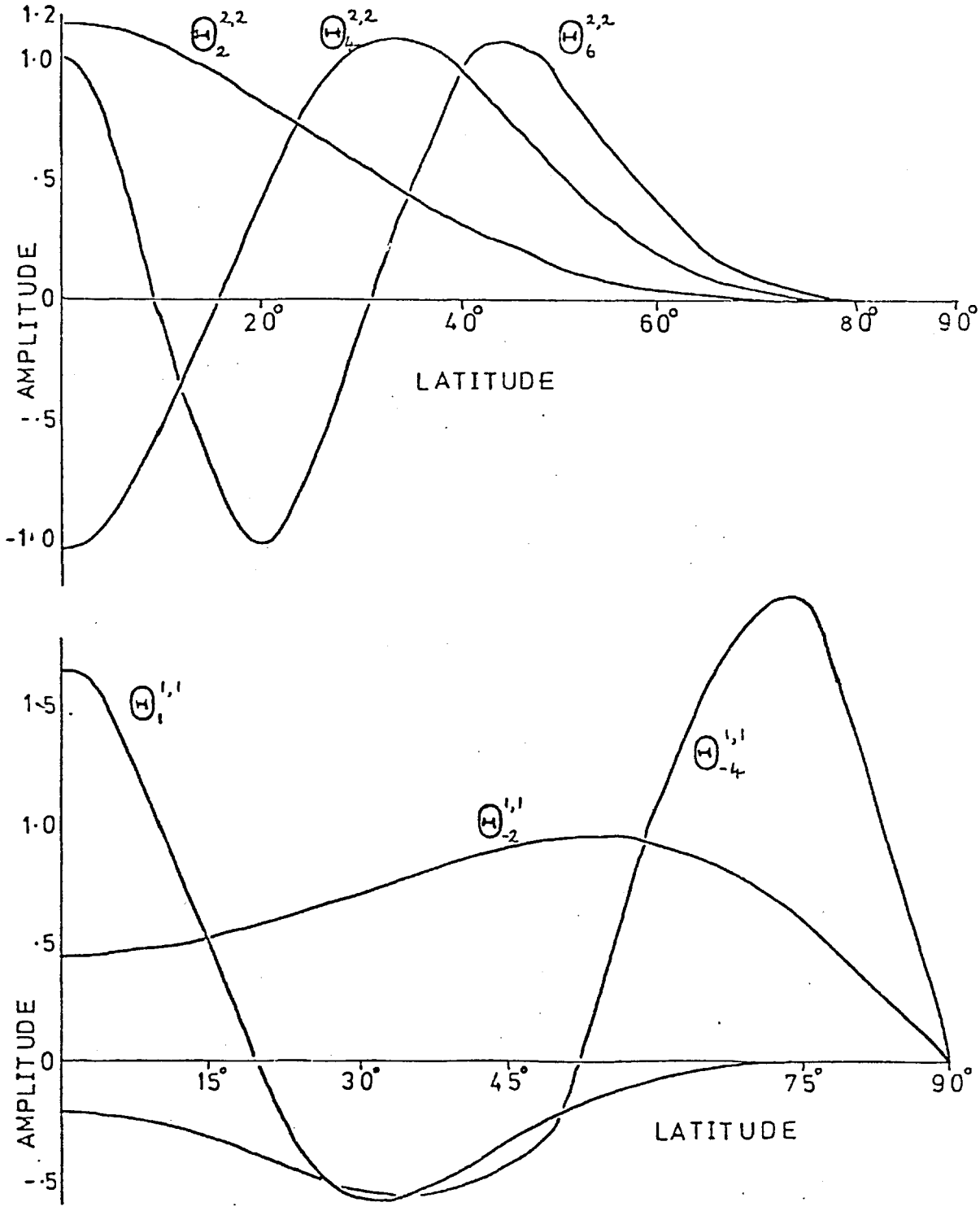

Figure 4.8 Latitudinal variation of the Hough functions used here.

the Laplace Tidal Equation.

4.4.3. The Laplace Tidal Equation

$$F_\theta[\Theta(\theta)] = \frac{-4a^2\omega^2}{gh}\Theta(\theta) \qquad (4.33)$$

It has the boundary conditions that $\Theta(\theta)$ is bounded at the poles ($\theta = 0, \pi$). For any fixed σ and s, (which occur in the definition of F_θ , Equation 4.32), 4.33 is an eigenvalue problem, which yields a set $\{h_n\}$ of eigenvalues. The Hough Functions (Θ) were first evaluated, by expressing them as a sum of associated Legendre Functions, by Hough (1898), hence their name. The six Hough Functions that are used here are illustrated in Figure 4.8. Those which have positive h (positive subscripts) are largest near the equator while those with negative h (negative subscripts) are largest near the pole.

The "equivalent depth", h, derives its name from comparison with the equivalent mode in an incompressible, uniformly deep, boundless ocean. In the case of negative equivalent depths, there is no obvious analogy as an ocean cannot be negatively deep. One important corollary of a mode having a negative h is that it has an imaginary vertical wavelength and so is vertically trapped (there is no vertical propagation of wave energy). When the vertical wavelength is positive the waves vary sinusoidally in the vertical, and so they propagate energy. Why the sign of h is so important can be seen by considering the z component of Equation 4.31, "The Vertical Structure Equation".

4.4.4. The Vertical Structure Equation

The z part of Equation 4.31 is transformed into a simpler form by using x, as defined by 4.25, as the vertical co-ordinate and removing a factor proprotional to $\rho^{\frac{1}{2}}$ from G, for as with most atmospheric waves the amplitude decreases with height roughly as $\rho^{\frac{1}{2}}$. So

$$y = e^{-x/2}\hat{G} \tag{4.34}$$

The Vertical Structure Equation can then be written in the form

$$\frac{d^2y}{dx^2} - \frac{1}{4}\left(1 - \frac{4}{h}\left\{\frac{dH}{dx} + \varkappa H\right\}\right)y = \frac{\varkappa e^{-x/2}}{\gamma g h}\hat{J} \tag{4.35}$$

This is the same form as the general Vertical Structure Equation given in the Appendix (Equation A.1) with

$$\nu^2(x) = \frac{1}{h}\left(\frac{dH}{dx} + \varkappa H\right) - \frac{1}{4} \tag{4.36}$$

From this, with the fact that H is a slowly varying function of x so $\frac{dH}{dx}$ is always much less than $\varkappa H$, it can be confirmed that if h is negative, so is ν^2. Similarly if h is positive and "small", then ν^2 is positive.

There are two boundary conditions for the Vertical Structure Equation. At the ground there can be no vertical velocity, while at the top the radiation condition implies that there is no downward propagation of energy (if ν^2 is positive) or else that the Kinetic Energy decays with height (ν^2 negative).

The top boundary condition is

$$\frac{dy}{dx} = i\nu y \tag{4.37}$$

where ν is positive if ν^2 is positive, or $i\nu$ is negative if ν^2 is negative.

The bottom boundary condition can be shown to be

$$\frac{dY(0)}{dx} + \left(\frac{H}{h} - \frac{1}{2}\right)Y(0) = 0 \qquad (4.38)$$

As well as the boundary conditions, we also need to know the heating function ($\hat{J}$) before solving the Vertical Structure Equation. This is where possible solar variability effects come in, as changes in UV will affect $\hat{J}(z)$.

4.4.5. The Heating Profile

As previously mentioned, the predominant forcing of atmospheric tides is by ozone and water vapour absorbing solar radiation. Other heating processes, which have been neglected here, are:-

(a) Cooling by infra-red emission. Though this is large (up to 30°C per day at the stratopause), it has only a small diurnal variation as temperature variations are only a few percent of the mean. For the diurnal forcing the effect of infra-red cooling is about 12% of the Ultra-Violet heating while for the semi-diurnal tide it is 3%.

(b) Heating by atomic oxygen absorbing UV at altitudes of about 100 km. This contributes neglibably to the diurnal and semi-diurnal tides at the ground (Green, 1965).

(c) Heating of the boundary layer by upward eddy heat transfer from the ground excites a tide that can be neglected at mid-latitudes (Siebert, 1961). In the tropics, however, it forces a large diurnal component whose neglect results in the diurnal pressure oscillation over India being underestimated

by a factor of 5. The semi-diurnal component is relatively small and its neglect results in only a small error.

(d) Heating due to the release of latent heat in cumulo-nimbus clouds. Lindzen (1978) suggested this as a possible tidal forcing that would explain the discrepancies between tidal theory and observations of the semi-diurnal tide. (The theory predicts that it is a maximum at 0900 and 2100 local time, while observations indicate that it is 40 minutes later. Also predicted is a phase reversal at 28 km, which is not observed.)

The heating (J), due to the absorption of solar radiation by a gas (G), varies with time of day, time of year, latitude, longitude, altitude, absorption coefficient of the gas (which varies with wavelength, and possibly other parameters) and solar output. Various assumptions therefore need to be made if the thermotidal heating is to be modelled. As ozone absorption is the only thermotidal forcing to be considered in detail, the comments will apply specifically to that case.

The heating depends on the elevation of the Sun, E, given by Equation 4.15. Assuming that at those wavelengths where gas G absorbs solar radiation it is the only significant absorber in the atmosphere, then the optical depth, u(z,E), defined as the total amount of G that the radiation has passed through, is given by

$$u(z,E) = \int_{\infty}^{z} \frac{\rho_G(z)dz}{\sin E} \qquad (4.39)$$

It has also been assumed here that the earth's curvature can be neglected and, more important, that the density of gas G is independent of latitude, longitude and time of day. Leovy (1964,

Figure 4) showed theoretically that in the mesosphere, ozone concentrations should vary diurnally by factors 2 (at 60 km), and 10 (70 km). However, this variation occurs during half an hour around sunrise and sunset, so it only slightly affects the diurnal and semi-diurnal Fourier components of the heating. To assume that ozone does not vary with longitude is consistent with neglecting topography, as a longitudinal variation in ozone would force those modes which move relative to the Sun. Using a latitudinal average ozone profile does introduce errors, in particular to the calculations of Chappuis Band absorption of visible radiation. This is discussed later.

The radiation having passed through an amount of gas u(z,E), its intensity at a wavelength λ will have been reduced to

$$I(\lambda,z,E) = I_o(\lambda) \exp(-\kappa_G(\lambda)\, u(z,E)) \qquad (4.40)$$

where $I_o(\lambda)$ is the intensity at the top of the atmosphere and $\kappa_G(\lambda)$ is the absorption coefficient. Following Lindzen and Will (1973), κ_G is assumed to be independent of temperature and pressure.

Knowing the intensity of radiation at a particular height, the heating can then be evaluated thus:

$$Q(z,E) = \rho_G(z) \int_\lambda \kappa_G(\lambda) I(\lambda,z,E)\, d\lambda \qquad (4.41a)$$

where the integration is over all wavelengths that contribute significantly to the heating. These equations (4.39 to 4.41a) obviously only apply when the Sun is above the horizon ($E > 0$). At night

$$Q(z,E) = 0 \qquad \text{and} \qquad E < 0 \qquad (4.41b)$$

Q is the total heating per unit volume per unit time, while J (Equation 4.28) was heating per unit mass per unit time. So

$$J(z,E) = \frac{Q(z,E)}{\rho(z)} \tag{4.42}$$

where the density of air, $\rho(z)$, is assumed to depend only on height.

To evaluate the forcing of a given mode, J(z,E) needs to be decomposed into separate components, $\hat{J}_n^{\sigma,s}(z)\Theta_n^{\sigma,s}(\theta)e^{i(\sigma t+s\phi)}$. Because of the approximations made above, the only components calculated here are those which depend on local time, $H = \omega t + \phi$, and are otherwise independent of time and longitude. These are the components that are fixed relative to the Sun as $\sigma'(\equiv \sigma/\omega) = s$. With ρ_G and ρ independent of time, Q depends on H only through sin E. Defining H = 0 at local noon, $J(z,E) \equiv J(z,H,\theta,\text{time of year})$ is symmetric in H and so all the sin $\sigma' H$ terms are zero. Hence

$$J(z,E) = \sum_{n=0}^{\infty}\sum_{\sigma'=0}^{\infty} \hat{J}_n^{\sigma',\sigma'}(z)\,\Theta_n^{\sigma',\sigma'}(\theta)\cos\sigma' H \tag{4.43}$$

The case considered here is that of the equinox so Equation 4.15 simplifies to

$$\sin E = \cos\theta\cos H \tag{4.44}$$

and E > 0 if and only if $|H| < \frac{\pi}{2}$. J in this case is also symmetrical about the equator, and

$$\hat{J}_n^{\sigma',\sigma'}(z) = \frac{4}{\pi}\int_{H=0}^{\pi/2}\int_{\theta=0}^{\pi/2} J(z,E)\,\Theta_n^{\sigma',\sigma'}(\theta)\cos\sigma' H\, d\theta\, dH \tag{4.45}$$

Using Equations 4.40 to 4.45, $\hat{J}_n^{\sigma',\sigma'}(z)$ can be evaluated. This was first done for ozone forcing by Butler and Small (1963) using

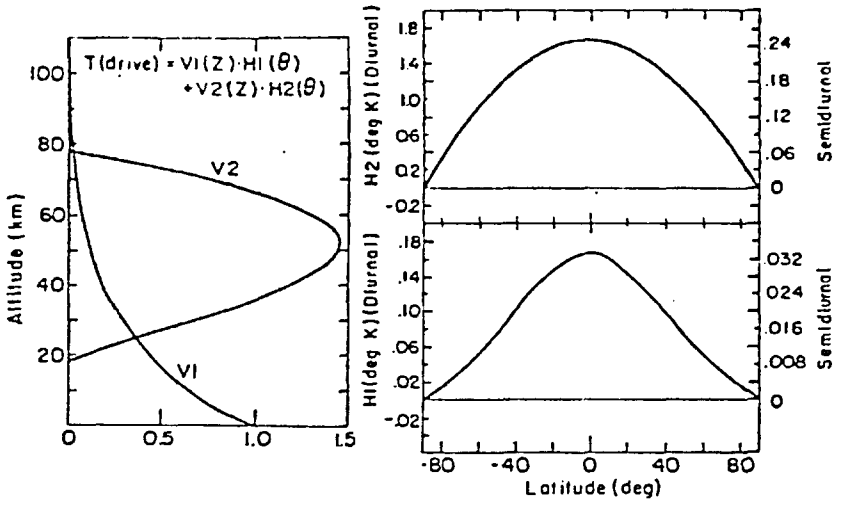

Figure 4.9 Distribution of the tidal excitation. (a)-left- due to Chapman (1968). V1 is due to H_2O, V2 to O_3. Similarly H1 and H2.

(b)-below- due to Forbes and Garrett (1978), decomposed into Hough function components.

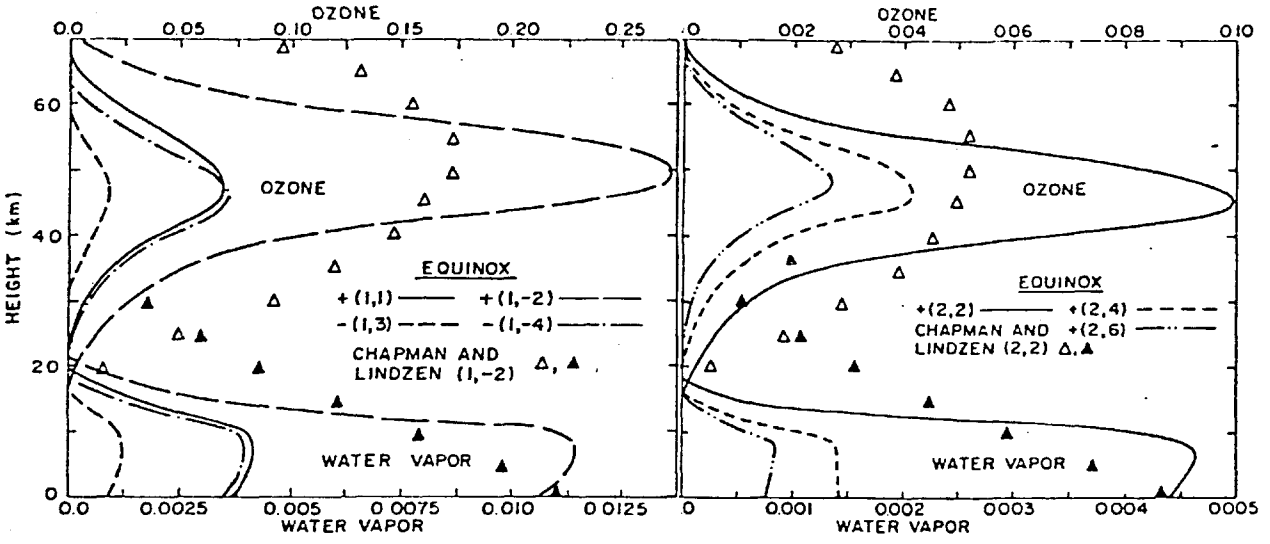

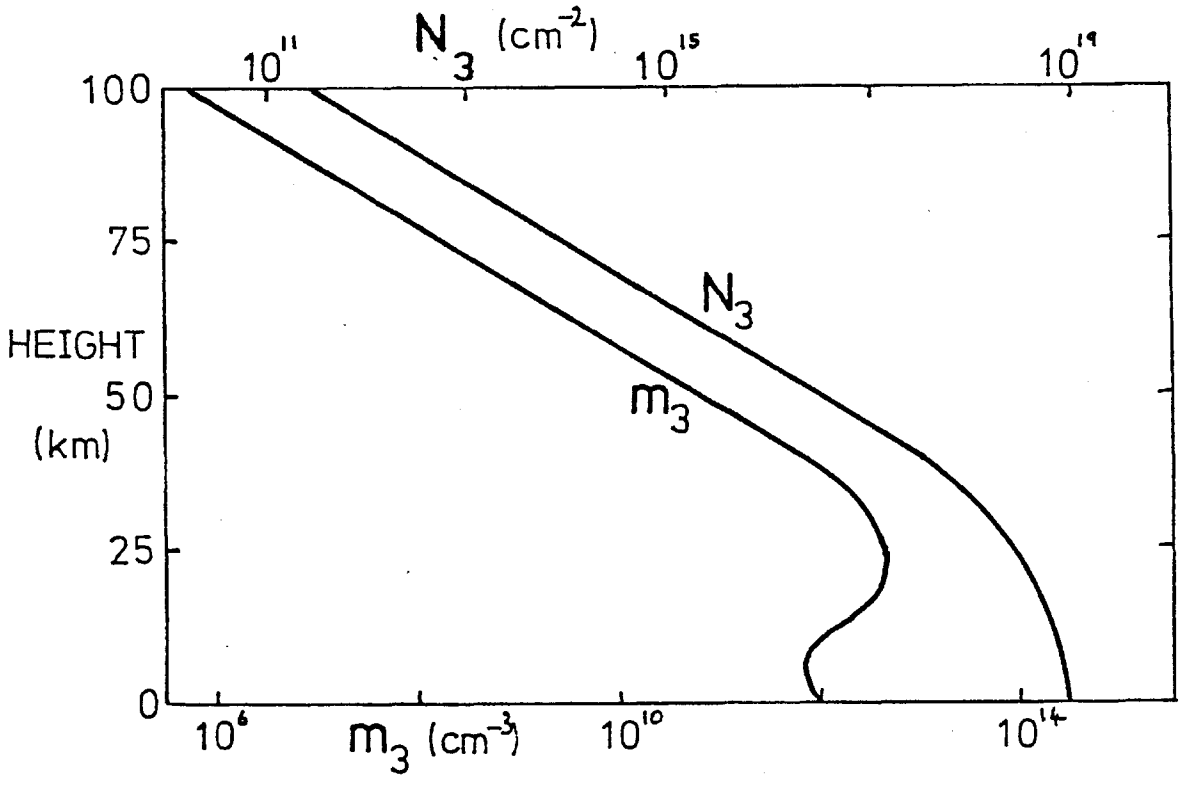

Figure 4.10 Vertical distribution of Ozone concentration(m_3) and total ozone column density (N_3) used in the calculations here.

the method just described. The next calculation (by Lindzen 1967, 1968, and used by Chapman and Lindzen, 1970) was based on values of J(z) obtained by Leovy (1964), who calculated the diurnal temperature range in the stratosphere and mesosphere. Lindzen (1968) assumed that the excitation of the semi-diurnal oscillation has the same altitude and latitude distribution as that of the diurnal oscillation (shown in Figure 4.9a) and that the forcing of every mode had the same vertical structure. The results of Forbes and Garrett (1978) show that these assumptions are wrong, as can be seen from Figure 4.9b.

In their calculations, Forbes and Garrett (1978) evaluated J(z,E) using a parameterisation of ozone heating first suggested by Lindzen and Will (1973), and given in a refined form by Schoeberl and Strobel (1978a). This parameterisation is

Chappuis Band (5000 - 7000Å)
$$Q_{CH} = m_3' \times 1.05 \times 10^{-16} \exp(-2.85 \times 10^{-21} N_3') \qquad (4.46a)$$

Huggins Band (3000 - 3500Å)
$$Q_{HU} = \frac{m_3'}{N_3'} \times [446 - 78 \exp(-1.77 \times 10^{-19} N_3') - 388 \exp(-4.22 \times 10^{-19} N_3')] \qquad (4.46b)$$

Hartley Band (2000 - 3000Å)
$$Q_{HA} = m_3' \times 4.8 \times 10^{-15} \exp(-8.8 \times 10^{-18} N_3') \qquad (4.46c)$$

Hertzberg Continuum (2060 - 2425Å)
$$Q_{HZ} = m_3' \times 7.35 \times 10^{-16} \exp(-4.9 \times 10^{-18} N_3') \qquad (4.46d)$$

where $m_3'(z)$ is the local number density of ozone (cm^{-3}), and $N_3'(z)$ is the slant path column density of ozone (cm^{-2}). Forbes and Garrett adopted a single ozone profile (independent of θ), the mid-latitude model of the US Standard Atmosphere (1976). For the new results presented here the ozone profile is from Nicolet (1975)

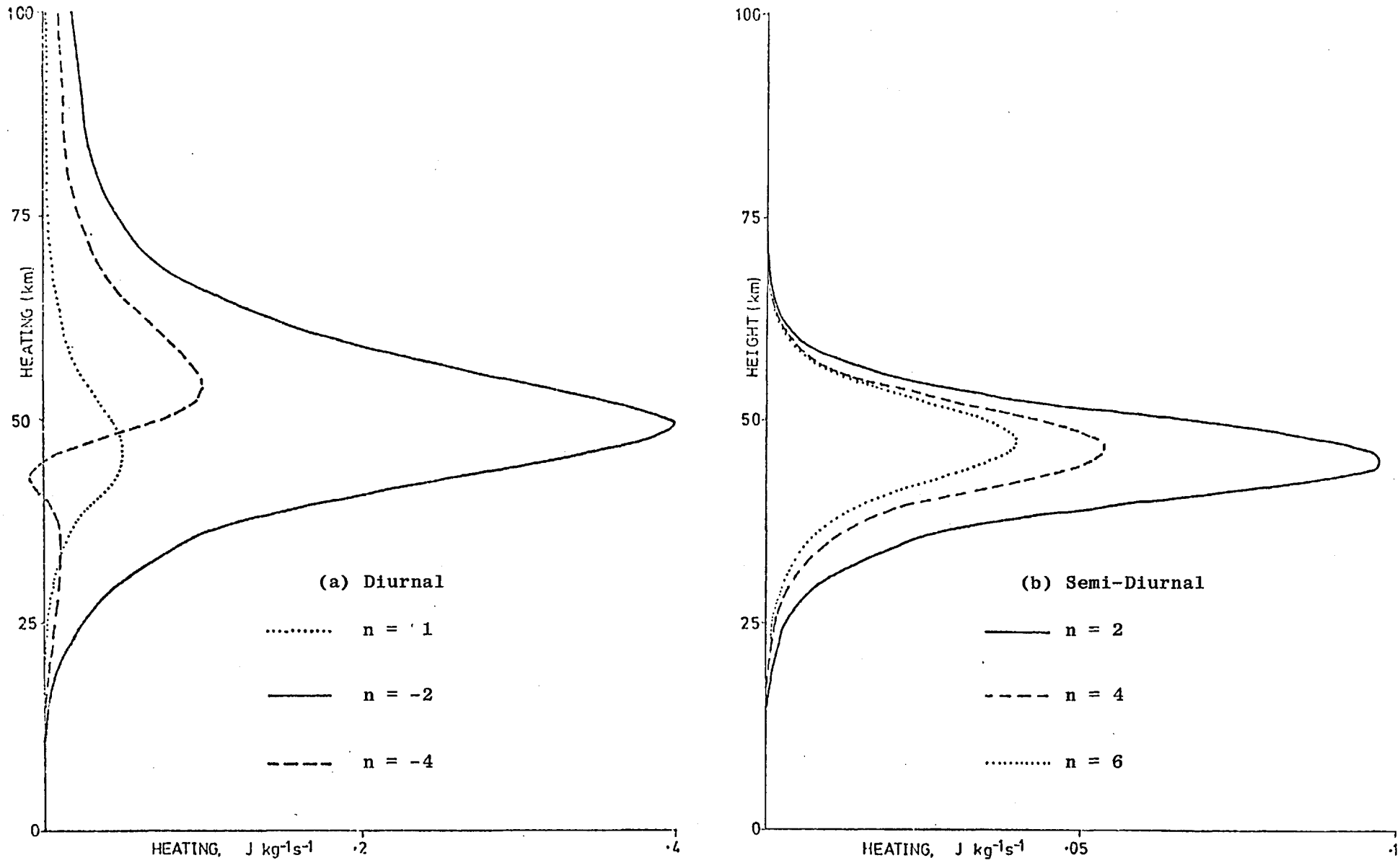

Figure 4.11 Forcing of the principal diurnal (a) and semi-diurnal(b) tides due to ozone absorption.

for heights up to 50 km while above this it is assumed to decay exponentially with height. The profiles of m_3 and N_3 (overhead Sun) are plotted on Figure 4.10.

From Equations 4.46a - d, the Q's can be evaluated, and hence the thermotidal heating,

$$J(z,\Theta,H) = (Q_{CH} + Q_{HL} + Q_{HA} + Q_{HZ}) / \rho(z) \qquad (4.47)$$

From this formula, $\hat{J}_n^{\sigma',\sigma'}(z)$ can be found by Equation 4.45. In that Equation the integrals can be approximated by sums, so

$$\hat{J}_n^{\sigma',\sigma'}(z) = \frac{4}{\pi} \sum_{i=1}^{k} \sum_{j=1}^{l} J(z,\Theta_i,H_j)\, \Theta_n^{\sigma',\sigma'}(\Theta)\, \cos(\sigma' H_j)\, w_i^{\Theta} w_j^{H} \qquad (4.48)$$

Figure 4.11 is plotted using Equations 4.46 to 4.48. The values (Θ_i, H_j) and weights (w_i^{Θ}, w_j^{H}) used were calculated as follows:

(a) Both summations in 4.48 were evaluated over 10 steps, so $k = l = 10$. For the accuracy needed here this number of points was sufficient, for with $k = 10, l = 20$ the results were changed by less than 0.1%.

(b) The times, H_j, were equally spaced so

$$H_j = \frac{\pi}{20}(j - \tfrac{1}{2}) \quad ; \quad w_j^{H} = \frac{\pi}{10} \qquad (4.49)$$

(c) The latitudes, Θ_i, were taken from Abramowitz and Stegun (1965, p. 916, Table 25.4, $n = 20$). The values they give are for Gaussian integration,

$$\int_{-1}^{1} f(x)\, dx \simeq \sum_{i=1}^{n} w_i\, f(x_i) \qquad (4.50)$$

Comparing the left hand side of this with 4.45 leads to

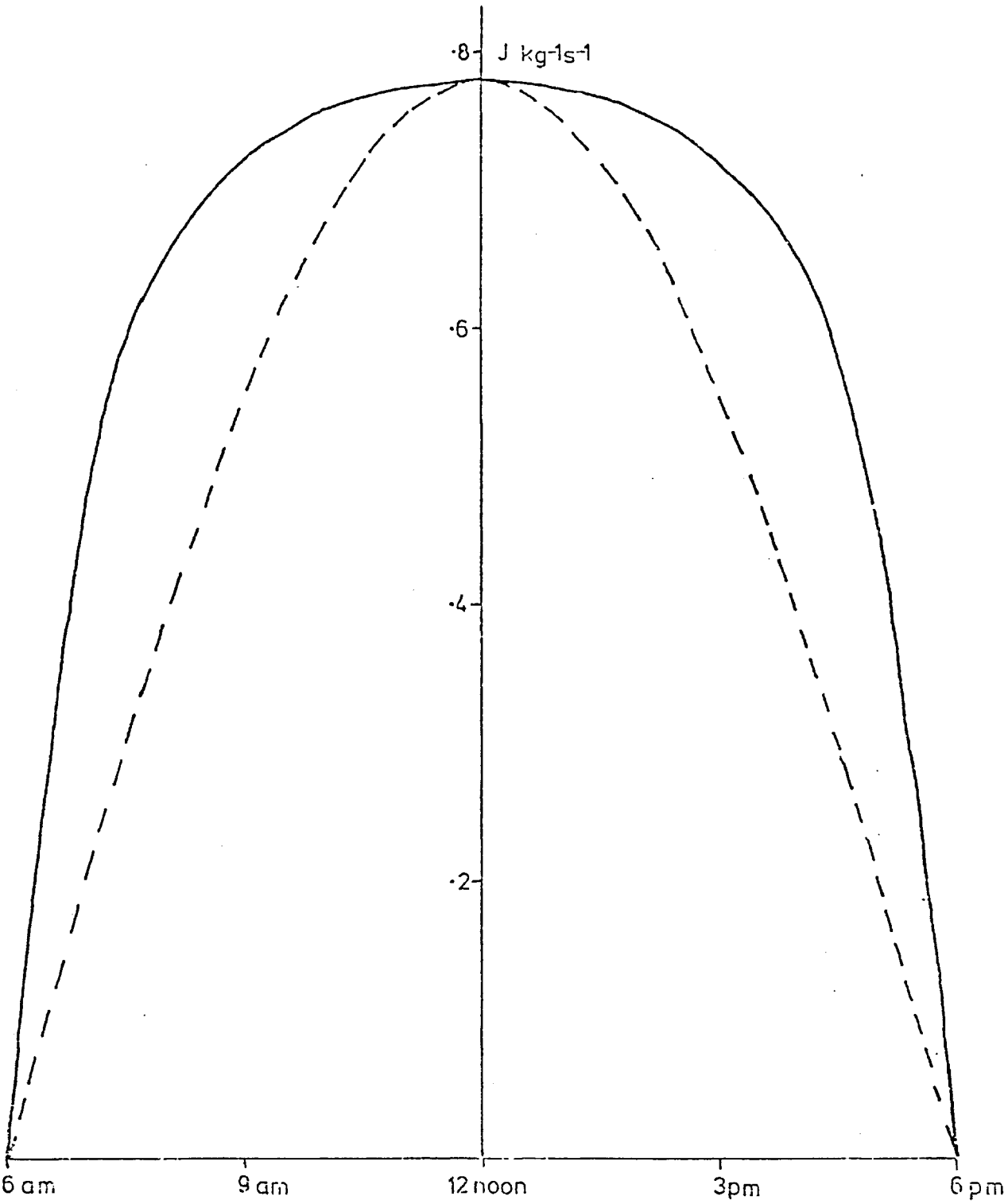

Figure 4.12 Calculated diurnal variation of heating at 50 km, 4.4° latitude (solid line) compared to the cosine profile assumed in the simple model of Section 4.3 (dashed line).

$$\int_0^{\pi/2} g(\sin\theta)\,d\theta \simeq \sum_{i=1}^{n/2} \frac{w_i}{\cos\theta_i}\, g(\sin\theta_i) \qquad (4.51)$$

where $\theta_i = \sin^{-1}(x_i)$. So the weights, w_i^{θ}, given by Abramowitz and Stegun are divided by $\cos\theta_i$. This leads to θ_i and w_i^{θ} having values very similar to H_j and w_j^{H}.

It is of interest here to see how $J(z,\theta,H)$ and $J'_{\sigma}(z,\theta) = \sum_{j=1}^{10} J(z,\theta,H_j)\cos(\sigma' H_j) w_j^{H}$ vary with latitude and time. Figure 4.12 illustrates how the heating varies during the day time (it is zero at night) at 50 km altitude and 4.4° latitude (the smallest value of θ_i). For comparison a cosine function with the same magnitude at noon is also plotted (cf theory of Section 4.3) and it can be seen that the actual heating has a much squarer profile than the cosine. This is because the heating due to atmospheric absorption depends on solar elevation only via the optical depth ($N_3' = N_3/\sin E$). The sin E factor, as in the simple theory due to the area the solar beam covers, is cancelled by the fact that it passes through a length of 1/sin E in crossing a unit depth. Hence the diurnal variation of heating is closer to a step function (constant for $|H| \leq \frac{\pi}{2}$, zero otherwise), then a cosine function. Because of this the diurnal component of the heating is larger (by about 16%) than that obtained using the simple model while the semi-diurnal component is only $\frac{2}{3}$ of the value obtained there. So quantitatively the simple model is inaccurate, but its results are useful qualitatively.

The latitudinal variation of the thermotidal forcing is illustrated by Figure 4.13. It is clear that, though there are similarities between the two components there are also large

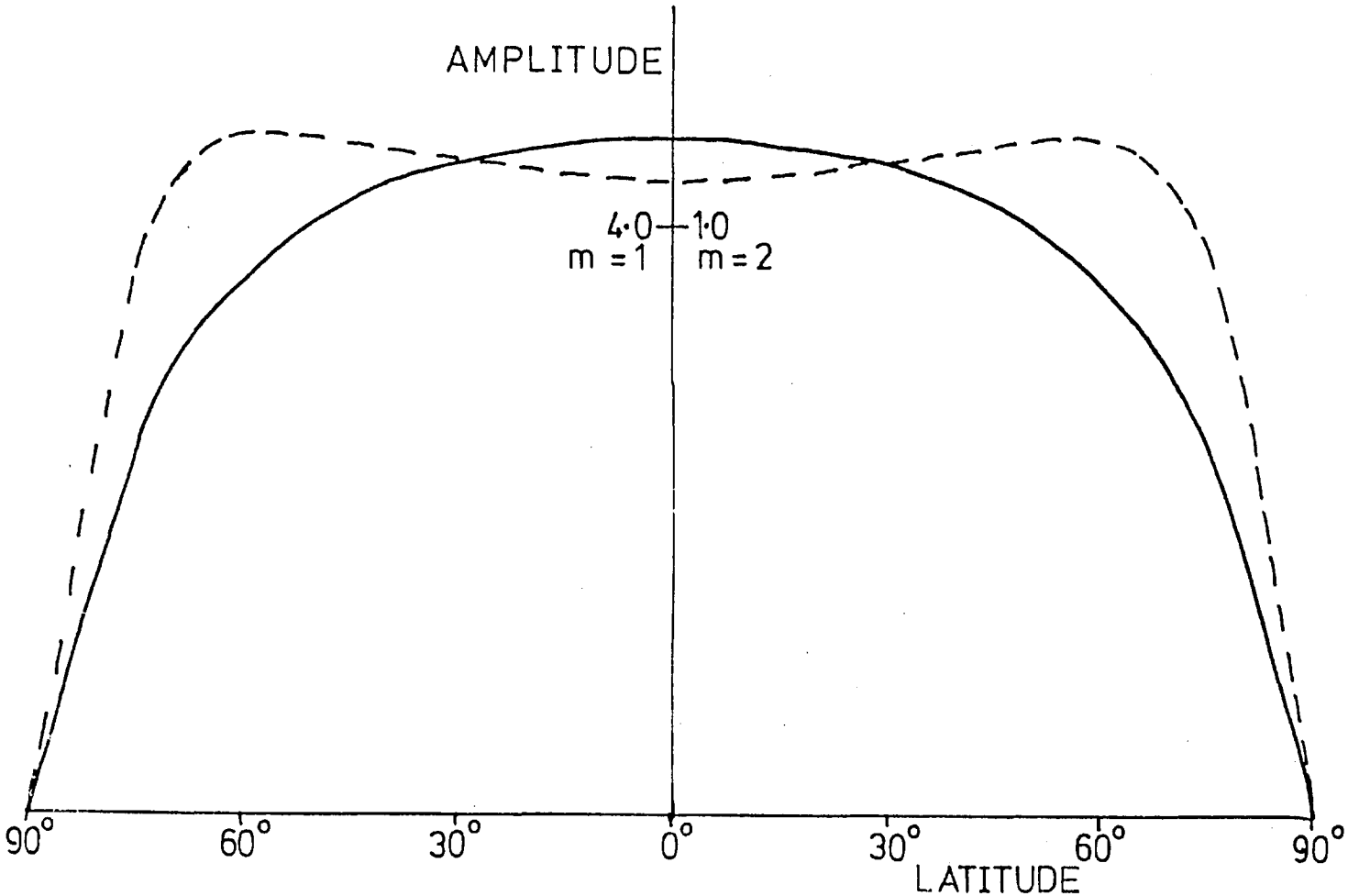

Figure 4.13 Latitudinal variation of the diurnal (solid line) and semi-diurnal (dashed line) heating due to ozone absorption of UV at 50 km.

σ, n	CL	FG	Here
1,1	0.39	0.26	0.12
1,-2	1.00	1.00	1.00
1,-4	0.35	0.27	0.25
2,2	1.00	1.00	1.00
2,4	0.26	0.42	0.55
2,6	0.15	0.27	0.41

Table 4.2 Normalised maximum amplitudes of the thermotidal forcings calculated by Chapman and Lindzen, 1970 (CL), Forbes and Garrett, 1978 (FG) and here. The normalisation is such that the maximum amplitudes are 1.0.

differences, contrary to the assumption of Lindzen (1968). Using Lindzen's model, Chapman and Lindzen (1970) noted that the ($\sigma' = 2$, $n = 2$) mode dominated the higher order semi-diurnal modes because its latitudinal variation was similar to that of the heating function. The results in Figure 4.13 show a different pattern, the forcing of the semi-diurnal tide (dashed line) being almost constant between $\pm 65^{o}$. Because of this the higher order modes are relatively larger than those obtained by Chapman and Lindzen, as can be seen in Table 4.2. These results agree with those of Forbes and Garrett (1978), also listed in Table 4.2. The diurnal forcing (solid line in Figure 4.13) shows a similar latitudinal variation to that given by Chapman and Lindzen (1970) and this manifests itself in the results of Table 4.2, though there still are significant differences between the relative amplitudes.

Later in this chapter the effect of solar variability on the tides will be considered. There are two, related, processes by which changes in UV may affect the heating in the ozone layer and hence the tides. The direct result of the Sun emitting more UV is that more will be absorbed. But this extra absorption will affect the radiative-chemical balance of the upper atmosphere resulting in changes in the ozone distribution, as calculated by Callis and Nealy (1978) and Penner and Chang (1978).

Changes in UV alter the radiation available for absorption by ozone in the Hartley and Huggins Bands and the Hertzberg Continuum. It is, therefore, of interest to know whether Chappuis Band absorption is important in thermotidal forcing. Hence the heating rate for a zenith Sun has been decomposed into the four heating

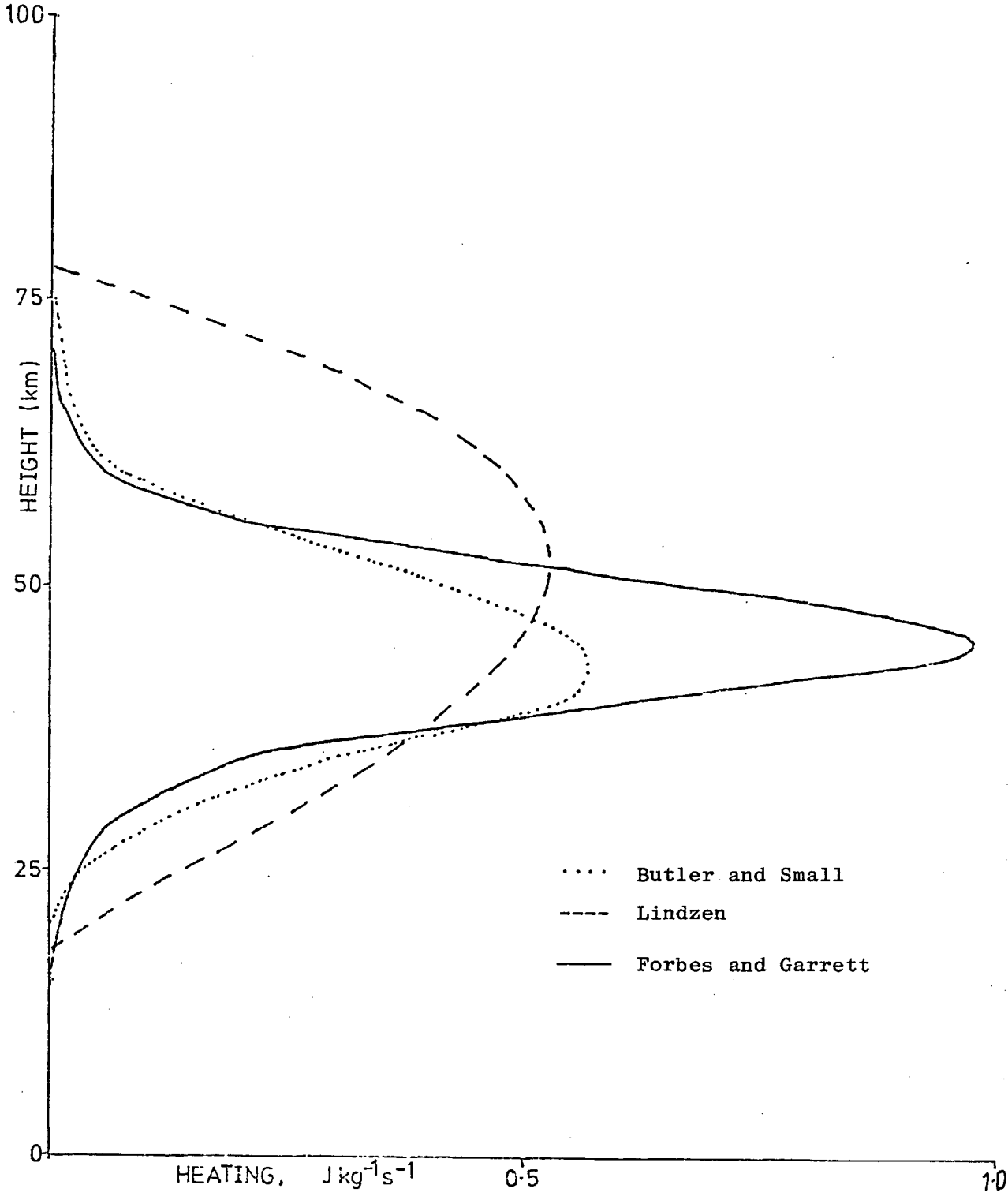

Figure 4.14 Comparison of the heating profiles of Butler and Small(1963), Lindzen (1968) and Forbes and Garrett (1978).

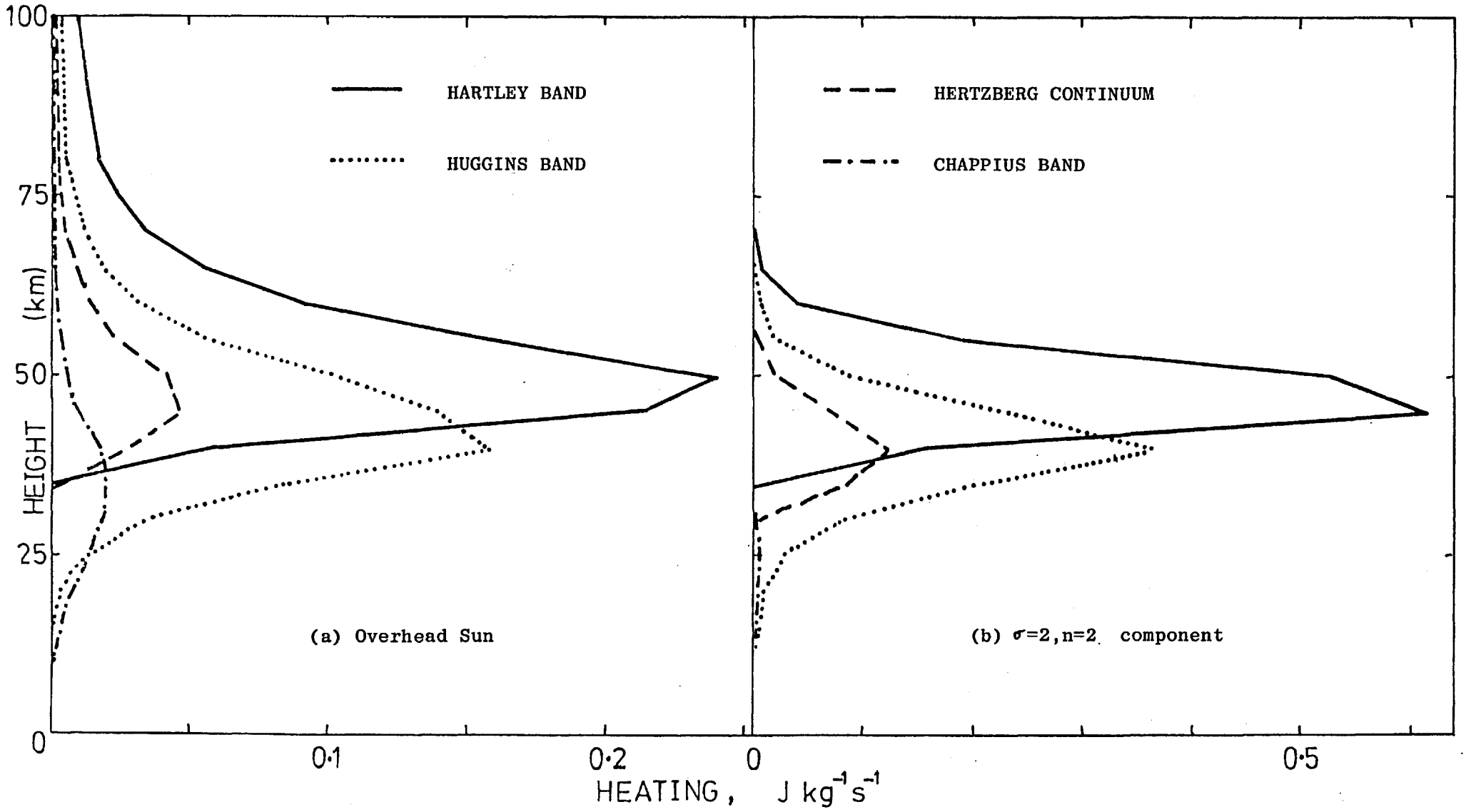

Figure 4.15 Vertical distribution of the thermotidal heating decomposed into the constituent heating components.

bands of Equation 4.46 (Q_{CH}, Q_{HU}, Q_{HA}, and Q_{HZ}).

Figure 4.15a shows that heating due to the Hertzberg continuum is always dominated by that in either the Hartley (high altitudes) or the Huggins Band (below 45 km). From this diagram it would seem that below 30 km Chappuis Band absorption would significantly contribute towards thermotidal forcing. However, as it is proportional to m_3/ρ and both m_3 and ρ were assumed independent of latitude, it is almost independent of latitude and so contributes insignificantly to the calculated tides. This can be seen in Figure 4.15b which illustrates the absorption bands' contributions to the thermotidal forcing of the ($\sigma' = 2$, $n = 2$) mode. For the same reason the tidal forcing above 65 km is negligible, for there, absorption is almost independent of latitude. With Chappius Band absorption unimportant, the thermotidal forcing by ozone is due only to absorption of UV.

As was mentioned at the start of this Section, the only other significant forcing of atmospheric tides is by tropospheric water vapour absorbing visible radiation. This has been evaluated, first by Siebert (1961) and more recently by Forbes and Garrett (1978). It is assumed here that this forcing is unaffected by solar variability, for the solar constant varies by less than 1% over the solar cycle while, it is claimed, UV varies by up to 20% (see Section 1.4.3.). The water vapour content of the atmosphere at any location is highly variable and no solar cycle effect has, as yet, been distinguished from this background noise. As the thermotidal forcing due to water vapour is assumed constant the results of Forbes and Garrett (1978) will be used here.

4.4.6. Results for Mean Conditions

For each mode (σ',n), J(z) and h are known and so y(x) may be evaluated by integrating the Vertical Structure Equation (4.35) with the appropriate boundary conditions. The pressure perturbation, δp, can be evaluated from y(x) using

$$\delta p(x) = \frac{P_0(0)\gamma h}{H(x) i\sigma} e^{-x/2} \left(\frac{dy(x)}{dx} - \frac{y(x)}{2} \right) \qquad (4.52)$$

By evaluating the main modes of frequency σ', the global distribution of the pressure anomaly can be derived from

$$\Delta p^{\sigma'}(x,\theta) = \sum_n \delta p_n^{\sigma'}(z)\, \Theta_n^{\sigma',\sigma'}(\theta) \qquad (4.53)$$

For an isothermal atmosphere δp can be evaluated analytically, as the Vertical Structure Equation can be directly integrated. Below the forcing

$$y(x) = \frac{(\cos \nu x - \frac{\alpha}{\nu} \sin \nu x)}{(\alpha + i\nu)} \frac{\pi}{\gamma g h} \int J(x_0) e^{(i\nu - \frac{1}{2})x_0} dx_0 \qquad (4.54)$$

where $\nu^2 = \frac{\pi H}{h} - \frac{1}{4}$, $\alpha = \frac{H}{h} - \frac{1}{2}$ and the integral is over those heights where ozone forcing is important.

The surface pressure oscillation is

$$\delta p(0) = \frac{P_0(0)}{H^2} \frac{i\pi}{g\sigma} \frac{(\alpha + 1/2)}{(\alpha + i\nu)} \int J(z) e^{(i\nu - \frac{1}{2})z/H} dz \qquad (4.55)$$

(cf Equation A.12) where z(= xH) has been substituted in the integral.

Note that both ν and J depend on the mode being considered. In the case of the ($\sigma = 2$,n = 2) mode, as ν is very close to zero the forcing has similar phases at all altitudes and so contributions from all heights add together. In contrast to this, the (1,1) mode has a vertical wavelength (28 km) so small that forcing over depths

σ',n	OZONE Amp	OZONE Phase	WATER VAPOUR Amp	WATER VAPOUR Phase	TOTAL Amp	TOTAL Phase	RATIO
1,1	.077	1731	.165	0155	.135	0004	.47
1,-2	.045	0600	.160	0600	.205	0600	.28
1,-4	.004	0600	.081	1800	.077	1800	.05
2,2	.584	0757	.268	0925	.798	0824	2.18
2,4	.111	0003	.042	0825	.105	1119	2.66
2,6	.042	0524	.019	0735	.053	0602	2.23

Table 4.3 Amplitudes (mb) and Phases (time of maximum) of the main tidal components, evaluated by the analytic solution of the vertical structure equation for the case of an isothermal atmosphere. The column on the far right is the ratio of the ozone to the water vapour forced components.

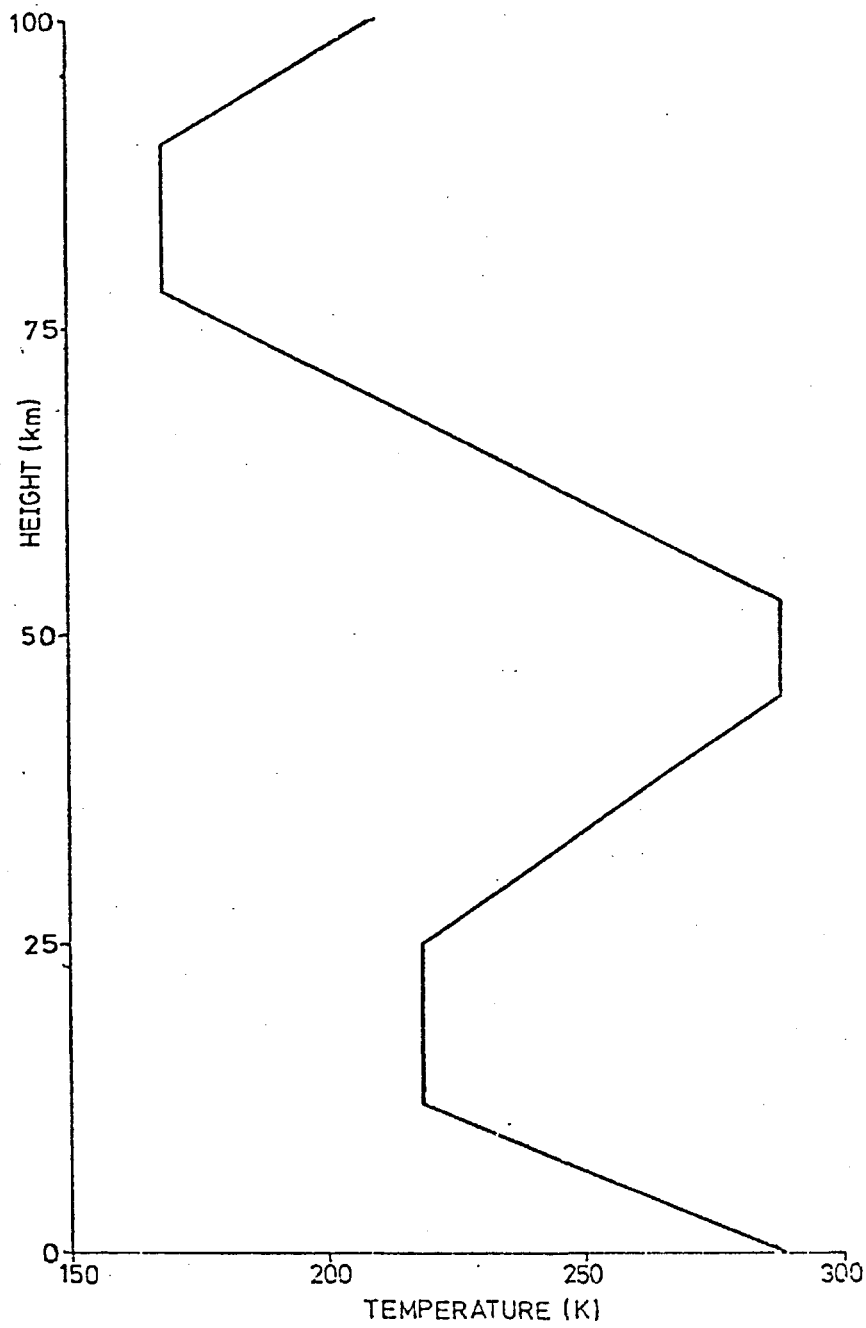

Figure 4.16 Temperature profile used in the model.

comparable with that of the ozone forcing will partially cancel.

The surface pressure perturbation, as given by this analytic solution, can be evaluated using the values of $J_n(z)$ shown in Figure 4.11. The integral in 4.55 is converted into a sum:

$$\int J(z) e^{(i\nu - \frac{1}{2})\frac{z}{H}} dz \doteq \sum_{j=1}^{l} J(z_j) e^{(i\nu - \frac{1}{2})\frac{z_j}{H}} w_j \qquad (4.56)$$

The values of z_j (and hence w_j) chosen so that this solution was directly comparable with the computational solution of the Vertical Structure Equation (4.35), where

$$z_j = \frac{17}{l} H (j-2) \quad ; \quad w_j = z_{j+1} - z_j = \frac{17H}{l} \qquad (4.57)$$

J was evaluated at 5 km intervals and linearly interpolated in between. When $l = 300$ the integration (4.56) is accurate to 0.01% in amplitude and 0.05° in phase. This precision is greater than that obtained by computational solution of the Vertical Structure Equation, hence $l = 300$ (corresponding to $w_j = 431$ metres) was used for all the analytic solutions.

The tides at the ground, for ozone and water vapour heating (individually and together), are given in Table 4.3. These solutions are for an isothermal atmosphere, but the atmospheric temperature varies greatly with height. The temperature profile used in the computational solutions, illustrated in Figure 4.16, is such that it is possible to solve the Vertical Structure Equation analytically, as was done by Pekeris (1937). (See Appendix Section A.2.3). However, it is much simpler to solve the Vertical Structure Equation computationally. The method for so doing is given in Section A.3 of the Appendix. The lower atmosphere, in this case

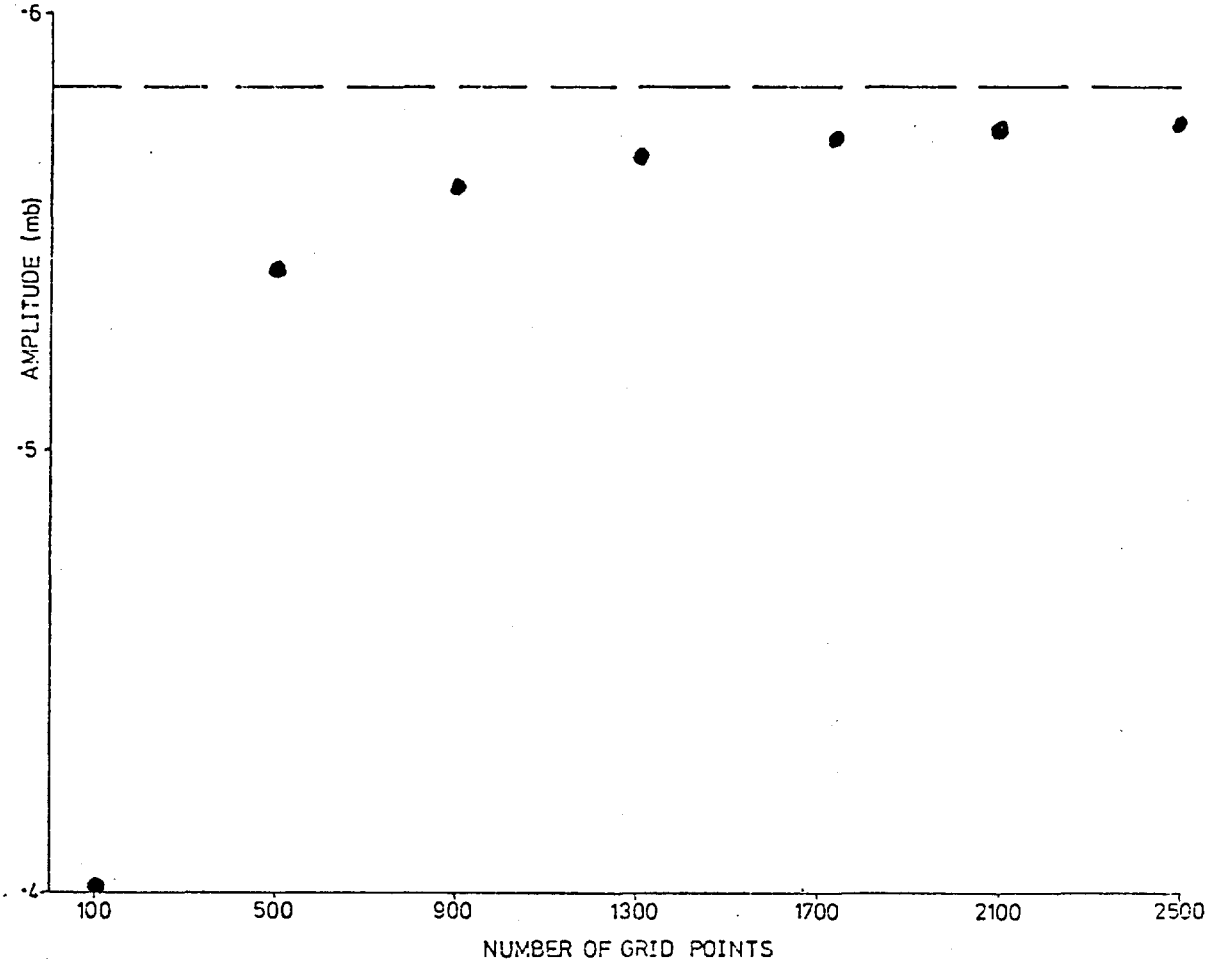

Figure 4.17 Variation of the computed surface amplitude of the (2,2) mode in an isothermal atmosphere (T=260 K) with the number of grid points. The dashed line is the value of the analytic solution.

			MODE			
σ', n	1,1	1,-2	1,-4	2,2	2,4	2,6
O_3	2.38	3.50	5.26	2.37	2.38	2.39
H_2O	3.58	8.53	9.37	4.66	4.84	4.37

Table 4.4 Percentage underestimation of computational solutions, with N = 1600, compared to analytic results.

	OZONE	WATER VAPOUR	TOTAL	RATIO
σ', n	Amp Phase	Amp Phase	Amp Phase	
1,1	.019 1351	.151 0304	.128 0437	.13
1,-2	.036 0600	.170 0600	.191 0600	.23
1,-4	.005 0600	.087 1800	.082 1800	.06
2,2	.598 0858	.272 0901	.856 0859	2.15
2,4	.020 1053	.035 0849	.047 0931	.55
2,6	.016 0404	.013 0813	.014 0550	1.19

Table 4.5 Same as table 4.3, but for computational solution for the realistic temperature profile (figure 4.16).

the bottom 17 scale heights, is split into N intervals of equal thickness in log-pressure co-ordinates, $dx = 17/N$.

It was suggested by Chapman and Lindzen (1970) that if the grid points (in the computational solution of the Vertical Structure Equation) are separated by 1% of the minimum wavelength then the amplitude evaluated will be within 1% of the actual solution. However, that was not found to be so here. Figure 4.17 shows the surface pressure amplitude plotted against N for the case of an isothermal atmosphere, with $T = 260^{o}K$ (so that $h_2^{2,2} = 292$ km). The above condition implies that only $N = 44$ points (of width ~ 3 km) are needed to obtain solution accurate to 1%, while the graph implies about 3,500 points (of width 36 metres) are needed. Increasing the number of points increases the energy input, but this is only a 0.05% increase in the energy. The calculation of values at the boundaries also introduces numerical errors, but as the expression for the boundary conditions given by Chapman and Lindzen are also employed here, they cannot be the cause of the difference between the predicted $N = 44$ and the calculated $N = 3,500$. This dichotomy is unresolved.

For the numerical integrations a value of $N = 1,600$ was chosen. This leads to the actual solutions being underestimated by between 2 and 9%. The error is larger for those modes which have an imaginary vertical wavenumber, ($\sigma' = 1$, n negative), and also larger for water vapour than for ozone forcing. It is assumed that there are similar errors in the solutions when the realistic temperature profile is used, and correcting multiplicative factors are introduced (so for the 1,1 mode the ozone forced amplitude is multiplied by 1.0238).

There are two main reasons why a change in the temperature profile affects the results. Firstly, when the temperature is changed so is the density and hence the total energy absorbed, $E = \int \rho J dz$, is as well. Secondly, the vertical wavelengths will be changed and hence the interplay between components forced at different levels altered. Changes in vertical wavelengths will also affect the vertical structure of the tides. The mode of primary concern here (2,2) is virtually unaffected, hence it seems to be insensitive to alterations in temperature. The water vapour forced components are only slightly affected by changes in the temperature profile as the forcing is localised. However, some of the ozone forced components (1,1; 2,4; 2,6) are radically reduced. This reinforces the pre-eminence of the (2,2) mode amongst the semi-diurnal components. Also, the phases of the tides are altered by changing the vertical temperature profile.

The results of Table 4.5 qualitatively agree with the observations (Haurwitz and Cowley, 1973) and with previous theoretical calculation (Walterscheid et al., 1980), but there are significant quantitative differences. Compared to the observations (Table 4.1) all the amplitudes are underestimated. Walterscheid et al. show that the effect of zonal winds is to increase the tides, so the model described above, which neglects winds, will underestimate the tides.

While the model is not perfect, it is adequate for the present needs, which are to consider the effect of solar variability on the tides.

4.5. The Tidal Response to the Sunspot Cycle

4.5.1. Theoretical

The results presented here are obtained by altering the heating profile and so simulating the effect of Ultra-Violet variability. Two basic models were used, one keeping the ozone distribution constant while UV changes, and the other with both varying. The same temperature profile (Figure 4.16) was used throughout, though Callis and Nealy (1978) and Penner and Chang (1978) predict a temperature oscillation of up to $\pm 8^{\circ}C$ (at 45 km) in response to the UV variations. This temperature change, with no alteration in the heating profile, was later found to significantly affect two modes, ($\sigma' = 1$, $n = 1$; and 2,2), which are 30% and 25% larger respectively using the temperature profile for the increased UV than for decreased. This accentuates the discrepancy between the theoretical and the observed changes in the semi-diurnal tide.

The observations of Heath and Thekaekara (1977) shown in Figure 1.9. imply the solar radiation changes by less than 20% above 3000Å over the sunspot cycle, but also that it changes by much more than 20% below 2500Å. The value of 20% is taken as representative, but, for the reasons just given, variations in Huggins Band absorption are overestimated while those in the more significant Hartley Band are underestimated.

The simplest case to consider is when the ozone density is unaltered by the UV variation. This leads to the heating being increased by 10% above 50 km (where Chappuis Band absorption contributes negligibly towards the heating) when the UV radiation (wavelengths less than 3500Å) is increased by 10%. The size of the

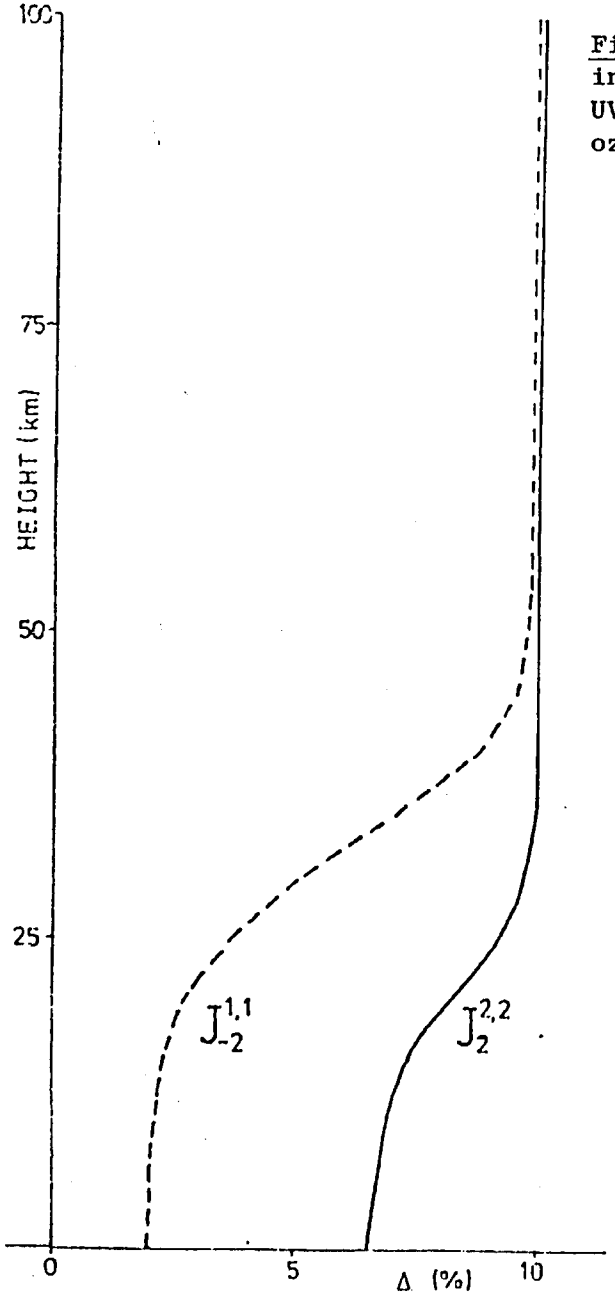

Figure 4.18 Percentage increase in the thermotidal forcing when UV is increased by 10% with the ozone concentration constant.

Figure 4.19 Changes in the ozone concentration, due to UV changes, evaluated by Callis and Nealy(1978) and Penner and Chang(1978). The dotted line is the estimated effect in the mesosphere used here. (The changes were only evaluated up to a height of about 50 km).

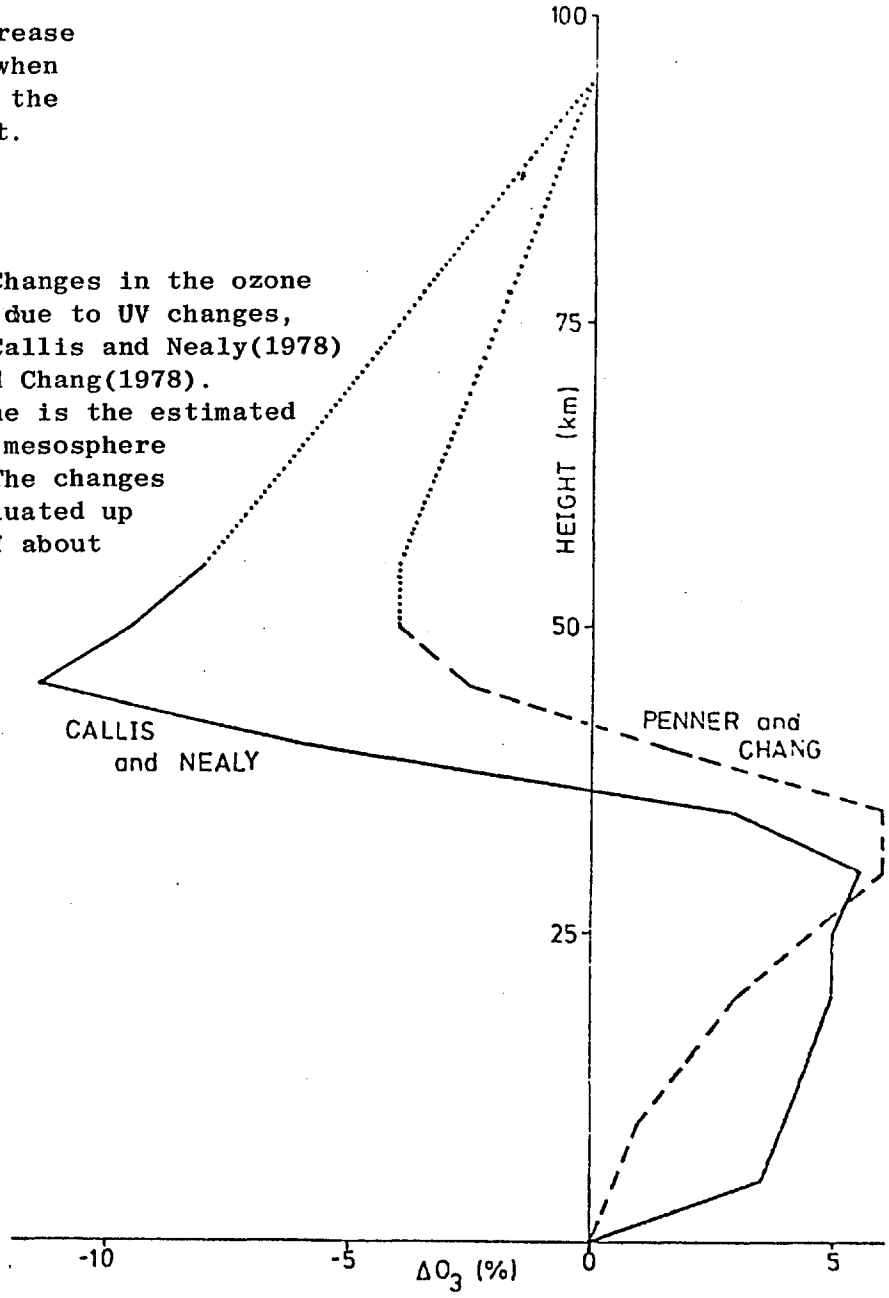

response decreases as the relative importance of Chappuis Band absorption increases. This more noticeably affects the (1,-2) than the (2,2) mode, as can be seen on Figure 4.18. (The heating profiles in this case of increased UV are referred to as P2, while those for average conditions are P1.)

Four further heating profiles were generated, using altered ozone density profiles, to calculate the heating with the Ultra-Violet changed by ± 10% from average. Profiles P3 and P5 use the ozone profile alterations calculated by Callis and Nealy (1978), profiles P4 and P6 those of Penner and Chang (1978). As both sets of results were for the change between sunspot minimum and sunspot maximum, they are divided by 2 to give the change between mean conditions and sunspot maximum. Figure 4.19 shows the evaluated ozone changes. The Callis and Nealy model only went up to 55 km, while that of Penner and Chang went to 50 km. Above these levels values have been estimated by assuming no variation at 95 km, a linear decrease in change between 55 km and 95 km, and, for the Penner and Chang profile, the change being the same at 55 km as at 50 km. The changes in column ozone (N_3) were evaluated by assuming that the total ozone in any 5 km interval (values were taken at 0,5,...100 km) is proportional to the mean of the ozone densities at the top and the bottom. The constant of proportionality at any height can be evaluated from the mean profiles of ozone density and column ozone.

Profiles P3 and P4 are obtained for sunspot maximum conditions, with the UV intensity increased by 10%, while P5 and P6 are for sunspot minimum (UV decreased by 10%). The heating profiles thus

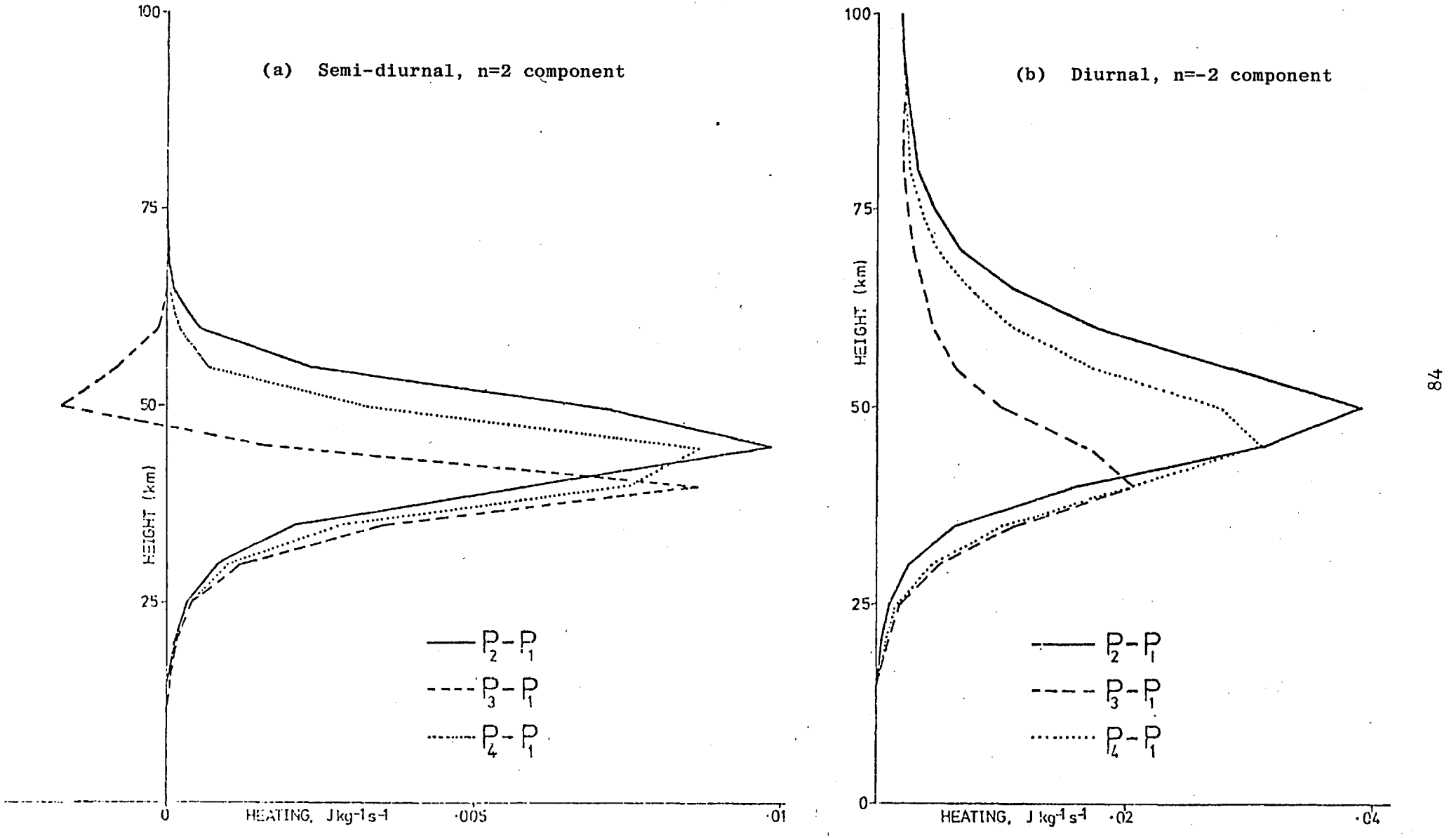

Figure 4.20 Changes in thermotidal forcing due to a 10% change in UV. P2, P3 and P4 refer to different ozone changes, as described in the text.

	P2		P3		P4		P5		P6	
σ,n	Amp	Pha	Amp	Pha	Amp	Pha	Amp	Pha	Amp	Pha
1,1	-0.67	-3.4	8.25	-1.4	3.34	-3.4	-5.86	2.5	-2.05	3.6
1,-2	1.22	0	1.70	0	1.61	0	-1.68	0	-1.64	0
1,-4	0	0	0.09	0	0.07	0	-0.16	0	-0.09	0
2,2	6.99	-0.9	5.37	-0.3	6.94	-0.8	-5.79	0.5	-6.97	0.9
2,4	10.32	2.1	5.06	4.8	9.11	3.4	-5.54	-4.7	-8.68	-3.9
2,6	7.76	-1.4	6.15	3.5	8.37	0.8	-6.58	-2.6	-8.17	-0.3

Table 4.8 Changes in the amplitude (percent) and the phase (degrees) of the tides due to changing the heating profile from P1 (mean conditions) to Pi (sunspot maximum or minimum). Analytic solution for an isothermal atmosphere.

	P2		P3		P4		P5		P6	
σ,n	Amp	Pha	Amp	Pha	Amp	Pha	Amp	Pha	Amp	Pha
1,1	-1.23	0.3	0.95	-2.1	-0.67	-0.9	-0.17	1.9	0.91	0.7
1,-2	0.82	0	1.27	0	1.11	0	-1.24	0	-1.16	0
1,-4	0	0	0.09	0	0.07	0	-0.19	0	-0.09	0
2,2	6.62	0	5.62	0	6.78	0	-5.91	0	-6.79	0
2,4	3.12	1.6	-4.29	2.4	0.34	2.1	2.76	-2.1	-0.43	-2.0
2,6	7.29	-4.9	6.83	2.0	8.56	-2.2	-7.21	-0.3	-7.92	3.3

Table 4.9 As Table 4.8, but for the computational solution with the realistic temperature profile of Figure 4.16.

obtained (P3 to P6) are similar to that for mean conditions (Figure 4.15), and the differences can be best illustrated by the change at each level. The results for the two main modes (2,2) and (1,-2) are shown in Figure 4.20. The deviations at sunspot maximum are nearly opposite to those at sunspot minimum and so are not plotted. In the upper atmosphere the non-linearity (e^{-KN_3}) in the expressions for Q (4.46a to d) breaks the symmetry. From Figures 4.20a and b it can be seen that the effect of altering the ozone as well as the UV is to accentuate the percentage change below 40 km but to reduce, even reverse, it above that level.

The heating profiles P1 to P6 are used to evaluate the changes in the atmospheric tides due to a 10% oscillation in UV. Both the analytic and the computational methods, outlined in the previous Section, are used, and the results are given in Tables 4.8 and 4.9 respectively. The largest effects (of around 7%), found in the semi-diurnal modes, are slightly reduced by including ozone perturbations (P3 to P6). Using the realistic temperature profile, rather than an isothermal atmosphere, devastates the results for the (1,1) and (2,4) modes so that their variations become negligible. So the major effect is that in the $n = 2$ semi-diurnal tide, where an increase in UV radiation of 20% (sunspot minimum to sunspot maximum) induces an increase of about 0.11 mb in the tide. As the observed tropical semi-diurnal tide has a standard deviation of only 0.04 mb the effect of a 20% change in UV would be readily observable. Contrarywise, the slight changes in the diurnal tide (the largest variation, 0.005 mb for a 20% increase in UV, occuring for the $n = 2$ mode) will be much more difficult to observe.

So when the tidal observations are analysed, the amplitude of any sunspot cycle induced variability should be an order of magnitude larger in the semi-diurnal than in the diurnal component. This is now shown not to be the case, and also doubt is cast on Heath and Thekaekara's (1977) value of 20%.

4.5.2. Observational

(a) Britain. Stagg (1931) noted that the diurnal tide showed variations dependent on the general state of the earth's magnetic field. His calculations, from observations made at Aberdeen over the years 1922-1928, showed that the diurnal tide on magnetically disturbed days peaked 2 hours later and was double the amplitude of that on "magnetically quiet" days. In contract to this, the semi-diurnal tide was independent of the amount of magnetic activity. Stagg also found that this effect was largest during a period of little solar activity (1922-1924). Because of the relatively small number of days he considered (7 years of 5 pairs of days per month), Stagg's results include large non-tidal fluctuations.

Further results given by Stagg (1931) show that the diurnal tide varies with the phase of the sunspot cycle, as well as with the earth's magnetic field. The diurnal tide was much larger during the dearth of sunspot activity, than during the remaining years when there were more sunspots. Using data from everyday, it can be calculated that the amplitude of the average diurnal tide was 0.173 mb for 1922-1924 compared to 0.066 mb for the following four years. However when many years of observations are considered the size of this effect is greatly reduced.

		DIURNAL		SEMI-DIURNAL	
		Amplitude	Phase	Amplitude	Phase
ABERDEEN	Mean (73)	104.1± 7.1	164±4	240.2±1.9	144±0.5
	SS Max(21)	94.5±11.8	164±7	238.1±3.2	144 ± 1
	SS Min(24)	111.6±11.8	158±7	240.9±3.7	143 ± 1
KEW	Mean (82)	144.5± 5.6	206±2	348.1±2.1	149±0.3
	SS Max(25)	145.9±11.1	202±4	353.6±3.9	149±0.6
	SS Min(26)	141.6± 8.3	207±3	345.9±3.9	148±0.7

Table 4.10 Variations in the diurnal and semi-diurnal tides at Aberdeen and Kew with the sunspot cycle. Amplitudes are in μb and phases in degrees. The numbers of years used for each set of results is given in brackets.

		DIURNAL		SEMI-DIURNAL	
		Amplitude	Phase	Amplitude	Phase
ABERDEEN	Mean	124.5	184.1	70.2	176.0
	SS Max	126.6	184.0	73.8	175.6
	SS Min	122.4	184.2	66.6	176.3
KEW	Mean	165.6	185.6	128.9	176.9
	SS Max	167.7	185.6	135.6	176.6
	SS Min	163.5	185.7	122.1	177.1

Table 4.11 Theoretical mean tides at Aberdeen and Kew, and predicted variations with the sunspot cycle. Amplitudes are in μb and phases in degrees.

Values for the diurnal and semi-diurnal tides at Aberdeen (57^{o}N, 2^{o}W) for 1871-1882 were obtained from Thompson (1891) and for 1887-1947 from a sequence of Meteorological Office publications (1887-1910, Hourly Observations; 1911-1921, British Meteorological and Magnetic Year Book; 1922-1947, The Observation Year Book). The same sources were used for the tides at Kew (51^{o}N, 0^{o}W), with, in this case, observations being published up until 1956 in the Observations Year Book.

The years for which observations were analysed were split into three subsets depending on their phase in the sunspot cycle. In each cycle R, the annual sunspot number, increases from below 20 to a maximum for the cycle (R_{max}, which for the years analysed is always greater than 40) and then decreases to less than 20. Any year for which $R < 20$ is defined to be in the sunspot minimum set, while if $R > \frac{1}{2}R_{max}$ it is allocated to the sunspot maximum set. Years not accounted for fall into the rising/falling set. The components of the tides (A_r and B_r of Equation 4.1) are then averaged over all the years for which data is available, and also over the years in the "maximum" and "minimum" sets. The results thus obtained are listed in Table 4.10, in which the standard error in the amplitudes (dA) is evaluated as the mean standard error of the two components (A_r and B_r). The standard error in the phase ($d\theta$) is dA divided by the mean amplitude.

From Table 4.10 it can be seen that the diurnal tide at Aberdeen varies with the sunspot cycle, with the ratio of the amplitude at sunspot minimum to that at maximum being 1.18, (compared to 2.62 for 1922-1978). No other tidal variation in Table 4.10

is significant at the 95% level - when the change is greater than 2 standard errors. To evaluate the standard error (se) of a difference between two sets of data, $\{a\}$ and $\{b\}$, the formula

$$[se(a-b)]^2 = [se(a)]^2 + [se(b)]^2$$

is used.

Although this result is statistically significant at the 95% level, the hypothesis that it is a tropospheric response to solar variability is unlikely to be true, for the change in the diurnal tide at Aberdeen has the opposite sign to that predicted by theory (Section 4.5.1.).

Before comparing the observed variations with the theoretical prediction, the validity of the theory for these latitudes is tested. This is done by comparing the values presented in Table 4.11 with those previously given in Table 4.10. The amplitudes of the semi-diurnal tides are underestimated by about a factor of 3. This difference is due, in part, to the stationary "Arctic Component" of the semi-diurnal tide which (at these longitudes) is in phase with the global modes considered. (The Arctic Component is only significant at high latitudes. It is a function of universal, not local time, and causes the nodes in Figure 4.1.) Also, higher order modes, not considered in Section 4.4, may be important, as the low order modes (particularly 2,2) are greatly reduced at these latitudes compared to the equator. The amplitude of the diurnal tide is well predicted by the theory. It will be assumed that the missing component of the tide at any station, not represented by the theory, varies with solar activity by the same

percentage as the theoretical tide.

The variation in the diurnal tide at Aberdeen is five times larger than that predicted by the theory, as well as of the opposite sign. This effect, then, cannot be explained by the theory and must be due either to some other atmospheric response to solar variability or else to chance. For Aberdeen the theory predicts a change in the semi-diurnal tide double that which can be explained from the observations. This implies that, unless the missing component is negatively correlated with the sunspot number, the solar UV output varies by, at most, a half of the value given by Heath and Thekaekara (1977).

The theory of Sections 4.4 and 4.5 is more accurate for the semi-diurnal tide at low latitudes, where the Arctic Component is relatively small. So tidal variations in the tropics, possibly caused by solar activity, are now considered.

(b) Tropics

Data for this Section was obtained from two sources of hourly averaged annual pressure. Results for Macau were from Resultados das Observações Meterológicas (1952-1978), while the Indian values were from Indian Weather Review, Annual Summaries, 1948-1963 (except 1955). Values for some of the Indian Stations were not always available, and on other occasions the data was obviously erroneous. Table 4.12 lists the eight stations used, their locations and for which years their data was used.

The amplitudes of the mean tides, averaged over the 107 station years, are 0.817 mb (diurnal) and 1.191 mb (semi-diurnal). These

STATION	LOCATION	YEARS USED	TOTAL
Bombay	18.9°N 72.8°E	1948-54,56-62	14 years
Calcutta	22.5°N 88.3°E	1948-54,56-63	15 years
Macau	22.2°N 113.6°E	1952-75	24 years
Madras	13.1°N 80.3°E	1951-54,56-61	10 years
Nagpur	21.2°N 79.1°E	1949-54,56,58-63	13 years
New Dehli	28.6°N 77.2°E	1949-53,56-63	13 years
Poona	18.5°N 73.9°E	1948-54,56-62	14 years
Seychelles	4.6°S 55.5°E	1951-54	4 years

Table 4.12 Details of the tropical stations whose observations were used here.

	Diurnal		Semi-Diurnal	
	Amplitude	Phase	Amplitude	Phase
Mean Theory	144.0	9.0	727.5	1.3
Mean Obs.	662.6±10.5	106.4±0.9	1033.7±7.4	315.0±0.4
Diff Theory	12.9	-0.2	125.6	-0.1
Diff Obs.	-20.2±19.2	-2.5±1.2	-8.4± 8.2	1.2±0.8

Table 4.13 Mean tide at Macau and its difference (Diff) between sunspot maximum and sunspot minimum, both theory and observation. Amplitudes are in μb and phases in degrees.

	Diurnal		Semi-Diurnal	
	Amplitude	Phase	Amplitude	Phase
Mean Theory	160.6	0.0	760.9	0.8
Mean Obs.	851.4	107.5	1222.3	305.3
Diff Theory	13.8	0.0	154.2	0.0
Diff Obs.	-47.3±15.8	3.7±0.9	8.3±14.3	-0.2±0.7

Table 4.14 As table 4.13, but for Indian stations.

are larger than the values the theory (Section 4.4) predicts (0.157 mb and 0.754 mb) by factors of 5 and 1.6 respectively. The cause of this disagreement between the observations and the theory is mainly local effects for, as can be seen from Figures 4.1 and 4.2, the tides are larger over India than at all other longitudes on the same latitude circle.

To begin with, observations at Macau are considered separately, (as they are independent of those from India). The theory underestimates the amplitudes by factors similar to those given above for the average of all the tropical stations. These factors are taken into account when predicting the theoretical changes in the tides. From Table 4.13 these can be compared with the observations. As at Aberdeen, the theory grossly overestimates the variations in the semi-diurnal tide while the diurnal tide shows no significant (at the 95% level) variation. There is also a significant phase change in the diurnal tide, not expected from the theoretical results of Section 5.4.1.

The results for the Indian Stations are considered en bloc (to reduce the standard errors). They are normalised at each station, before averaging over all the stations. The normalisation chosen is such that the mean tide at any station $(\bar{x},\bar{y})$ is the unit vector in the x-direction (1,0). So for that station any mean annual tide $(\bar{x},\bar{y})$ transforms to a point (ξ,η) given by

$$(\xi,\eta) = \left(\frac{x\bar{x}+y\bar{y}}{\bar{x}^2+\bar{y}^2} , \frac{y\bar{x}-x\bar{y}}{\bar{x}^2+\bar{y}^2} \right) \qquad (4.58)$$

The values thus evaluated are averaged for the seven Indian stations, over all years, years of sunspot maximum and years of

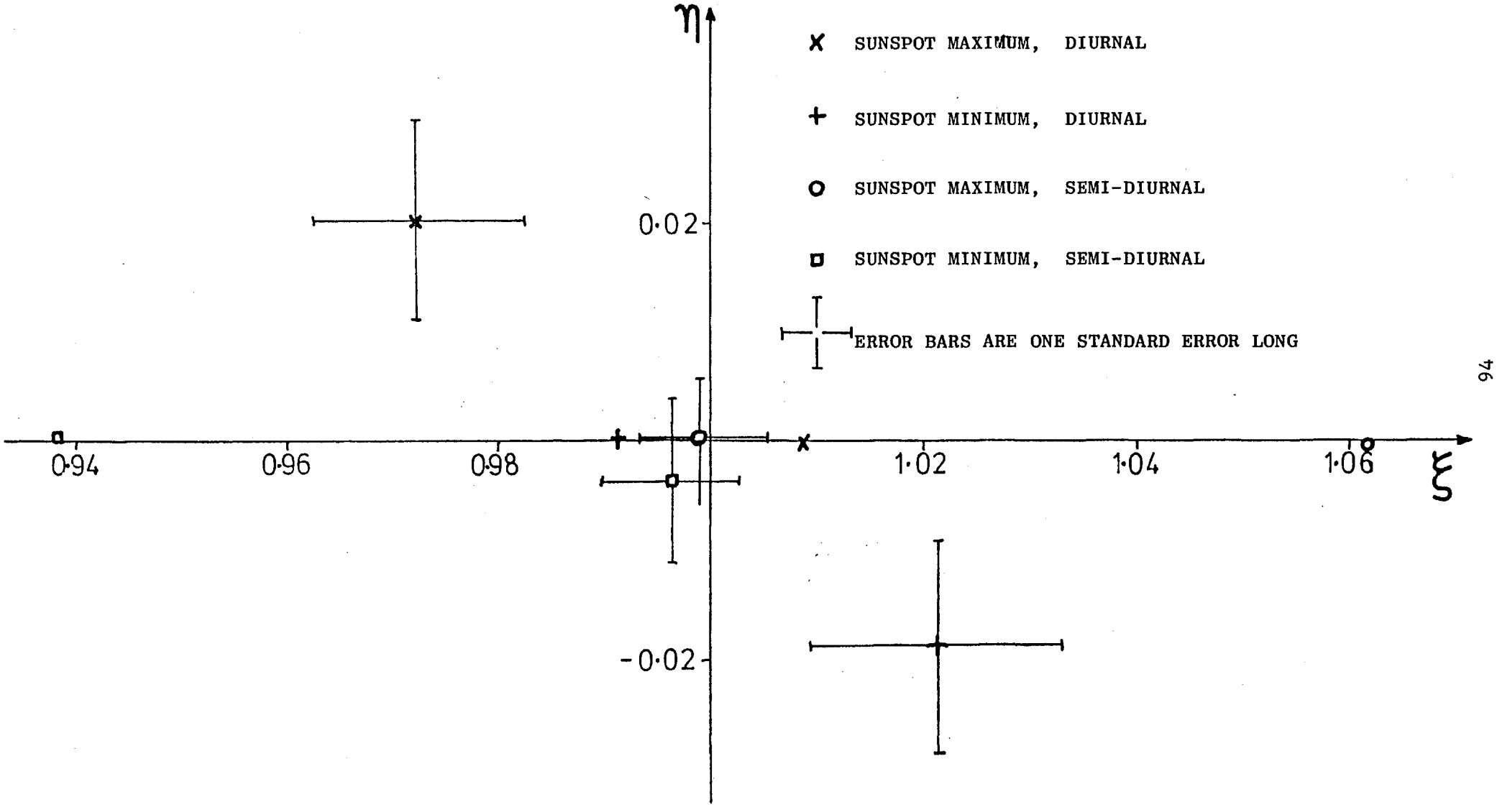

Figure 4.21 Theoretical and observed variations in the diurnal and semi-diurnal tides in the tropics. Observations from Macau and India, 31 years of data for the "Sunspot Maximum" results, 29 for those at "Sunspot Minimum".

sunspot minimum (as defined above). The results follow the same pattern as at Macau and Aberdeen, as can be seen from Table 4.14. The diurnal tide shows a significant (95%) variation of greater than 5% over the sunspot cycle, while the semi-diurnal tide varies by a tenth of the value expected (and with the opposite sign).

By normalising the results at Macau, they can be combined with those from India. The effect of this is to reduce the standard errors, while other properties are only slightly changed as they are similar in both sets of observations. The combined results are plotted in Figure 4.21. This diagram highlights the discrepancies between the theoretical prediction (Section 4.5.1) and the observations. The semi-diurnal tide is predicted to vary by 12.3% over the sunspot cycle, but it is observed to vary by only 0.3% ± 1.0%, while the diurnal tide shows much larger variations (-4.9% ± 1.6%) than predicted (1.6%).

Assuming that the change in the semi-diurnal tide is proportional to that in the UV, then from the observed variation in the tide a value for the sunspot cycle variation in UV can be estimated. As shown above, a 20% change in the UV would cause a 12.3% change in the semi-diurnal tide, so a 0.3% ± 1.0% variation in the tide is due to a $(0.3 \pm 1.0) \times (20/12.3)\% = 0.5\% \pm 1.6\%$ variation in the UV.

The variation in the diurnal tide is larger than its mean ozone absorption forced component, and hence it is not due to variations in UV. As the diurnal tidal forcing due to local tropospheric heat transport is important in the tropics, it is that which decreases by about 5% from sunspot maximum to sunspot minimum.

Hence there was, during the years 1948 to 1975, a tropospheric parameter which had a significant variation over the sunspot cycle.

4.6. Conclusion

From the results for the semi-diurnal tide it is concluded that the UV decreases by only 0.5% ± 1.6% from sunspot minimum to sunspot maximum. This agrees with the assertation of Smith and Gottlieb (1974) that for wavelengths longer than 1500Å there is no variation over the 11 year sunspot cycle, but is contrary to the claims of Heath and Thekaekara (1977) that the UV (at 3000Å) varies by 18% over the sunspot cycle. No suggestion is ventured to explain the observations of the diurnal tide. They show that there was, during the period analysed, a tropospheric parameter which varied significantly between sunspot maximum and sunspot minimum.

CHAPTER 5

PLANETARY WAVES

5.1. Introduction

The general circulation of the atmosphere at mid-latitudes is dominated by eddy processes. These are important for, as well as determining pressure distributions, they transfer large amounts of heat and momentum. There are two main types of large scale eddies, baroclinic waves and planetary waves. The former are transient phenomena, with zonal wavenumbers at least six. The latter, which have zonal wavenumbers one, two and three, are considered in detail here.

Planetary waves are forced by airflow over orography and over longitudinal asymmetrics in heating (Shutts, 1978). Changes in the solar constant would affect the tropospheric heating and, if the zonal wind was altered, the orographic forcing. However, a more important process is the sensitivity of planetary waves to changes in the middle atmosphere (Schoeberl and Geller, 1976, Bates, 1977, and Geller and Alpert, 1980). So, if solar activity alters the middle atmosphere, it could affect planetary waves and hence the troposphere. This amplification mechanism is considered further in Section 5.3.

There is evidence that planetary waves are affected by solar variability (Parker, 1976, King et al., 1977). Parker found a $\pm$ 2 mb variation in surface pressure over the sunspot cycle, while King et al. found a $\pm$50 m variation in 500 mb height over the solar rotation period. These observations are considered in Sections 5.4.1 and 5.4.2 respectively.

5.2. Theory of Planetary Waves

The predominance of low wavenumber planetary waves in the winter stratosphere was explained by Charney and Drazin (1961) using quasi-geostrophic theory. They showed that all but the largest scale waves are "trapped", the amplitide decaying exponentially away from the forcing. Whether a wave propagates or is trapped in the vertical is determined by the Vertical Structure Equation, (VSE).

In the idealised case the waves are independent of time (stationary), and the vertical structure of the atmosphere (in particular zonal wind, u, and static stability, B) is independent of height. Charney and Drazin (1961) derived the quasi-geostrophic potential vorticity equation, on the mid-latitude beta plane (i.e. replacing f by $f_o + \beta y$).

$$\frac{d^2\Psi'}{dz^2} + \nu^2 \Psi' = 0 \qquad (5.1)$$

where $$\nu^2 \equiv \frac{gB}{f_o^2}\left[\frac{\beta}{u} - (k^2+l^2)\right] - \frac{1}{4H^2} \qquad (5.2a)$$

and $$\psi' = \Psi'(z) \exp\left[i(kx+ly) + \frac{z}{2H}\right] \qquad (5.3a)$$

k and l are horizontal wavelengths in the x (eastward) and y (northward) directions.

B is the static stability

ν is the vertical wavenumber

H is the density scale height

Vertical propagation occurs if, and only if, ν^2 is positive. For if it is negative, Ψ is an exponential function of z, and decays in amplitude away from the forcing. Propagation occurs if the wind

is westerly and less than the wave's critical velocity, $u_c = \beta/(k^2 + l^2 + f_o^2/4g\ B\ H^2)$. Using representative values for the stratosphere, only those waves whose wavelengths are greater than 20,000 km propagate. These values are quantatively changed when spherical co-ordinates are used (Shutts, 1978). For in that case

$$\nu^2 \equiv \frac{gB}{f_o^2}\left[\frac{2\Omega}{\chi} - \frac{(n+2)(n-1)}{R^2}\right] - \frac{1}{4H^2} \qquad (5.2b)$$

$$\psi' = \Psi'(z)\, P_n^m(\cos\theta)\exp\left(im\lambda + \frac{z}{2H}\right) \qquad (5.3b)$$

and $\chi = Ru/\sin\theta$ is assumed independent of height and longitude. Then

$$\left.\begin{array}{l} u_c = 78\ ms^{-1} \text{ for } n = 2 \\ \quad\ 45\ ms^{-1} \text{ for } n = 3 \end{array}\right\} \text{ at } 45^\circ, \text{ independent of m}$$

The most important modes are those with $n = m+1$, which have a single, mid-latitude, peak. The ($m = 1$, $n = 2$) mode has a longitudinal wavelength, at 45°N, of about 30,000 km. During the winter, the $n = 2$ waves propagate up to 100 km while the $n = 3$ waves become evanescent above 50 km. In the summer, all stationary planetary waves are confined to below 40 km.

In obtaining the Vertical Structure Equation (5.1) various assumptions were made, many of which were also made for the complex tidal theory, Section 4.4.1. The relevant approximations are:- (a) perfect gas, (b) thin layer, (c) hydrostatic, (d) sphericity, though orography is not ignored here, (e) dissipation neglected, (f) linearised equations. The important extra approximation made here is that the horizontal wind is approximated by the non-divergent part (but the vertical velocity is not set at zero). This leads to vorticity advection, twisting and baroclinic generation of vorticity being neglected in the vertical component of the

vorticity equation.

Following Shutts (1978) stationary perturbations on an atmosphere whose angular velocity depends only on height are considered, so

$$u(\theta, z) = \frac{1}{R} \sin\theta \, \chi(z) \tag{5.4}$$

The waves are assumed stationary in time ($\frac{\partial}{\partial t} = 0$) and sinusoidal in longitude ($\frac{\partial}{\partial \phi} = im$). Then separation of variables yields that the θ dependence is given by Associated Legendre Functions, $P_n^m(\cos\theta)$. So the stream function (Ψ) and entropy source term (S) are replaced using

$$\begin{aligned} \Psi &= -\cos\theta \, \chi(z) + \mathrm{Re}\left(\Psi'(z) P_n^m(\cos\theta) e^{im\phi}\right) \\ S &= \mathrm{Re}\left(iS_0(z) P_n^m(\cos\theta) e^{im\phi}\right) \end{aligned} \tag{5.5}$$

In this case the VSE becomes

$$\frac{d^2\Psi}{dz^2} + \frac{B}{\rho_0}\frac{d}{dz}\left(\frac{\rho_0}{B}\right)\frac{d\Psi}{dz} + \frac{gB}{f_0^2}\left\{\frac{2\Omega}{\chi} - \frac{(n+2\chi)(n-1)}{R^2} - \frac{f_0^2}{g\rho_0}\frac{1}{\chi}\frac{d}{dz}\left(\frac{\rho_0}{B}\frac{d\chi}{dz}\right)\right\}\Psi' = -\frac{gBR^2}{f_0 m \chi \rho_0}\frac{d}{dz}\left(\frac{\rho_0 S_0}{B}\right) \tag{5.6}$$

The boundary conditions are zero normal velocity at the ground and a radiation condition at the top. Shutts (1978) introduced an "energy-transmitting" upper boundary condition by assuming that above the integration region the atmosphere is in solid body rotation. This leads to the condition

$$\frac{d\Psi'}{dz} = \left\{\frac{1}{\chi}\frac{d\chi}{dz} + i\nu + \frac{1}{2H}\right\}\Psi' \quad \text{at } z = z_T \tag{5.7}$$

where ν^2, the vertical wavenumber squared, is derived by setting $\Psi' = (B/\rho_0)^{\frac{1}{2}}F$. When this is substituted in the VSE (Equation 5.6),

and the resulting equation normalised so that the coeficient of $\frac{d^2F}{dz^2}$ is 1, then the coefficient of F is ν^2.

The effect of orography is included, so the bottom boundary condition, in linear form, is

$$\frac{d\Psi'}{dz} - \frac{\Psi'}{\chi}\frac{d\chi}{dz} = -\frac{g\beta}{f} a_{mn} - \frac{gR^2}{mf\chi} S_o \quad \text{at } z = 0 \qquad (5.8)$$

where a_{mn} is the (m,n) component of surface elevation.

The VSE (5.6) can be solved with the boundary contions 5.7 and 5.8 computationally or, if the vertical structure is "simple", analytically (see Appendix, Section A.2). Knowing $\Psi'(z)$, δp can be calculated from

$$\delta\rho(z) = \rho_o(z) f \Psi'(z) e^{-z/2H} \qquad (5.9)$$

with u and β independent of height, an analytic solution can be found. A method is outlined in Appendix A.2.1. The solution, at the ground, is

$$\Psi'(0) = \frac{-gR^2}{mf\chi} \int_0^\infty e^{(i\nu - \frac{1}{2H})z_o} S_o(z_o) dz_o - \frac{g\beta a_{mn}}{f_o(i\nu + \frac{1}{2H})} \qquad (5.10)$$

Using typical values for a_{mn} (200 m) and S_o $[(1.5 \text{ K day}^{-1}/260 \text{ K}) \exp(-z/4 \text{ km})]$, the relative importance of the two terms in the solution 5.10 can be found. They each have an amplitude of about 5 mb for wave number m = 1, n = 2 implying that both tropospheric heating and orography are important. Ozone absorption of Ultra-Violet radiation (UV) forces a component that is negligible, as is now shown.

5.2.1. Ozone Forcing

Ozone absorbs about 30 Wm^{-2} of solar radiation when the sun is at zenith (see Section 2.2). The globally averaged amount is a quarter of this (7.5 Wm^{-2}). Ozone varies only slightly with longitude (at those altitudes where its absorption causes most heating), and it is assumed here that the forcing of planetary waves is 1% of the longitudinal mean heating. This assymetry is due to the upward propagation of planetary waves. Using typical values ($f = 10^{-4} s^{-1}$, $u = 30\ ms^{-1}$, $H = 7600$ m, $T = 260$ K, $B = 4 \times 10^{-5} ms^{-1}$, $n = 2$, $m = 1$) then at 45°, $\nu^2 = 1.1 \times 10^{-4} m^{-1}$ and

$$|\Psi'(0)| = 1.15 \times 10^5$$

so $$|\delta p| = 0.14 \text{ mb}$$

This is only 1% of the tropospherically forced component. However, the values given in Chapter 1 for changes over the sunspot cycle (of ± 10% for UV, ± 0.1% for the solar constant) imply a change of 0.01 mb in both tropospherically and ozone forced planetary waves. This is similar to the result of Green (1979) of 0.04 mb (Section 3.1), but two orders of magnitude less than the observed effect of 2 mb (see Section 5.4).

Altering the height that the UV is absorbed results in the planetary wave having a different amplitude. If a fixed quantity of energy is absorbed at height h, then the amplitude is proportional to $1/\sqrt{(\rho(h))}$, which in turn is proportional to exp (z/2H), in an isothermal atmosphere. (For details of the calculation see Section A.2.1). So for every kilometre the heating is raised, the amplitude of the planetary waves will be about 7% larger. Concurrent with this would be a phase change $d\theta$ = (change in height) x ν. This

could alternatively be expressed as an additional component of amplitude $dA = 2 \sin \frac{1}{2} d\theta \times |\delta p|$. Assuming that changes in heating profile are proportional to those for the equator with the Sun at zenith, $\delta h \lesssim 0.3$ km. So the redistribution in height can be represented as an additional component with amplitude of less than $0.035 |\delta p|$ - again negligible compared to the observed variations.

So perturbations in the longitudinal variations of ozone heating, due to possible UV changes, cannot change the amplitude of planetary waves at the ground by more than 0.02 mb.

5.3. Variations in the Atmospheric Profile

5.3.1. Previous Models

Bates (1977) and Geller and Alpert (1980) consider the effect of zonal wind variations on planetary waves. However, the wind changes they use are larger than those calculated for the effect of solar variability (see Section 2.2).

Bates (1977) derived, in a different method to that outlined in Section 5.2, a vertical structure equation for planetary waves. The wind profiles were chosen so that the vertical wavenumber was constant in the troposphere, in the stratosphere and above the mesospheric jet. This severely restricts the form of the wind profile, and there is a discontinuity in the wind shear, at the tropopause. The distance between the tropopause and the mesospheric jet is, in Bates' model, very close to one wavelength. He considered various wind profiles, as illustrated in Figure 5.1 where the height $x = \ln(p(0)/p)$.

The basic profile, P, has the mesospheric jet at $x = 6.8$ with

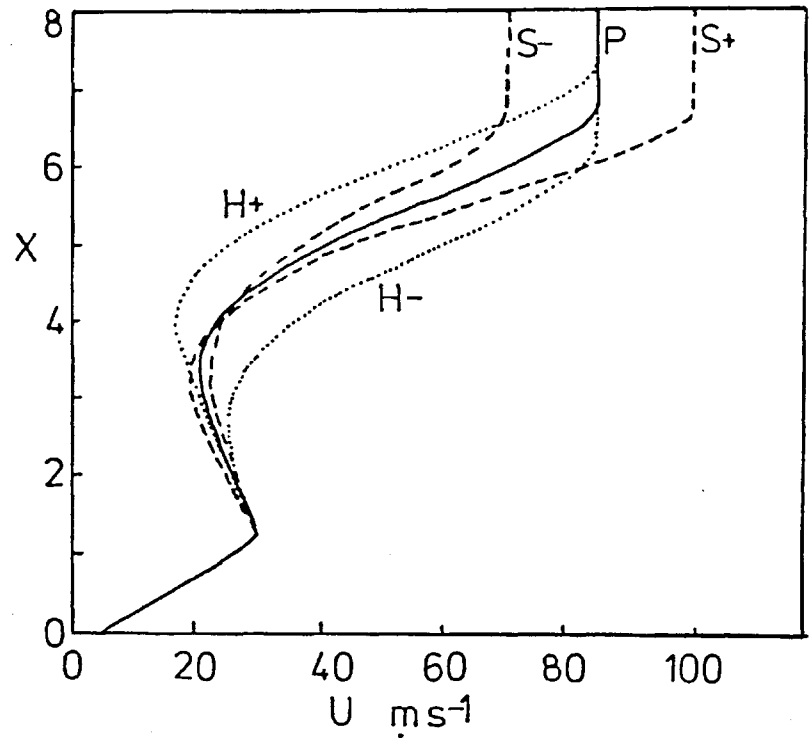

Figure 5.1 The vertical velocity profiles used by Bates (1977). P is the mean profile, S+ and S- involve changes in the mesospheric jet strength of 15 m/s and H+ and H- changes in the mesospheric jet height of 0.5 scale heights.

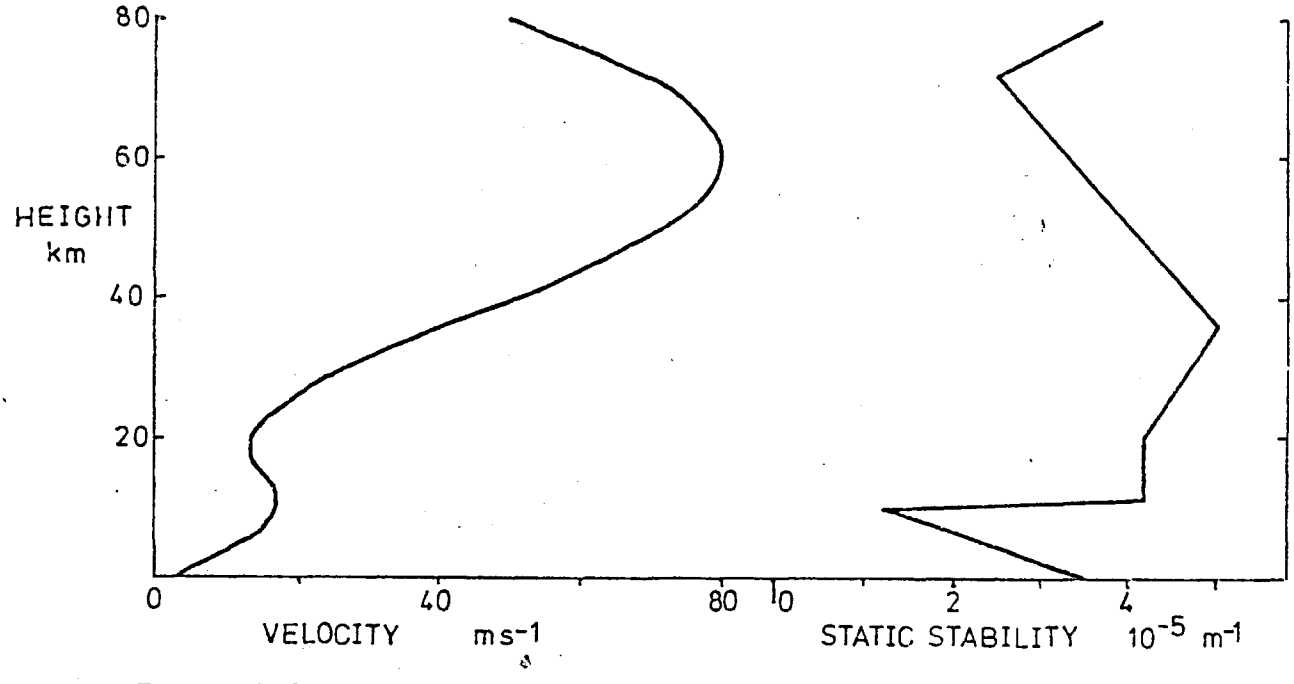

Figure 5.2a Mean zonal wind velocity and static stability profiles used in the new results here. They are typical mid-latitude winter profiles, and are based on those of Charney and Drazin (1963).

a strength 85 ms^{-1}. Profiles S+,S- are used to investigate the sensitivity of planetary waves to changes in the jet strength, in this case $du_{Jet} = \pm 15\ ms^{-1}$. Profiles H+,H- involve changes in the jet height of $dx_{Jet} = \pm 0.5$, with the jet strength unaltered. However, a change in the jet height causes a large change in the wind strength between $x = 3$ and $x = 6$.

Bates found that the surface amplitude of the planetary wave-number 1 is increased by 7.6% for a 15 ms^{-1} increase in the jet strength. There is a concurrent phase change of 2.1^{o}. Similarly, when the jet is raised by half a scale height the surface amplitude is increased by 7.8% and there is a non-linear phase change of $\pm 10^{o}$. In his model the thermally forced component is about five times the amplitude of the orographic one. As the changes are of a similar magnitude for each component, the fractional effect is much larger on the orographic component. These results may be due to resonance, as one layer is very close to one wavelength deep.

Geller and Alpert (1980) consider the effect of a vertically localised decrease in velocity of 20%. For their calculations they use the two dimensional, quasi-geostrophic model of Schoeberl and Geller (1977) with the Θ and z dependence of ψ unseparated. The velocity profile used is two dimensional, and when altered only a region of width $dx = 2$, centred at x_o, is changed. More than three scale heights below x_o there is no "measurable change in planetary wave structure". However, when the velocity near $x_o = 4$ is decreased by 20%, then at 500 mb ($x = 0.7$) there are changes in height of up to 20 m (10% of the mean amplitude). In this model the unrealistic restriction of the width of wind-changes to two scale heights

introduces rapid variations of the vertical wavelength with height. This affects the vertical propagation in a different way to more realistic (smoother and wider) wind changes.

The magnitude of the change considered (6 ms^{-1} at 30 km) is an order of magnitude larger than would be expected from a 10% change in UV. Hence their conclusion that "planetary wave coupling between the troposphere and the upper atmosphere appears to be a plausible mechanism to give a tropospheric response to solar activity" cannot be inferred from their results.

Though Bates (1977) and Geller and Alpert (1980) found large tropospheric responses to stratospheric wind changes, the changes themselves are unrealistic. From Bates' results, assuming a linear response, a 7 ms^{-1} increase in jet velocity causes an increase in surface amplitude of 3.6% and a phase change of -1.0° while a 1 km increase in jet height causes a 2.1% increase in amplitude.

However, for these results it was assumed that radiative damping is negligible below the mesospheric jet. As is shown in the following Section, this leads to enhanced sensitivity to upper atmospheric variations. Hence Bates' (1977) results overestimate the effect of stratospheric wind changes on planetary waves.

5.3.2. New Results

The model uses the VSE (5.6) with boundary conditions 5.7 and 5.8. The vertical profiles of zonal wind and static stability used for mean conditions are those of Charney and Drazin (1961), shown in Figure 5.2a. The wind profile above 18 km is given by

$$u(z) = \left(\frac{14+4J}{2}\right) - \left(\frac{4J-14}{2}\right)\cos\left[\frac{\pi(z-18)}{2J-18}\right] \qquad (5.11)$$

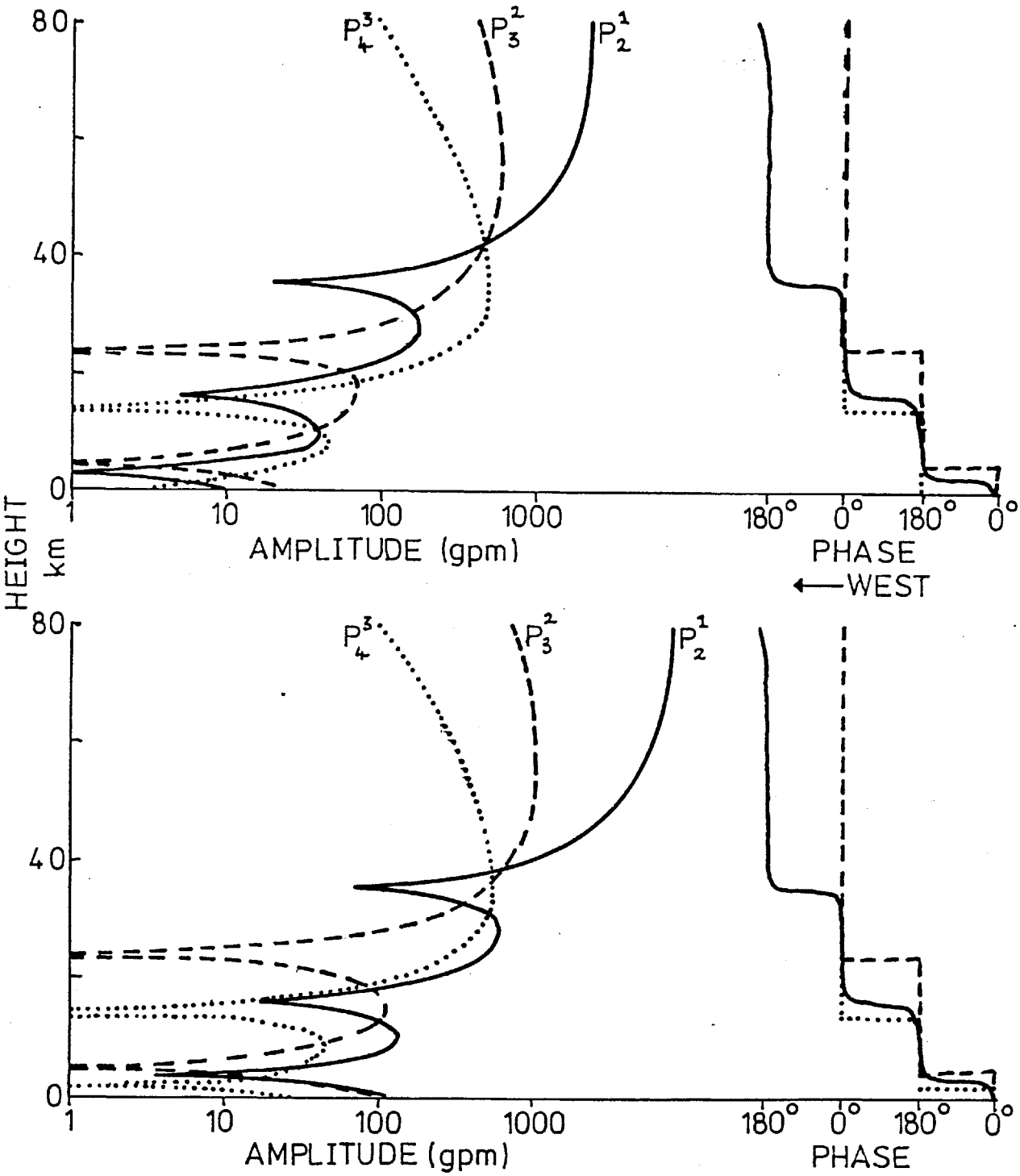

Figure 5.2b Vertical profile of the three planetary waves considered here, with mean vertical wind profile. The top figure is for the case of orographic forcing while the bottom one is for thermal forcing.

where UJ (= 80 ms^{-1}) is the maximum zonal velocity of the mesospheric jet, occurring at height ZJ (= 60 km).

The method of integration is the same as that for atmospheric tides (see Section 4.4.6), outlined in Appendix A.3. The region of integration ($0 \leq z \leq 80$ km) is split into 1,600 subintervals. The results, for constant u and B, were then accurate to $\pm 0.2\%$ in amplitude and $\pm 0.2^{\circ}$ in phase for orographic forcing. The accuracy of integrations with thermal forcing is less as the heating profile is approximated. However, this approximation is the same for differing velocity profiles if the tropospheric wind is unaltered.

The forcings used are

$$S_o = (1.5\,K\,day^{-1}/260\,K)\exp(-z/4km)\,P_n^m(\cos\theta)\cos\lambda \qquad (5.12a)$$

$$a_{mn} = 200\ gpm\quad P_n^m(\cos\theta)\cos\lambda \qquad (5.12b)$$

The vertical profiles of the waves are plotted on Figure 5.2b. Only wavenumber 1 propagates in the vertical, the other waves are trapped. However, Shutts (1978) found that both the (1,2) and (2,3) waves propagated. This disparity is discussed later, and it is found that the introduction of radiative cooling improves the model.

The amplitude and phases at the ground of the three waves considered here (m = 1, n = 2; 2,3; 3,4), with both constant and realistic vertical profiles, are given in Table 5.1. For the former $u = 20\ ms^{-1}$, $B = 3 \times 10^{-5}$m, while for the latter the profiles in Figure 5.2a are used. From this table it is apparent that the thermally forced components increase and the orographic components decrease

	THERMAL				OROGRAPHIC			
	CONSTANT		REALISTIC		CONSTANT		REALISTIC	
m,n	Amp	Pha	Amp	Pha	Amp	Pha	Amp	Pha
1,2	5.2	22	16.2	1	4.9	118	1.5	4
2,3	2.6	19	10.2	0	5.5	121	2.8	0
3,4	1.8	14	3.5	0	6.8	130	0.3	180

Table 5.1 Amplitude (mb) and phase (Degrees) of the three main planetary waves at Sea Level. "Constant" is the analytic solution when $u(z) = 20$ m/s and $B(z) = 3\times10^{-5}$ m^{-1}; "Realistic" is the computational solution with u(z) and B(z) as in figure 5.2a.

WAVE	m=1, n=2				m=2, n=3				m=3, n=4			
FORCING	Thermal		Orographic		Thermal		Orographic		Thermal		Orographic	
HEIGHT	0	5	0	5	0	5	0	5	0	5	0	5
P1	1622	299	154	116	1019	28	278	49	345	193	34	220
P2	+54	-26	+15	-8	+13	-7	+8	-5	+31	-17	-30	-17
P3	-62	+31	-18	+8	-13	+7	-7	+4	-41	+24	+39	+22
P4	-137	+68	-39	+19	-27	+15	-16	+8	-91	+52	+87	+49
P5	+112	-55	+32	-16	+36	-19	+22	-12	+57	-32	-55	-32
P6	-6	+3	-2	0	-2	+1	-1	0	-1	+1	0	0
P7	-98	+49	-28	+14	+113	-60	+68	-36	+43	-24	-26	-24

Table 5.2 Amplitudes of the waves forced by thermal and orographic forcing at both the ground (0, measured in 10^{-2} mb) and at 5 km (5, measured in 10^{-2} m). The velocity profiles are defined as follows:-

P1 ZJ = 60, UJ = 80

P2 ZJ = 61, UJ = 80

P3 ZJ = 59, UJ = 80

P4 ZJ = 60, UJ = 85

P5 ZJ = 60, UJ = 75

P6 as P1, but with a localised increase of velocity near the jet so that maximum jet strength = 85 m/s. No alteration for $|z - 60| > 5$

P7 as P1, but with a localised decrease near 25 km, so that $u_{P7}(25\text{km}) = 0.8\ u_{P1}(25\text{km})$. No alteration for $|z - 25| > 5$

Values for P2 to P7 are differences from the results for mean conditions (P1).

when, instead of the constant profiles, realistic profiles are used. The reason for the thermally forced waves' result can be seen from the VSE (5.6). The effect of thermal forcing at any height is inversely proportional to the zonal wind velocity, $\chi \sin\theta / R$. As the thermal forcing is predominantly tropospheric, where the real wind is less than 20 ms^{-1}, it is larger in the realistic wind than in the constant wind. The cause of the change in the orographic component is less easy to isolate. With a constant wind profile, the amplitude is independent of the wind velocity (see Equation 5.10). When integrated with the realistic wind profile with, in the lowest 100 metres, χ altered so that $\frac{d\chi}{dz} = 0$ at the ground, the results are very similar to those with $\frac{d\chi}{dz} \neq 0$. Hence the difference between the results with constant and realistic wind profiles is due to changes in the vertical wavenumber, (ν).

The effect of altering the zonal wind profile is now considered, and in particular whether resonance occurs. The main profile alterations considered are those involving changes in only ZJ or UJ. From Section 2.2, zonal wind changes associated with the sunspot cycle may be as large as ± 5 ms^{-1} in UJ and ± 1 km in ZJ. Also considered is a change of small altitudinal extent (10 km), for comparison with the results of Geller and Alpert (1980). Some of the profiles used are shown in Figure 5.3, along with the wind change predicted by Schoeberl and Strobel (1978b).

The tropospheric responses to these zonal wind alterations are listed in Table 5.2. Localised changes in the mesospheric jet (profile P6) has much less effect than when changes lower down also occur (P4). The effect of a 5 ms^{-1} change in UJ is about 2.2 times

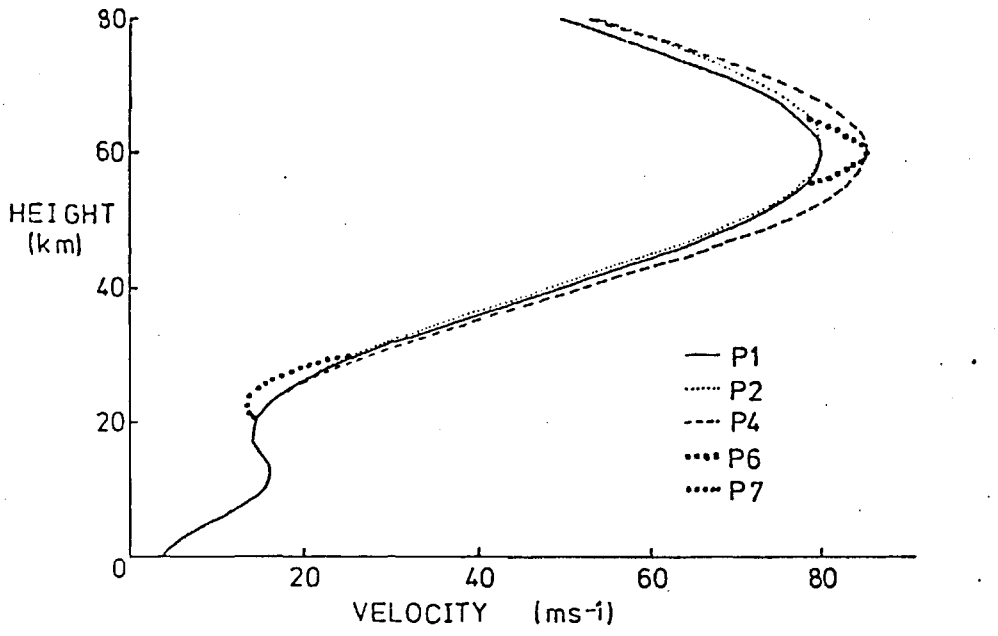

Figure 5.3 Some of the wind profiles used to calculate the values in Section 5.3.2.

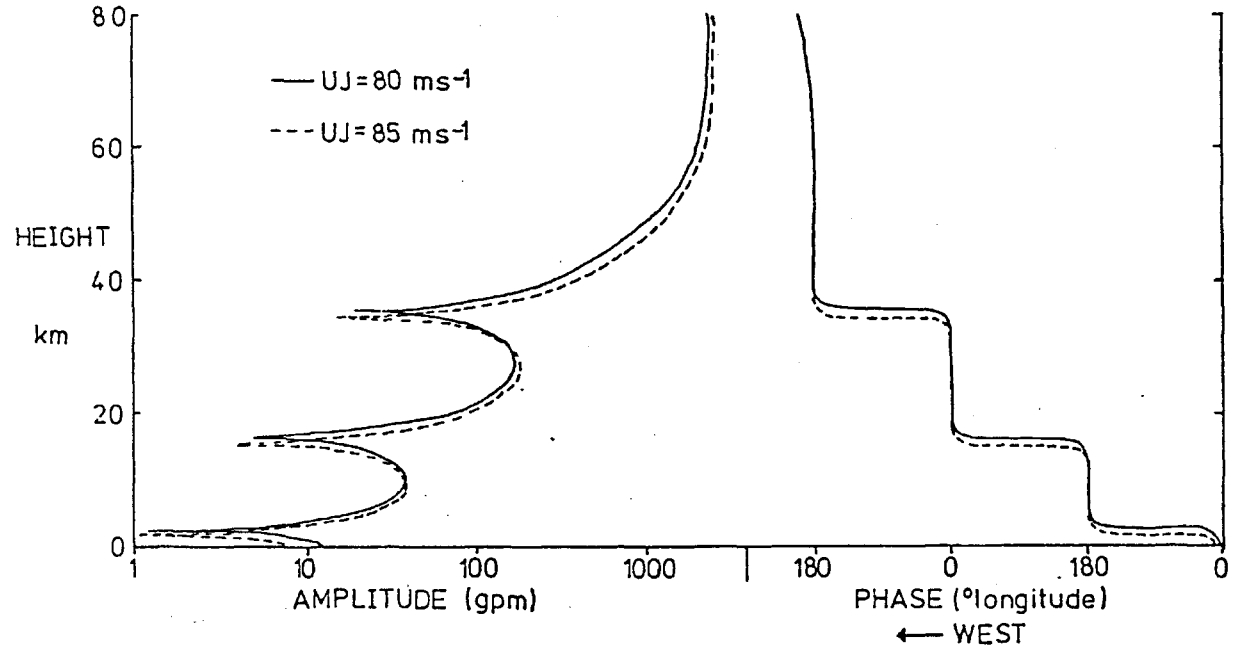

Figure 5.4 Effect on the orographically forced (1,2) wave of increasing the mesospheric jet strength (UJ). The results are similar for thermal forcing, and for the other wave numbers.

larger than that due to a 1 km change in ZJ. This is because the former causes stratospheric wind changes which are about double those from the latter (see Figure 5.3). The effect of a 20% decrease in the lower stratosphere (P7) is very large - of the order of 15%. This concurs with Geller and Alpert in showing that such wind changes would, if they occured, be very important. However, as shown in Section 2.2, such changes do not occur in response to UV variability.

For all but one wave (the orographically forced (3,4)), the changes at the ground are opposite in sign to those at 5 km. The reason for this is found when the vertical structure of the waves is considered. The orographically forced (1,2) wave, typical in this respect, is shown in Figure 5.4 for ZJ = 60 with UJ = 80 and 85. The graph shows that increasing the stratospheric wind results in the wave's nodes being lowered, in this case by about 1 km. This, in turn, affects the amplitude (A) as $\frac{dA}{dz} \neq 0$. For all but the orographic (3,4) wave;

$$\frac{dA}{dz}(0\ \text{km}) < 0\ ; \quad \frac{dA}{dz}(5\ \text{km}) > 0$$

(see Figure 5.2b). So increasing the stratospheric wind reduces the amplitude at the ground, but increases that at 5 km. Obviously this is only true for "small" changes, such that the node which occurs in the bottom 5 km of the atmosphere remains there. However, no such node occurs for the orographic (3,4) wave in the reference state, hence its idiosyncracy.

If the stratospheric winds are sufficiently increased, by reducing ZJ, the node is lowered to the ground. For the orographic (1,2) mode this occurs for ZJ = 54.955 km, when the phase is 90° and

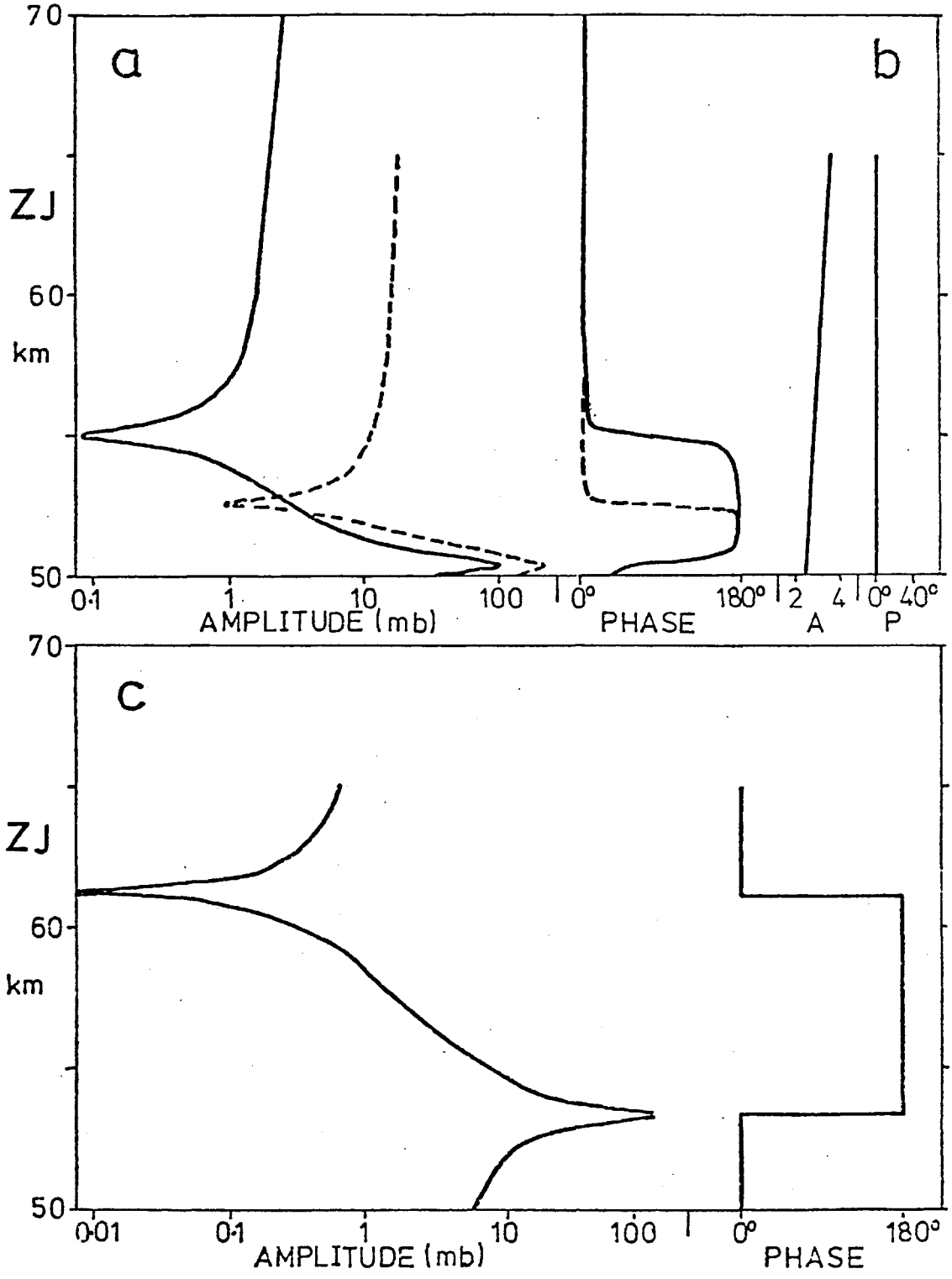

Figure 5.5 Variation of the wave amplitude and phase with the mesospheric jet height (ZJ). Solid lines are for orographically forced waves, while the dashed lines are for the thermally forced (1,2) wave. (a) m=1, n=2; (b) m=2, n=3; (c) m=3, n=4.

its amplitude is 0.64 m. Lowering the height of the mesospheric jet even further results in resonance. So at ZJ = 50.357 km the amplitude is 812 m - though this is not realistic for the approximation of linearity will have broken down. This resonance occurs when

$$\frac{d}{dz}(\ln \Psi') \simeq \frac{d}{dz}(\ln \chi) \quad \text{at } z = 0 \qquad (5.13)$$

For when 5.13 is true the left hand side of Equation 5.8 is 0 Ψ. But the right hand side is non-zero - hence the resonance. For those values of ZJ which yield very large or very small amplitudes, the phase is also very sensitive to ZJ. This can be seen from Figure 5.5. If the stratosphere was well represented by values of ZJ between 49 and 56 km, then the orographic (1,2) wave would be very sensitive to ZJ. At the realistic ZJ = 60 km, a change of 1 km in ZJ results in an 11% change in the surface pressure - by no means negligible.

Similarly the (3,4) wave is very sensitive to changes in ZJ, including when ZJ = 60 km (Figure 5.5c). However, in that case $|\delta_{p(0)}| = 0.4\ P_3^4$ mb, so large fractional changes are of small absolute amplitude. The (2,3) wave shows no resonance or sensitivity to ZJ (for ZJ in the range 50 to 70 km), a 1 km change in ZJ resulting in a 3% change in amplitude.

The above results are for orographic forcing. When thermal forcing is considered resonance still occurs at the same height as for orographic forcing, but the slope above ZJ = 55 km is noticeably reduced, (figure 5.5a shows response of the (1,2) wave).

However, for the above results, as ZJ is reduced the profile becomes less realistic, as the zonal velocity at 80 km is reduced.

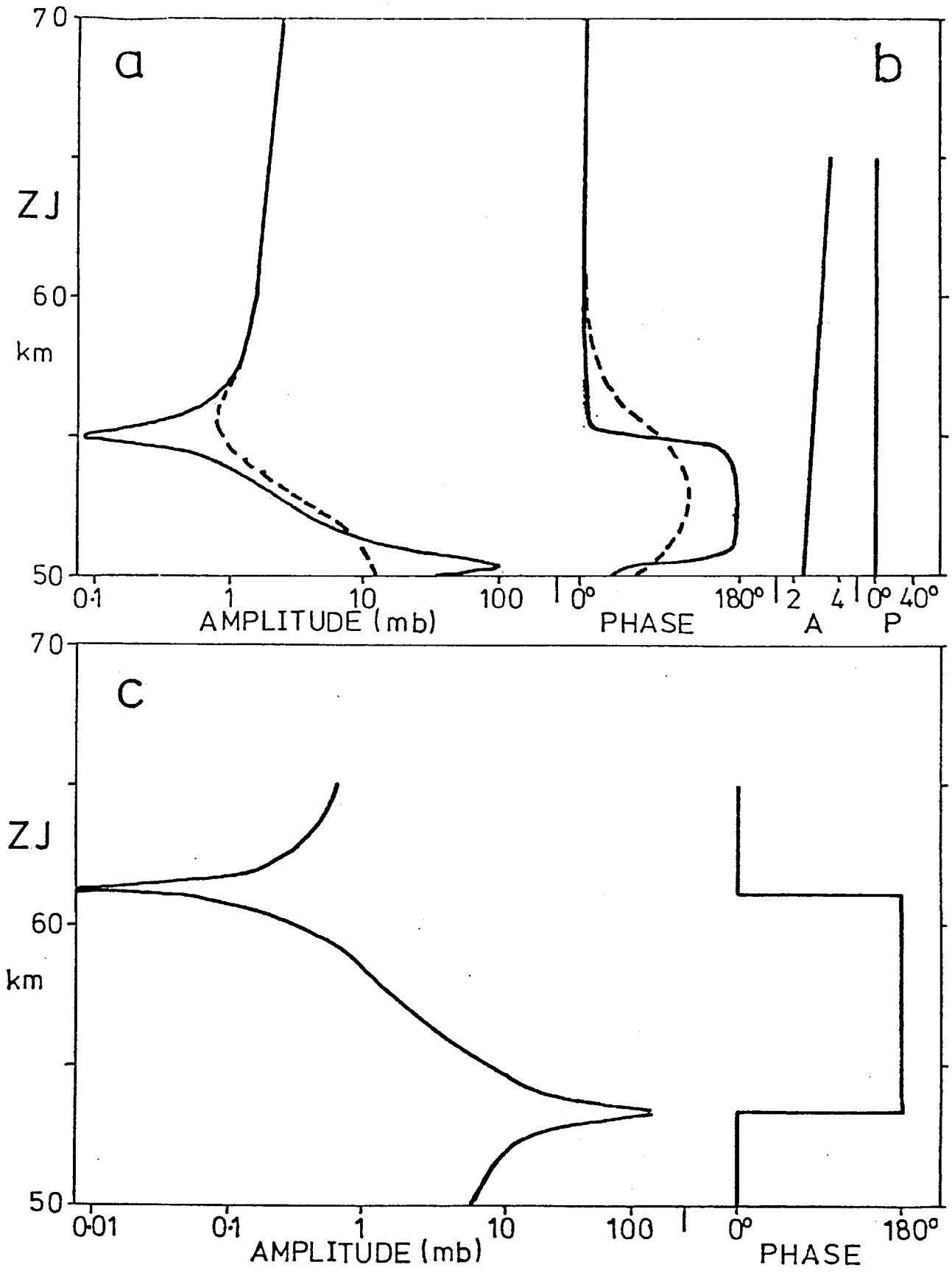

Figure 5.6 As Figure 5.5, but the dashed line is for u(z) = UJ for z > ZJ. This change only affects the (1,2) wave.

When ZJ = 50 km, $u(80) = 15\ ms^{-1}$. So an alternative model is used in which

$$u(z) = UJ \quad \text{for} \quad z \geq ZJ \tag{5.14}$$

This alteration has a negligible effect on the waves when ZJ is larger than 60 km. For lower values of ZJ the sensitivity of the surface amplitude to changes in the mesospheric jet height is reduced. So the amplitude of the orographically forced (1,2) wave, which with the previous model varied by a factor of 1000, now varies by a factor of 10 (see Figure 5.6). Similarly phase changes are smoothed to a maximum of 4^{o}/100 m compared to 36^{o}/100 m.

The (2,3) wave is virtually unaffected by this change - there was nothing to be smoothed! The trapped nature of the (3,4) wave results in it being insensitive to wind above the mesospheric jet.

When comparisons are made with the results of Shutts (1978) and with observations, it is found that the model traps waves to a greater extent than it should (see Figure 5.7). This is because the upper boundary is taken at 80 km, compared to 40 km in Shutts. The large zonal wind velocities in the mesospheric jet act as a rigid lid and the waves take on "trapped" characteristics. In the atmosphere the region between 30 and 60 km is a sink of planetary wave energy (Shutts, 1978), and so the effect of the mesospheric jet as a rigid lid is reduced. This sink is here modelled using infra-red cooling (radiative damping).

Following Holton (1975) and Hartmann and Garcia (1979), the Vertical Structure Equation with cooling is

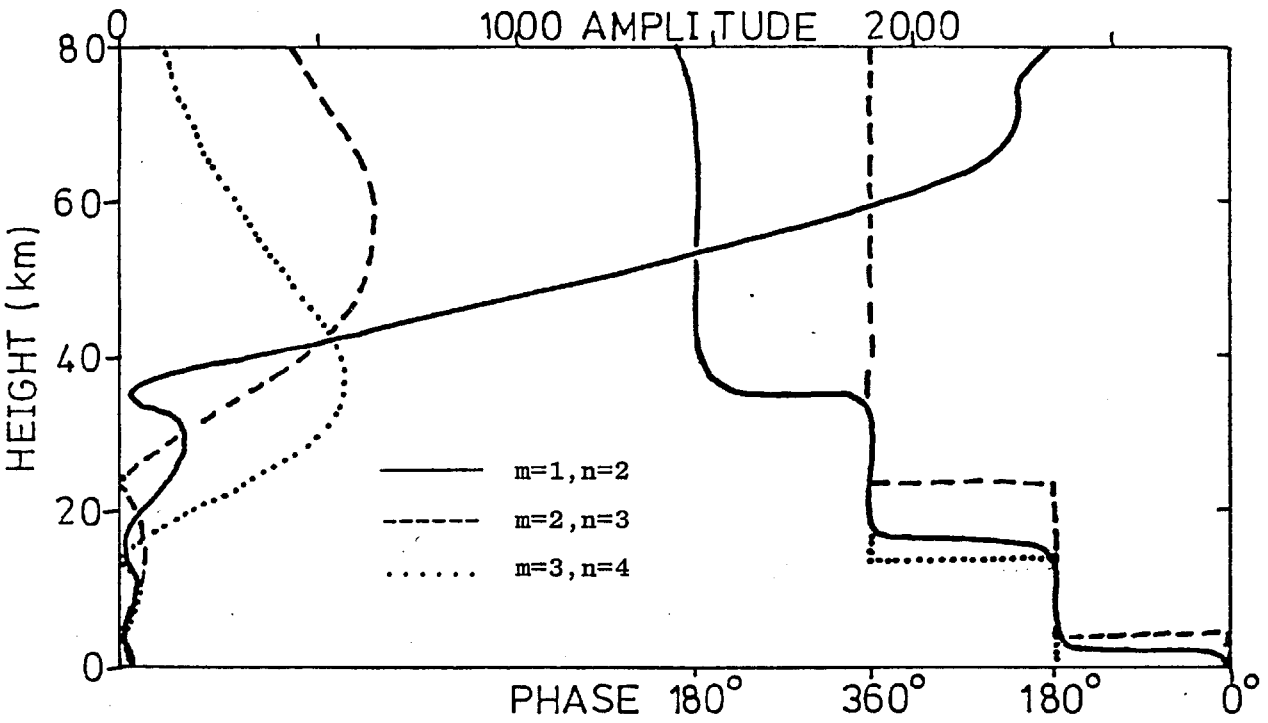

Figure 5.7 Vertical structure of orographically forced planetary waves.

(a)-above- Calculated here using UJ=80, ZJ = 60

(b)-below- From Shutts (1978)

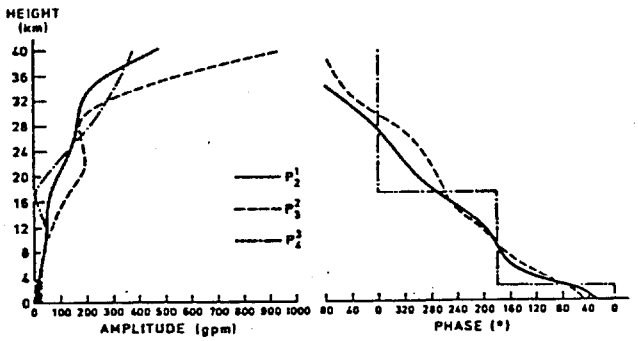

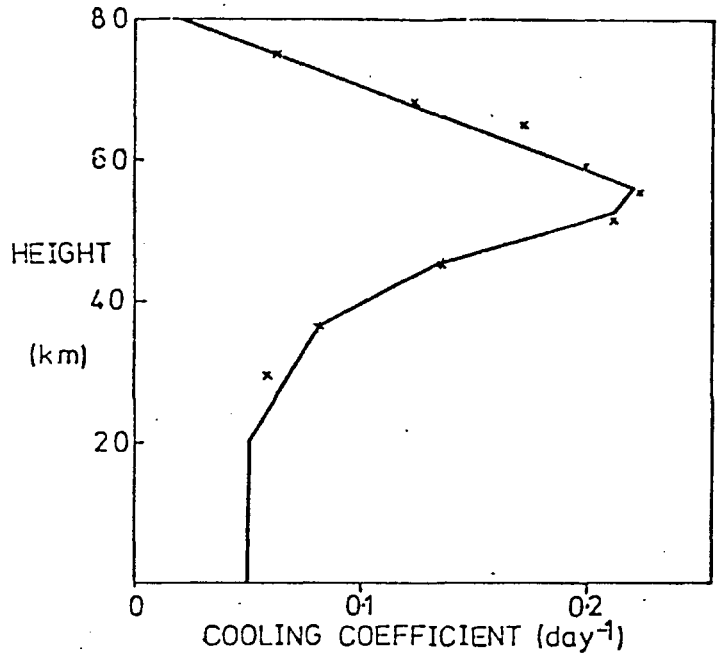

Figure 5.8 Vertical profile of Newtonian cooling coefficient used here (solid line). The crosses indicate the values calculated by Dickinson (1973)

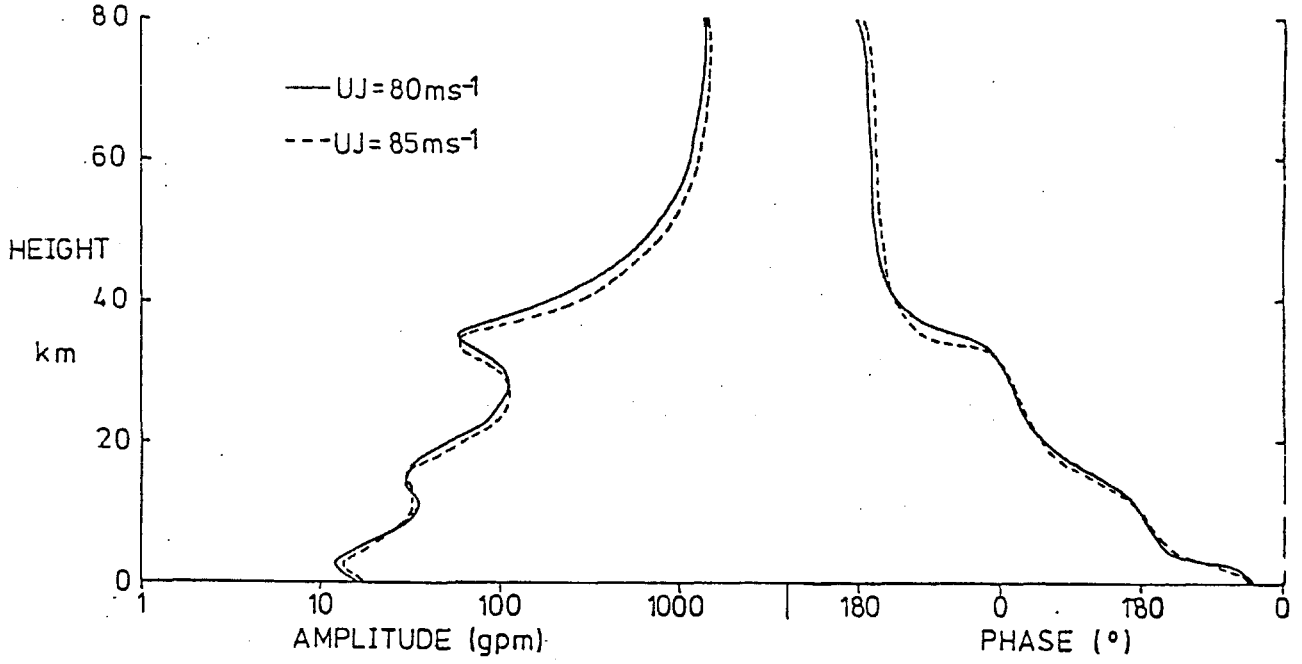

Figure 5.9 As Figure 5.4, but with Newtonian cooling included.

$$\left(1+\frac{\alpha R^2}{i\chi m}\right)\frac{d^2\Psi'}{dz^2}+\left[\left(1+\frac{\alpha R^2}{i\chi m}\right)\frac{B}{\rho_0}\frac{d}{dz}\left(\frac{\rho_0}{B}\right)+\frac{R^2}{i\chi m}\frac{d\alpha}{dz}\right]\frac{d\Psi'}{dz}$$

$$+\frac{gB}{f_0^2}\left\{\frac{2\Omega}{\chi}-\frac{(n+2\chi n-1)}{R^2}-\frac{f_0^2}{g\rho_0}\frac{1}{\chi}\frac{d}{dz}\left(\frac{\rho_0}{B}\frac{d\chi}{dz}\right)\right\}\Psi'$$

$$=-\frac{gBR^2}{f_0 m\chi\rho_0}\frac{d}{dz}\left(\frac{\rho_0 S_0}{B}\right) \qquad (5.15)$$

where α is a Newtonian cooling coefficient. Figure 5.8 shows the vertical profile of α used here, based on the values given by Dickinson (1973), shown as asterisks in the Figure. The boundary conditions are as before (Equations 5.7 and 5.8), but the vertical wavenumber squared is now

$$\nu^2=\frac{gB}{f_0^2}\left[\frac{2\Omega}{\chi}-\frac{(n+2\chi n-1)}{R^2}-\frac{f_0^2}{g\rho_0}\frac{1}{\chi}\frac{d}{dz}\left(\frac{\rho_0}{B}\frac{d\chi}{dz}\right)\right]\Big/\left(1+\frac{\alpha R^2}{i\chi m}\right)$$

$$-\frac{1}{2}\frac{B}{\rho_0}\frac{d^2}{dz^2}\left(\frac{\rho_0}{B}\right)+\frac{1}{4}\left[\frac{B}{\rho_0}\frac{d}{dz}\left(\frac{\rho_0}{B}\right)-\frac{1}{\left(1+\frac{\alpha R^2}{i\chi m}\right)}\frac{d\alpha}{dm}\right]^2$$

$$-\frac{1}{2\left(1+\frac{\alpha R^2}{i\chi m}\right)}\frac{d^2\alpha}{dz^2} \qquad (5.16)$$

The effect on orographically forced waves of introducing cooling can be seen from Figure 5.9. The vertical profiles of waves are smoothed, particularly near nodes. This results in the phase variations of P_2^1 being very similar to those of Shutts (1978), shown in Figure 5.7b. Another consequence of cooling is that maximum amplitudes (near the mesopause) are reduced, for wave energy is absorbed lower in the atmosphere. Similar effects occur in the thermally forced waves.

This smoothing also applies to the dependence of the surface wave on the stratospheric winds (parameterised by ZJ), as can be

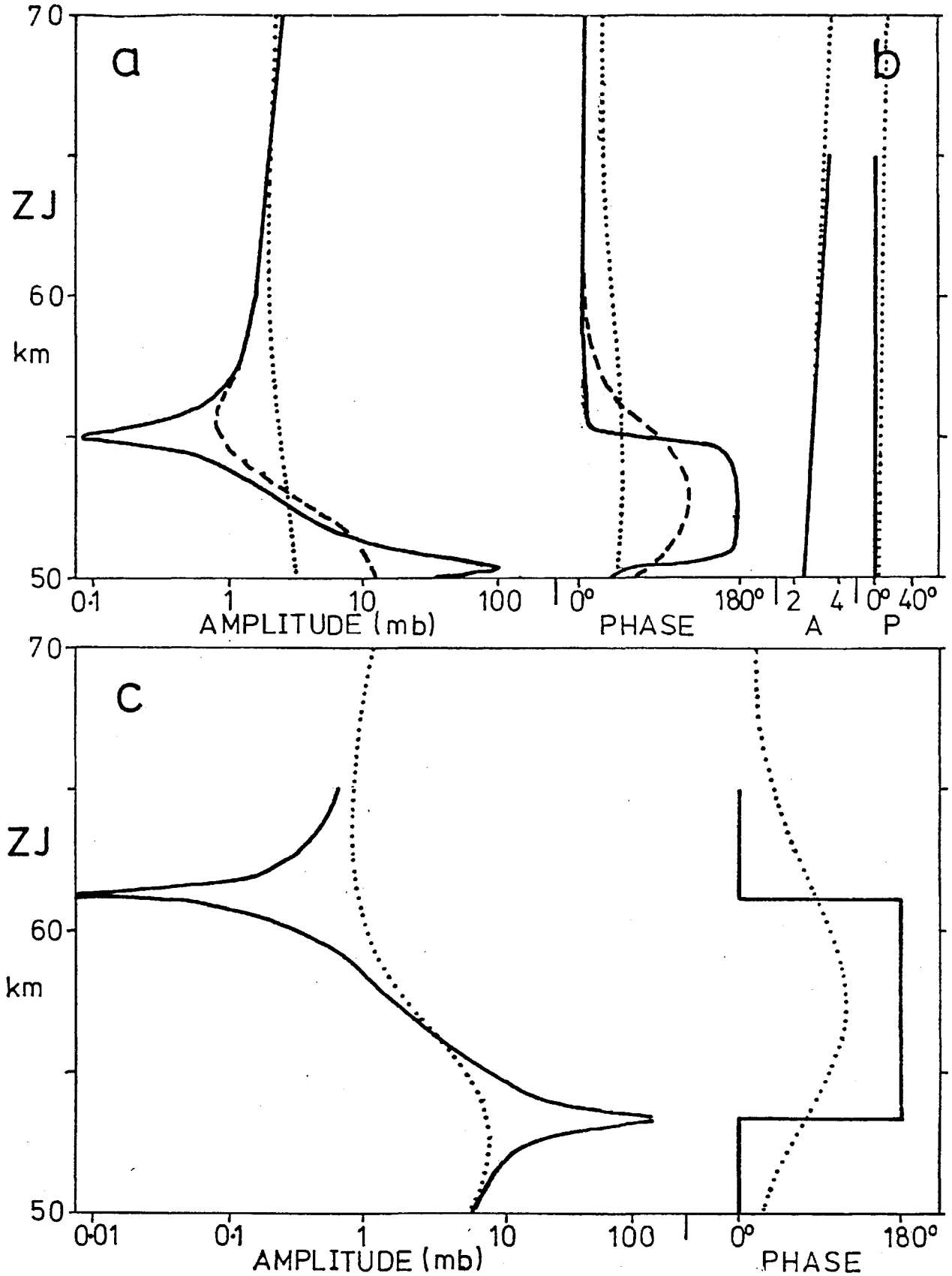

Figure 5.10 As Figure 5.5, but with the effect of Newtonian cooling also included (dotted line). For the results with cooling, $u(z) = UJ$ for $z > ZJ$.

seen from Figure 5.10. The orographically forced (1,2) wave in this latest model varies by a factor of only 1.5, and the maximum phase variation is 0.25°/100 m. For ZJ = 60 km, the percentage change in amplitude is +1% for every 1 km increase in ZJ, a tenth of the value when cooling is not included.

The (2,3) wave is virtually unaffected by changing the model, except for the phase being shifted by about 15°. The rate of change of amplitude with mesospheric jet height is slightly reduced, to 2.4% for every 1 km when ZJ = 60 km. Like the (1,2) wave, the (3,4) wave is smoothed so the resonance disappears. However, the (3,4) wave still increases by a factor of 10 between ZJ = 61 and ZJ = 53 km, while the maximum phase variation is 1.5°/100 m.

So resonance does not occur when cooling is included.

To examine the effect of stratospheric wind changes in surface pressure and 500 mb height, the planetary waves are summed. Before this is done realistic forcings are introduced.

The orographic forcing used is that given by Sankar-Rao (1965). The thermal forcing is less easily modelled. Geller and Avery (1978) evaluated the heating rates from a global circulation model. The values used here, given in Table 5.3, are based on those of Geller and Avery for 900 mb at 50°N. It is assumed that Fourier analysing those values yield the forcings of P_1^2, P_2^3, and P_3^4, which in turn are assumed to decay exponentially with height.

The global response to these forcings is shown in Figure 5.11. Comparison with the observed values of van Loon et al. (1973),

	OROGRAPHIC		THERMAL	
m,n	Amp	Phase	Amp	Phase
1,2	150	-91^{o}	1.01	73^{o}
2,3	242	-150^{o}	0.74	96^{o}
3,4	196	55^{o}	0.28	86^{o}

Table 5.3 Amplitude and phase of the realistic forcings. The orographic forcing is in metres and the thermal forcing in K day^{-1}. The thermal forcing is evaluated from values in Geller and Avery (1978) for winter heating.

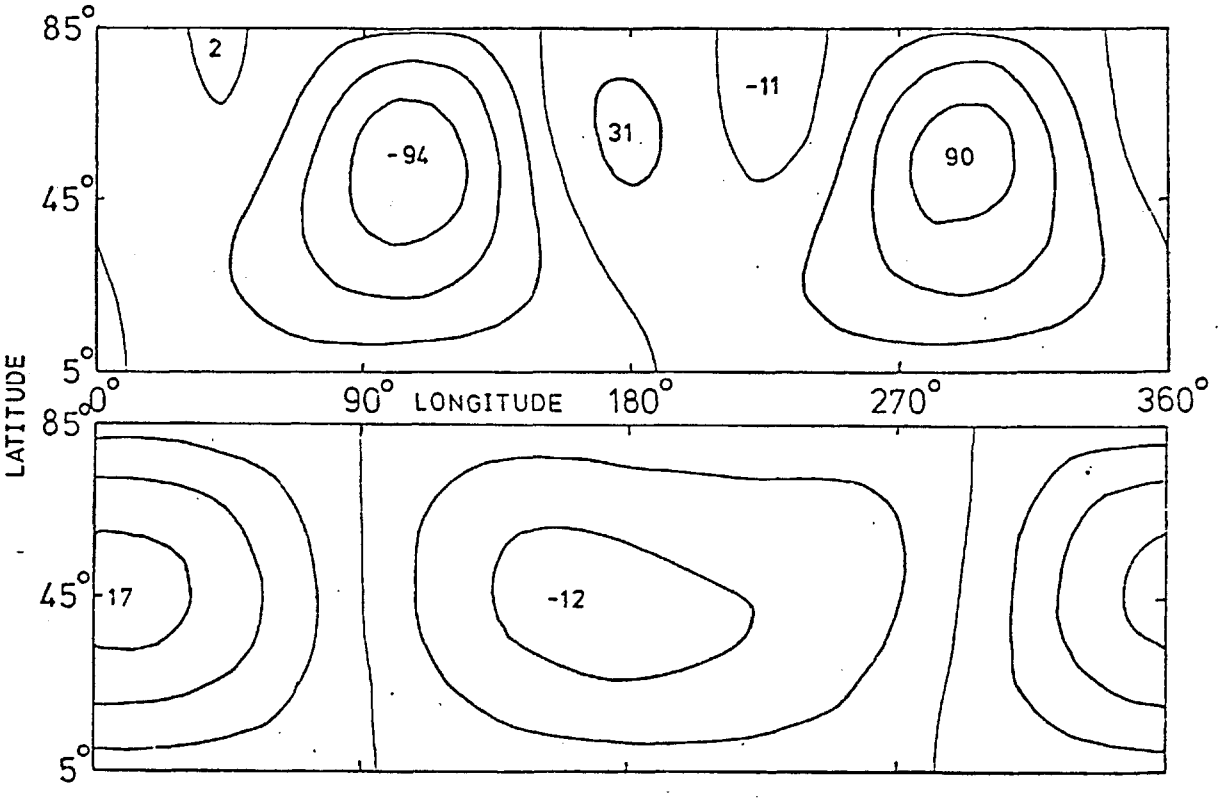

Figure 5.11 Mean global perturbation due to the forcings given in Table 5.3, at sea level (lower diagram) in mb and at 5 km (upper diagram) in metres, for mean conditions.

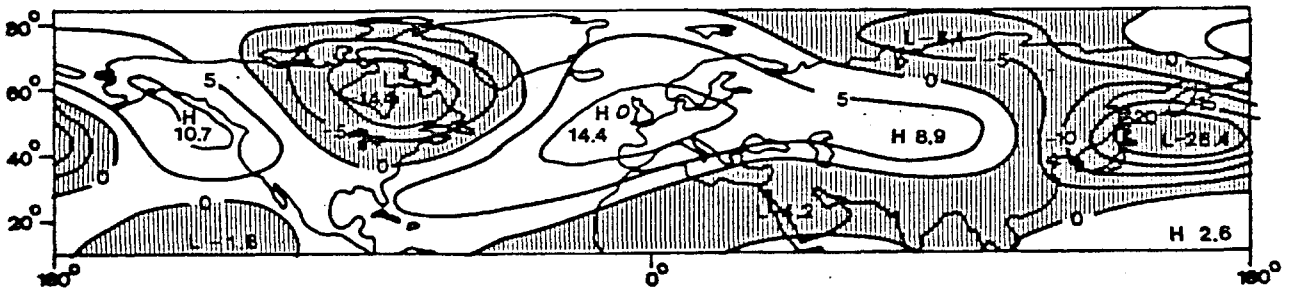

Figure 5.12 Observed mean Northern Hemisphere January 500 mb planetary wave height pattern (in decametres) due to zonal harmonics 1,2 and 3, using the results of van Loon et al.(1973). From Geller and Alpert (1980).

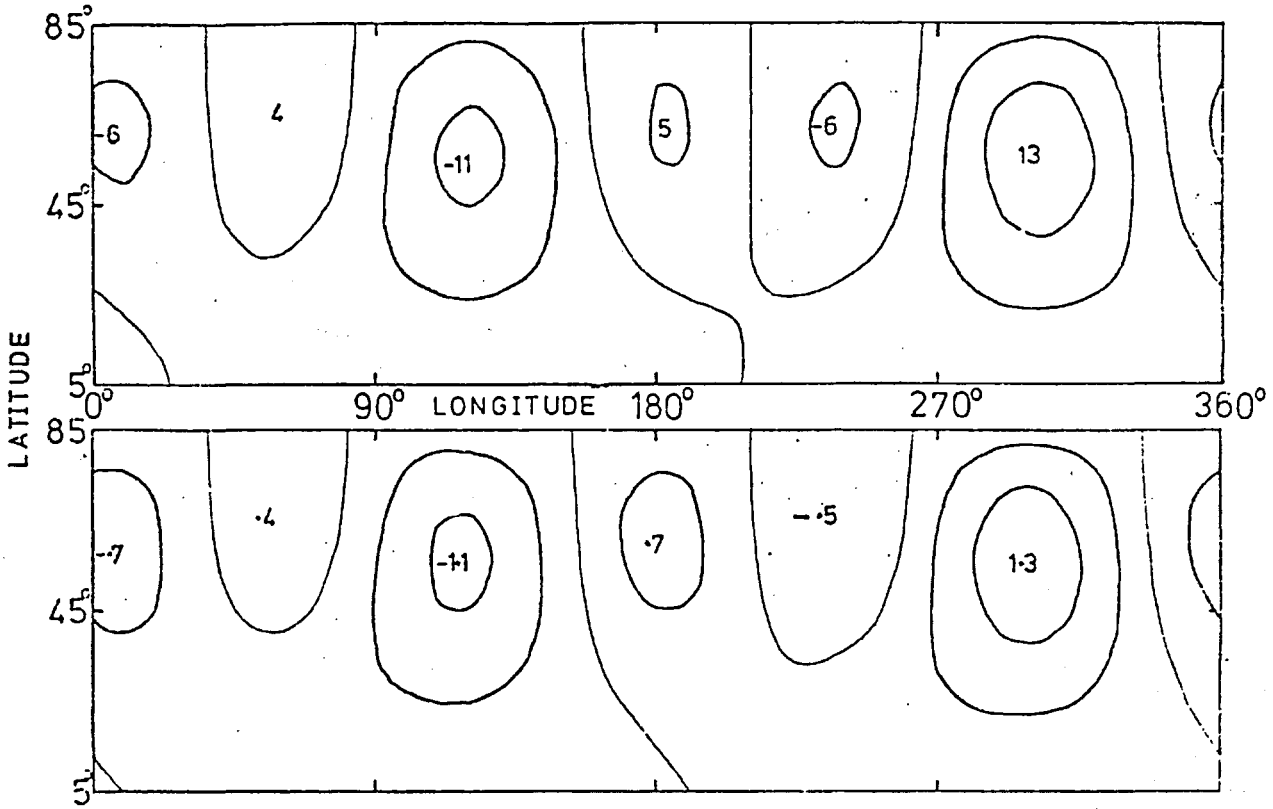

Figure 5.13 Difference between the global structure for ZJ = 60, UJ = 80 (as in Figure 5.11) and that for ZJ = 60, UJ = 85. Values at the ground (below) are in mb, while those at 5 km (above) are in metres.

	GROUND		500 MB	
m,n	Amp	Phase	Amp	Phase
1,2	.56 mb	82°	5.3 m	64°
2,3	.11 mb	106°	1.0 m	96°
3,4	.76 mb	180°	7.3 m	174°

Table 5.4 Amplitudes and phases of the waves which comprise figure 5.13.

shown in Figure 5.12 (from Geller and Alpert, 1980), shows that the model underestimates the amplitude of planetary waves at 5 km. This is probably due to the assumption that the thermal forcing decays exponentially with height. For that means S(5 km) = 0.3 S(0 km) while Geller and Avery show that the forcing at 5 km has a similar magnitude to that near the surface. So the forcing, and hence the amplitude, at z = 5 km has been underestimated. At the surface the model produces a pressure pattern dominated by wavenumber 1, for the wavenumber 3 component, evident at 5 km, is no longer significant.

The effect of increasing UJ to 85 ms^{-1}, as would occur if the UV increased by 10%, is shown in Figure 5.13. As the pressure and height patterns are very similar to those of Figure 5.11, the difference between values for UJ = 80 ms^{-1} and UJ = 85 ms^{-1} are plotted. The dominant changes at both levels are in wavenumbers 1 and 3, as is verified in Table 5.4, where the amplitudes and phases of the perturbation waves are listed. Hence the effect of changes in the middle atmosphere winds on the surface pressure and 50 mb height will, at mid-latitudes, be largest for wavenumbers 1 and 3. However, Parker (1976) and King et al. (1977) both observed variations which were predominantly wavenumber 2. As well as this qualitative disparity, the observed fluctuations are much larger than the predictions of the model for a 10% change in UV.

So the observed planetary wave variations are not due to solar UV variations changing the middle atmosphere zonal winds and thence planetary waves at all levels, including the troposphere.

It can be seen from Table 5.4 that the phases of the perturbation waves change little ($< 20^{o}$) between the ground and 5 km

while Ψ changes by over 100^{o}. The reason for these small phase changes is that the bottom boundary condition for the perturbation waves implies that phase lines are vertical at the ground. For, as $\chi(0)$ is unaltered, the RHS of Equation 5.8 is unaffected by the middle atmosphere wind changes. So

$$\frac{d\Psi_o}{dz} - \frac{\Psi_o}{\chi}\frac{d\chi}{dz} = \frac{d\Psi_1}{dz} - \frac{\Psi_1}{\chi}\frac{d\chi}{dz} \quad \text{at } z=0 \qquad (5.17)$$

where the subscript o refers to mean conditions (UJ = 80), while 1 refers to UJ = 85. Rearranging 5.17 gives

$$\frac{1}{(\Psi_o-\Psi_1)}\frac{d}{dz}(\Psi_o-\Psi_1) = \frac{1}{\chi}\frac{d\chi}{dz} \qquad \text{at } z=0 \qquad (5.18)$$

Expressing the perturbation wave ($\delta\Psi = \Psi_o - \Psi_1$) in polar form ($Ae^{i\theta}$), substituting in to equation 5.18 and equating real and imaginary parts yields

$$\frac{1}{A}\frac{dA}{dz} = \frac{1}{\chi}\frac{d\chi}{dz} \quad ; \quad \frac{d\theta}{dz} = 0 \qquad \text{at } z=0 \qquad (5.19)$$

So phase lines of $\delta\Psi$ are vertical at the ground, while the amplitude is proportional to the zonal wind velocity.

The Vertical Structure Equation of $\delta\Psi$ is found by subtracting that for Ψ_1 from that for Ψ_o. Then, neglecting cooling,

$$\frac{d^2}{dz^2}\delta\Psi + \frac{B}{\rho_o}\frac{d}{dz}\left(\frac{\rho_o}{B}\right)\frac{d}{dz}\delta\Psi + \frac{gB}{f_o^2}\left\{\frac{2\Omega}{\chi} - \frac{(n+2)(n-1)}{R^2} - \frac{f_o^2}{g\rho_o}\frac{1}{\chi}\frac{d}{dz}\left(\frac{\rho_o}{B}\frac{d\chi}{dz}\right)\right\}\delta\Psi + \Psi_o\chi(\delta\chi) = -\frac{gBR^2}{fm\rho_o}\left(\frac{-\delta\chi}{\chi_o-\chi_1}\right)\frac{d}{dz}\left(\frac{\rho_o S_o}{B}\right) \qquad (5.20)$$

where $\delta\chi = \chi_o - \chi_1$ and X is a linear operator in $\delta\chi$, so when $\delta\chi$ and its derivatives are zero, $X(\delta\chi) = 0$. As $\delta\chi$ is zero in the troposphere, the mean tropospheric wavelength for all three

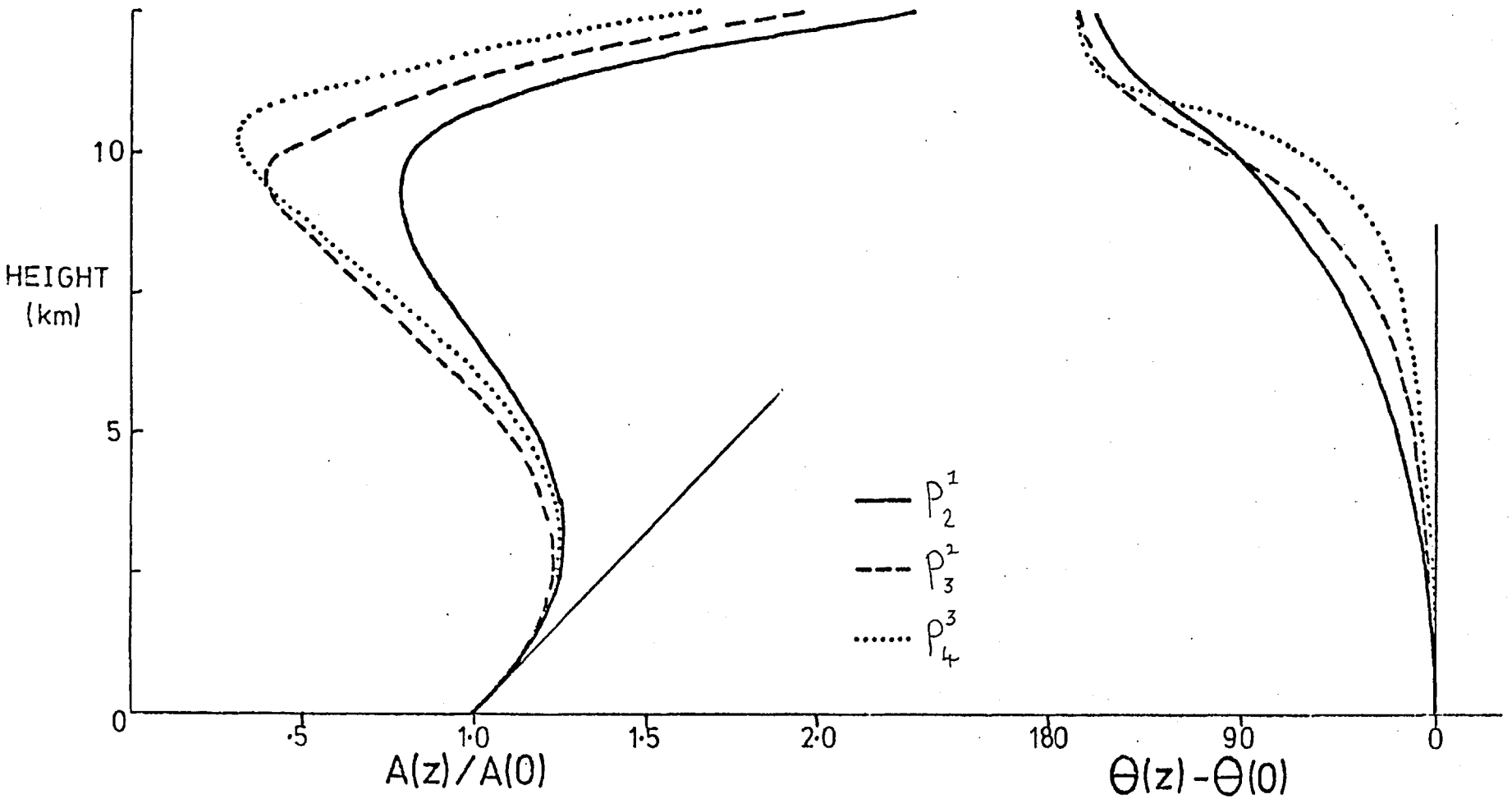

Figure 5.14 Vertical variation of the perturbation waves, $\delta\Psi$, with height. A and θ are respectively the amplitude and the phase of $\delta\Psi$. The amplitude of the wave = $\frac{Af}{g}$ x exp $(-z/2H_o)$

waves (1,2; 2,3; 3,4) is, as before, about 40 km and so phase changes are, on average, 90^{o}/10 km.

The vertical profile of $\delta\Psi$ is, when normalised so that $\delta\Psi(0) = 1$, almost identical for orographically and thermally forced waves. This is because $\delta\chi$ is zero where heating is significant, so the RHS of 5.20 is negligible, and hence S_o and a_{mn} are not explicitly used to calculate $\delta\Psi$. They are implicitly involved in the Ψ_o term of 5.20, but this term only occurs when $z > 18$ km. At these levels the orographic component differs by a constant multiple from the thermal one, so normalisation leads to identical results.

The tropospheric variation of the three waves is shown in Figure 5.14. Though these results were obtained using meridional variation of zonal wind which is independent of height (Equation 5.4) similiar results would follow from a two dimensional model. For in that case the bottom boundary condition is similar to that used here (Schoeberl and Geller, 1977) and Equation 5.18 still applies. Vertical wavelengths, at mid-latitudes, are also similar to those for the above results (van Loon et al., 1973). Hence the profiles of Figures 5.14, of the effect middle atmosphere wind changes have on planetary waves at mid-latitudes, are similar to those which would be obtained from a two dimensional model, such as that of Schoeberl and Geller (1977) used by Geller and Alpert (1980).

It has been observed by Edmonds (1980), that geopotential height and temperature anomalies have little westward phase tilt with height. One possible explanation of this is that the effect of middle atmosphere wind changes on planetary waves are a major

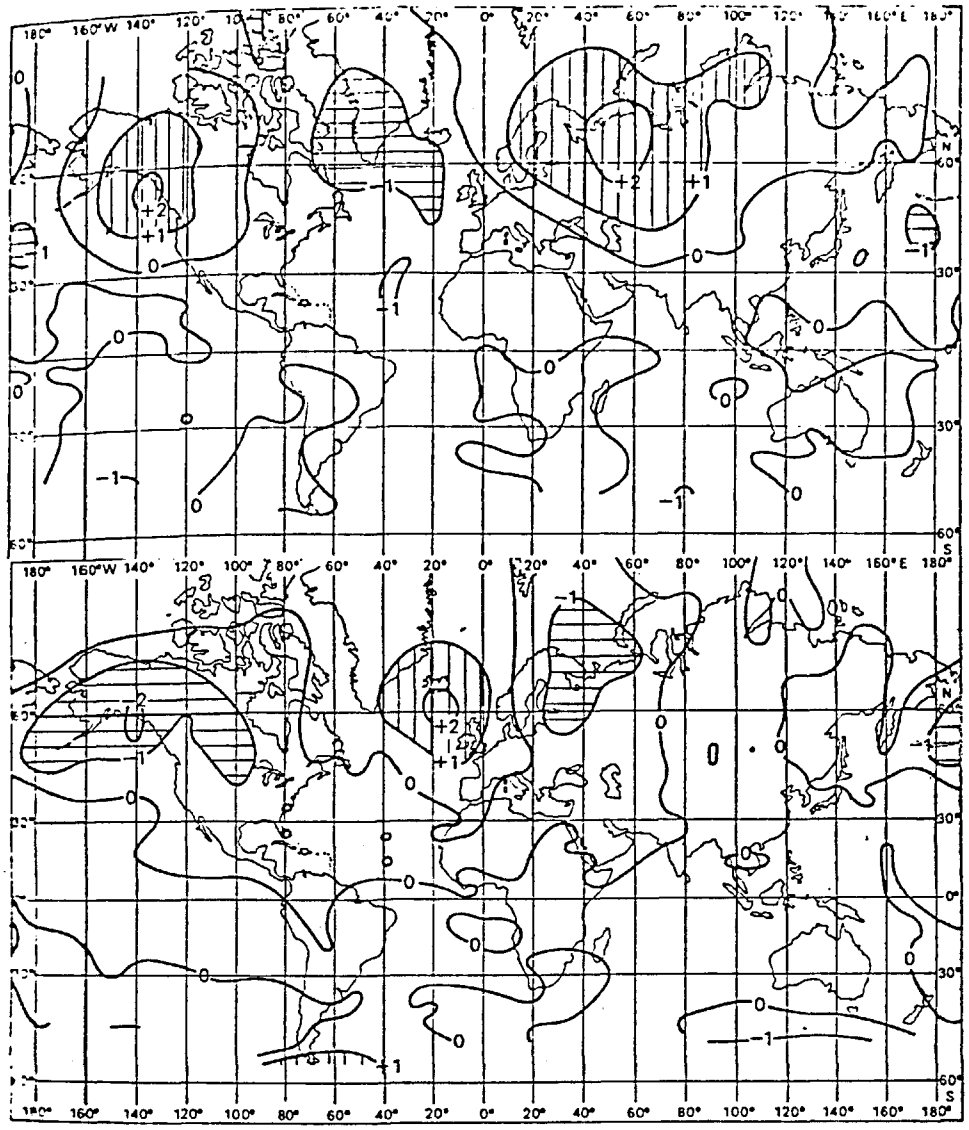

Figure5.15 Pressure anomalies associated with the sunspot cycle, for Januarys 1750-1958. (a)-above- for within a year of sunspot maximum. (b)-below- for within a year of sunspot minimum. From Parker (1976)

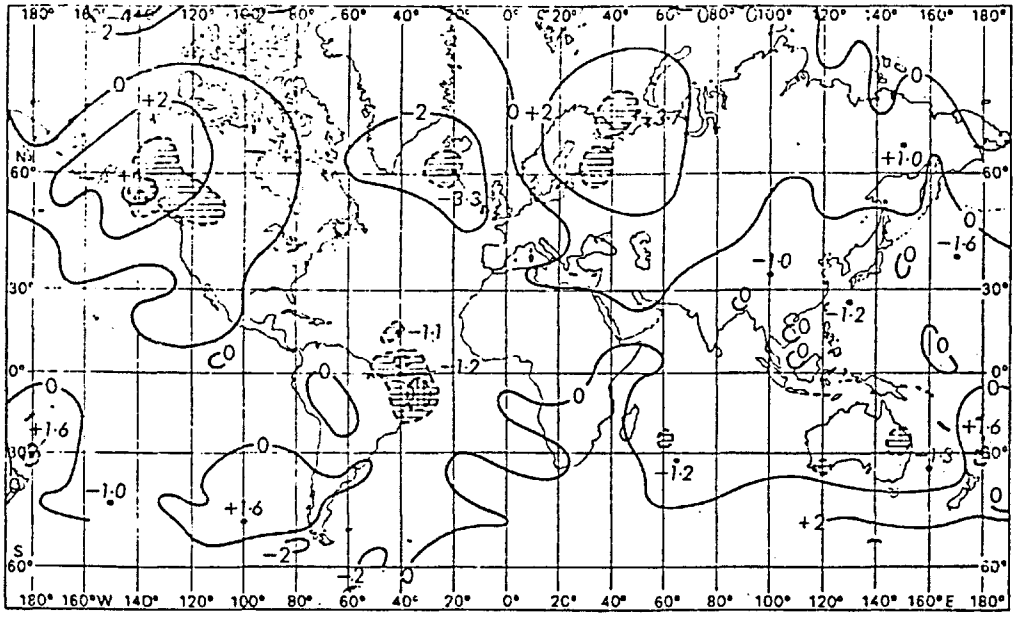

Figure 5.16 Difference between Figures 5.15a and b. Hatched areas are significant at 5% level, cross hatched at the 1% level. From Parker (1976)

contributor to such anomalies. However, this would imply a minimum in the effect at 10 km, while that is where Edmonds observed the maximum effect. Also, the above results gave large phase changes between 7 and 12 km, while Edmonds observed little phase tilt below 15 km.

So changes in the stratospheric winds, not induced by solar variability, may be a major cause of tropospheric anomalies.

5.4. Observations

5.4.1. Effect of Sunspot Cycle

Parker (1976), presenting results from 200 years data, illustrates how the surface pressure varied over the sunspot cycle. His charts for January are reproduced here (Figure 5.15). The largest effect is the winter hemisphere polewards of 30°, where planetary waves, and hence variance of the annual mean pressure, are largest. Similarly, the effect is larger in the northern than in the southern winter, for then the planetary waves have a larger mean amplitude.

By Fourier analysing the values in Figure 5.15 around a mid-latitude circle, it is found that the largest effect is on wave number 2. This result is inconsistent with the above theory, which implied that increased UV would have the greatest effect on wave-numbers 1 and 3 not, as observed, on wavenumber 2. Also, the change in wavenumber 2, of about 1 mb, is double that which the theory predicts (Table 5.4).

Parker plots the difference in surface pressure between sunspot maximum and sunspot minimum (Figure 5.16) and shades the areas with significant variations. 5% of the area has variations significant

at the 95% level, while less than 1% is significant at the 99% level. Also, there is no preference for particular latitudes in the significant areas. Hence the effects are probably random fluctuations.

5.4.2. Effect of Solar Rotation

The change in insolation due to solar rotation is much less than that due to the sunspot cycle (see Section 1.4). The ratio of the two effects is approximated here as a tenth, which probably results in an overestimation of the rotation effect. This factor is carried over into the models of Section 5.3.2. So the maximum effect of solar rotation, according to the model is ± 0.13 mb at the ground and ± 1.3 m at 5 km (about 500 mb).

Calculations by King et al. (1977) showed effects of ± 2.1 mb at the ground and ±70 m at 500 mb, much larger than the theory predicts. These observations are now considered in more detail.

The data used by King et al. (1977) was the daily 500 mb heights for the years 1963-1972. The average values appropriate to each location and each day of the year were subtracted from the daily values. These deviations from the climatic mean were then analysed to find the effect of solar rotation. Superposed epoch analysis was used with key dates successively, 27 then 28 days apart. For each key date, the 500 mb heights for up to 80 days after the key date are found. So by considering a number of key dates, sets of heights are formed for 0,1,2...80 days after key dates. These values in each set can then be analysed and variations between sets found.

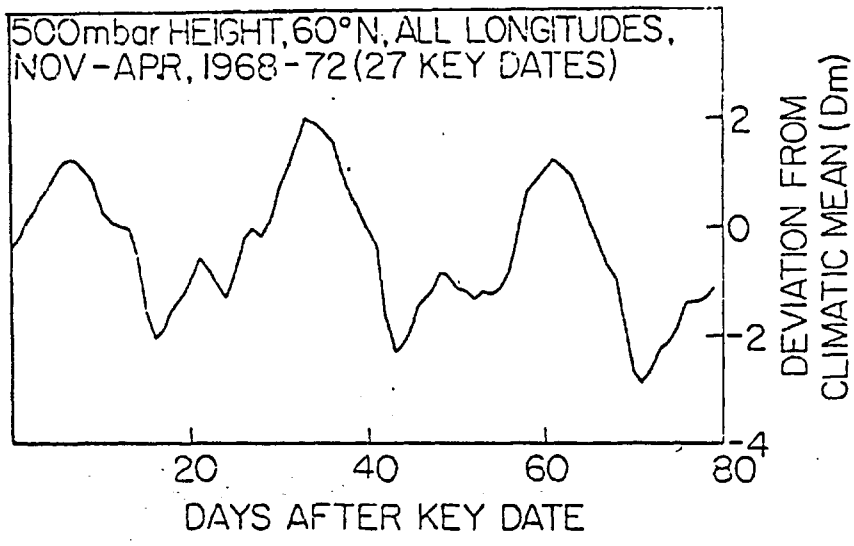

Figure 5.17 Superposed epoch analysis of the mean 500 mb height at 60° N, using key dates 27.5 days apart. From King et al. (1977).

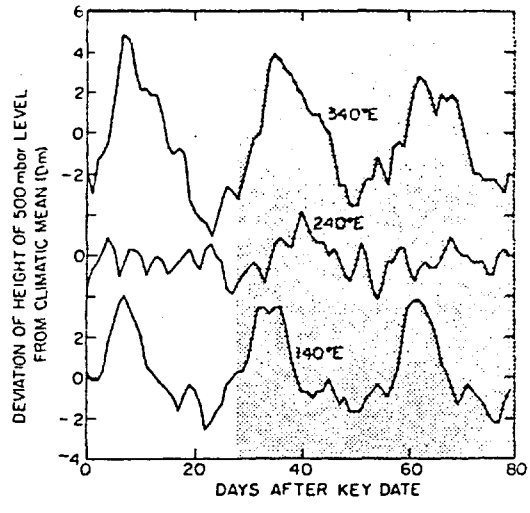

Figure 5.18 Superposed epoch analysis of the 500 mb height for three longitudes at 70° N, for the winters 1963/64 to 1971/72. From King et al. (1977)

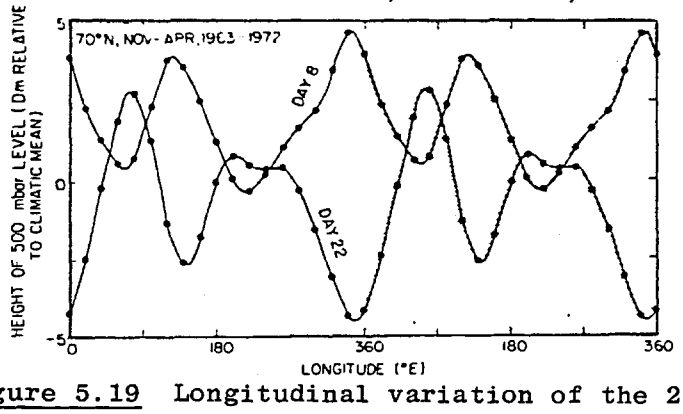

Figure 5.19 Longitudinal variation of the 27.5 day oscillation in the 500 mb height. Results on day 8 and day 22 of the 27.5 day superposed epoch analysis at 70° N. from King et al (1977).

A period of 27.5 days was chosen as representative of variations in solar output (see Figure 1.4). The sunspot number and 500 mb heights are then analysed for the winters 1963/4 to 1971/2. The results are illustrated in Figure 5.17. The sunspot number varied by 20%, being a maximum on day 6 (six days after the key dates). The zonal mean 500 mb height at 60°N showed variations of ±20 metres with a similar phase. This result cannot be a planetary wave effect as it is a zonal mean. However, the response varied with longitude, as Figure 5.18 shows for 70°N. While the amplitude was large at 140°E and 340°E, there was no effect at 240°E. This is further illustrated by Figure 5.19, demonstrating the longitudinal variations on days 8 and 22. As well as a change in the mean height of 30 metres, there was also a change in wavenumber 2, equivalent to a wave of amplitude 50 metres. With there having been no variation at 50°N,340°E, the mean pressure gradient between 50 and 70°N,340°E varied by 50%, and hence so did the mean zonal wind, (Holopainen, 1979, showed that the wind is 93% of the geostrophic value at 500 mb over Great Britain). Also, variations in the 500 mb height imply variations in the mean tropospheric temperature. A 100 m increase in the 500 mb height, as at 70°N, 340°E, implies a 5K warming. This is only slightly affected by the concurrent changes in surface pressure.

So during the winters 1963-1972 there were very large 27.5 day oscillations in the 500 mb height, the zonal wind and the tropospheric temperature.

Other authors have found tropospheric periodicities between 20 and 30 days. Fraedrich and Bottger (1978) found a period of

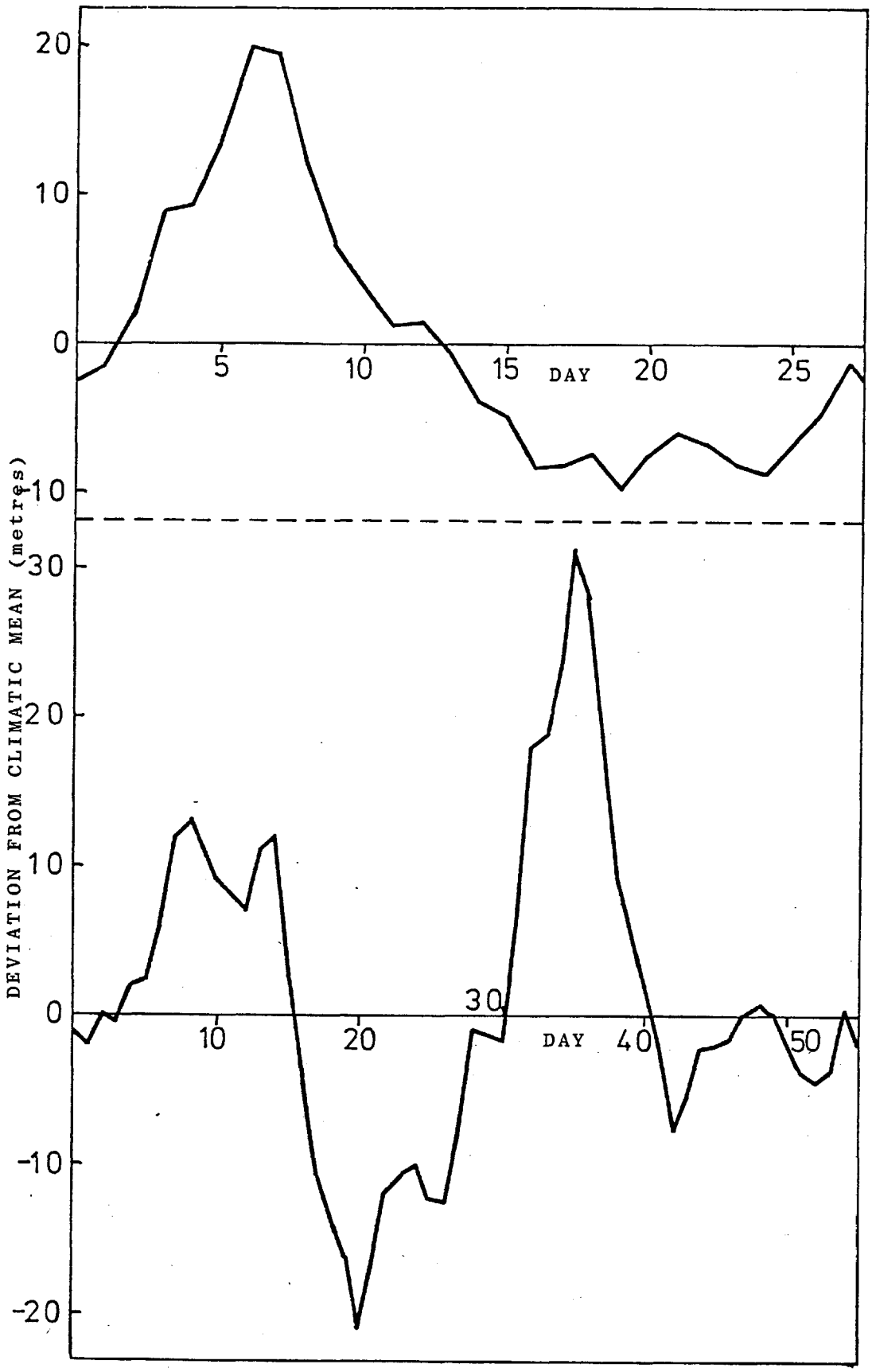

Figure 5.20 Superposed epoch analysis of the mean 500 mb height at 70°N using key dates 27.5 days (top) and 55 days (bottom) apart. The 27.5 day period is dominant in both.

about 25 days for planetary waves in winter at 50°N and 500 mb. McGuirk and Reiter (1976) found a "strong, persistent and significant oscillation of about 24 days periodicity in hemispheric-scale energy parameters during the winter season". Craddock (1968, p. 158) found a period of 23-25 days in the surface pressure at Aberdeen. So King et al.'s results could be another manifestation of this periodicity. Their results could be due to either chance, a coincidence of high/low pressure occurring a multiple of 27.5 days apart, or else solar variability affecting the troposphere, as King et al. suggest.

Williams (1979) suggests that the results obtained by King et al. (1977) were due to a property of superposed epoch analysis when periodic key dates are used. He shows that such a method will result in the fundamental mode, in this case with period 27.5 days, dominating its harmonics, if the data have a "red" spectrum (greater power in lower frequencies). However, when key dates 55 days apart are used the first harmonic, and not the fundamental mode, dominates (see Figure 5.20). So the dominance of the 27.5 day period is not due to the method used. When using key dates 20 and 40 days apart it is the fundamental that dominates, as predicted by Williams' theory.

The location of the largest effect found by King et al. (1977), 70°N,20°W, is close to Jan Mayen Island. Green (1979) found that for the winter of 1957/58 the 500 mb height did not have the large variations with a period of 27.5 days which King et al. found for the winters 1963 to 1972.

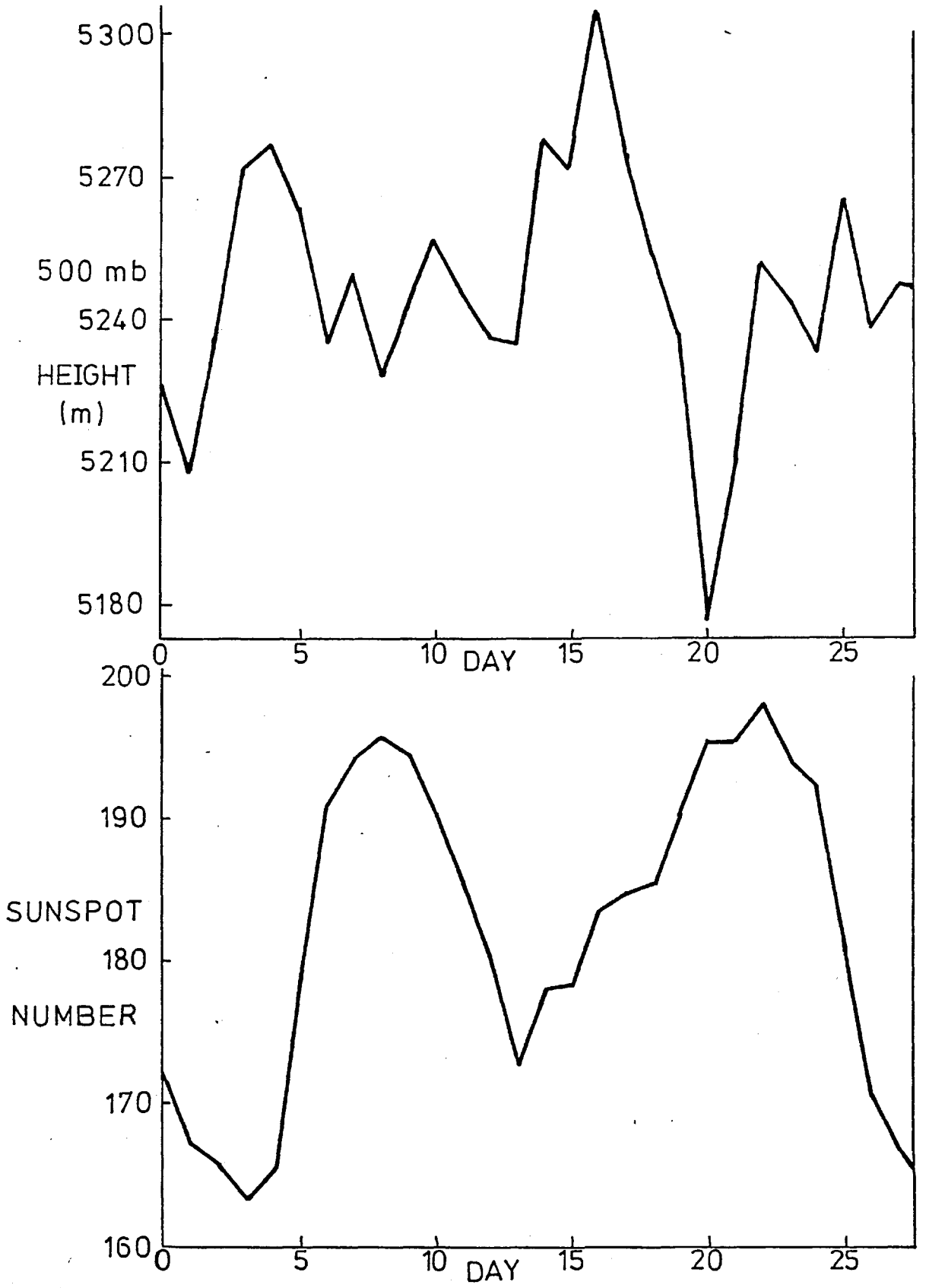

Figure 5.21 Superposed epoch analysis using key dates 27.5 days apart. (a)-top- 500 mb height at Jan Mayen Island (71°N, 9°W) (b)-bottom- sunspot number. Both are for the winters 1956/57 to 1958/59. A total of 19 key dates were used.

This is also true when the three winters 1956/57 to 1958/59 are considered together, as shown in Figure 5.21a. However, the sunspot number for the same period also fails to show a clear 27.5 day cycle (Figure 5.21b), indicating that the effect of rotation on solar output may have been reduced at that time of high solar activity. Hence these negative results do not disprove the hypothesis that the observations of King et al. were due to variations in solar output.

To investigate the behaviour for 1963-72 in more detail Fourier analysis is used. King et al. (1977) suggest that the main wave is a standing wave with period 27.5 days and longitudinal wavenumber 2. Two-dimensional Fourier analysis could be used to express the heights in terms of propagating waves, thus

$$h(x,t) = \sum_{m=0}^{M/2} \sum_{\sigma=0}^{S/2} A_{m\sigma} \sin(mx+\sigma t+a_{m\sigma}) + B_{m\sigma} \sin(mx-\sigma t+b_{m\sigma}) \qquad (5.21)$$

where M is the number of points in the x-direction (in this case 18) and S is the number of points in the t-direction (in this case 27 and 28 were used and the mean taken as representative of the 27.5 day period). Standing waves, which have the formula $C \sin(mx+c) \sin(\sigma t+d)$, are not uniquely definable from Equation 5.21, for the sum of two propagating waves of equal amplitude and wavenumber moving in opposite directions is equal to one standing wave of double their amplitude:

$$A \sin(mx+\sigma t+a) + A \sin(mx-\sigma t+b) = 2A \sin\left(mx+\frac{a+b}{2}\right) \cos\left(\sigma t+\frac{a-b}{2}\right) \qquad (5.22)$$

This ambiguity is resolved by assuming that there is only one

propagating wave, the one which has the larger amplitude in Equation 5.21, so

$$h(x,t) = \sum_{m=0}^{M/2} \sum_{\sigma=0}^{S/2} \alpha_{m\sigma} \sin(mx \pm \sigma t + \phi_{m\sigma}) + \beta_{m\sigma} \sin(mx + \theta^x_{m,\sigma}) \sin(\sigma t + \theta^t_{m,\sigma}) \qquad (5.23)$$

The amplitudes of $\alpha_{m,\sigma}$ $(m\sigma > 0)$ and $\beta_{m,\sigma}$ are listed in Table 5.5 for $m = 0,1,2,3$, $\sigma = 0,1$. The largest wave is, as stated by King et al., the standing wavenumber 2, but its amplitude of 12 m is only a quarter of that which they attribute to it. Linearly extrapolating the theory of Section 5.3.2, there would need to be an oscillation of amplitude 80 ms^{-1} in the mesospheric jet to produce this response. This in turn would need a change on 110% in the solar UV, which does not occur. Hence the mechanism of the previous Section does not explain the large standing wave with period 27.5 days.

King et al., using the notation of Schoeberl and Geller (1976), suggest that it is the (2,4) mode which is altered. As Schoeberl and Geller use Hough Functions, not Associated Legendre Functions, to describe the latitudinal dependence of planetary waves, this predominantly polar mode is not modelled in the previous Section. The large oscillation of 11 m in the zonal mean height $(m = 0, \sigma = 1)$ is not a planetary wave effect.

The data was now split into two subsets, one for the winters 1963/64 to 1966/67 and the other 1967/68 to 1970/71 - the results for 1971/72 being neglected. The former were at a period of low sunspot activity, the latter when it was high and so they are

σ \ m	0	1		2		3	
	S	S	T	S	T	S	T
0	0.3 m	6.1 m	-13^{o}	3.3 m	-78^{o}	1.8 m	-97^{o}
1	11.0 m	6.8 m	+4.9 m	11.9 m	+3.6 m	5.5 m	+0.7 m

Table 5.5 The main planetary waves at 70^{o}N, for the winters 1963/64 to 1971/72. The mean waves, $\sigma = 0$, have both their amplitude and their phase given. The waves with a period of 27.5 days ($\sigma = 1$), both standing (S) and travelling (T) have only their amplitude given. For the travelling waves a positive amplitude indicates eastward propagation, negative westward.

σ \ m	0	1		2		3	
	S	S	T	S	T	S	T
0	-8.7 m	9.2 m	60^{o}	3.4 m	0^{o}	9.9 m	-117^{o}
1	10.5 m	9.8 m	+9.4 m	6.5 m	+5.0 m	2.8 m	-4.0 m

Table 5.6a As Table 5.5 but for MIN, the winters 1963/64 to 1966/67

σ \ m	0	1		2		3	
	S	S	T	S	T	S	T
0	12.6 m	7.8 m	-98^{o}	16.1 m	-108^{o}	1.9 m	57^{o}
1	15.4 m	2.1 m	+15.7 m	17.7 m	-0.9 m	7.6 m	+4.3 m

Table 5.6b As Table 5.5 but for MAX, the winters 1967/8 to 1970/71

σ \ m	0	1		2		3	
	Amp	Amp	Phase	Amp	Phase	Amp	Phase
0	21.3 m	16.7 m	-110^{o}	17.4 m	-119^{o}	11.8 m	62^{o}

Table 5.6c Difference between the standing waves, MAX - MIN.

referred to as MIN and MAX respectively. The amplitudes of the main waves for MIN and MAX are listed in Table 5.6. There are several interesting properties:-

(a) The standing wavenumber 2 is large only in MAX. This supports the chance theory, that high pressure coincidentally occurred a multiple of 27.5 days apart.

(b) The travelling wavenumber 1 has a large amplitude in both MIN and MAX. The reason for the small component over the whole period 1963/64 to 1971/72 is that the two waves have a phase difference of 120°, and so partially cancel.

(c) There are large changes (10 to 20 m) in the time averaged ($\sigma = 0$) waves. As they are averaged, they cannot be due to solar rotation, but may be due to the sunspot cycle. If the two standing waves, with periods 27.5 days and 11 years, were due to the same process then their longitudinal phases should be similar. This is not the case, for their phases are different by more than 60° for all three waves. As these observations are only over one solar cycle, no conclusion can be drawn as to whether the change is solar induced, (Pittock, 1978).

5.5. Conclusions

Planetary waves are affected by changes in the middle atmosphere winds. However, the effect is not as large as suggested by Bates (1977) because radiative damping reduces the sensitivity of the waves. Even so, a 20% increase in UV over the sunspot cycle, as is claimed by Heath and Thekaekara (1977) to occur, would have a maximum effect of 2.6 mb at the ground. In agreement with Schoeberl and Strobel (1978b), it is found that wave number 2 is virtually

unaffected by changes in UV. However, both Parker (1976) and King et al. (1977) find that the largest changes coincident with solar activity are in wave number 2. Hence these changes are not explained by the theory of Section 5.3.2.

The observations by Parker, of variations in surface pressure over the sunspot cycle, are not statistically significant and are probably random fluctuations. The largest component wave in the observations of King et al. is the standing wave number 2 (with a period of 27.5 days) which has an amplitude of 12 m. Because this component is much larger than the theory predicts, and is only large for part of the period considered, it is probably also a random fluctuation.

One corollary of the theory applies to all middle atmosphere wind changes, not necessarily induced by solar variability. This is that while the mean waves have large westward phase tilts with height in the troposphere, the perturbation waves have almost vertical phase lines in the lowest 5 km.

APPENDIX

THE VERTICAL STRUCTURE EQUATION

A.1. Introduction

The two waves considered in depth, planetary waves and atmospheric tides, have many similarities. Both are assumed to have a given periodic behaviour in the horizontal, parameterised by horizontal wavenumbers, while their vertical structures are governed by the "Vertical Structure Equation". The absorption of heat forces both, though planetary waves are also forced by orography.

The generalised form of the Vertical Structure Equation (VSE) used in this appendix is:

$$\frac{d^2\xi}{d\eta^2} + \nu^2(\eta)\xi = F(\eta) \qquad \text{(A.1)}$$

where η is the height

$\xi(\eta)$ is the wave amplitude

$\nu(\eta)$ is the vertical wavenumber

and $F(\eta)$ is the forcing due to periodicity in the absorption/emission of radiation.

There are boundary conditions at $\eta = 0$ (ground) and at $\eta = \eta_T$. The boundary conditions used are

(a) No vertical velocity at the ground, $w = 0$.

(b) No propagation of energy downwards from above the forcing.

They are initially represented as

$$\frac{d\xi}{d\eta} + \alpha\xi = \beta \qquad \text{at} \quad \eta = 0 \qquad \text{(A.2)}$$

$$\frac{d\xi}{d\eta} + \gamma\xi = \delta \qquad \text{at} \quad \eta = \eta_T \qquad \text{(A.3)}$$

A.2. Analytic Solutions

When ν is independent of height, Equation A.1 can be solved analytically by a Green's Function method. The analytic solution has the advantage of giving $\xi(\eta)$ exactly in terms of the heating function and other parameters of interest.

In the real atmosphere ν is far from constant. To solve for realistic vertical structures, a computational method is needed (see Section A.3). However, these solutions, by their very nature, fail to give formulae relating variations of $\xi(\eta)$ with changes in vertical profiles. Therefore analytic solutions for "simple" vertical profiles, which are more realistic than constant ν, are of interest. These "simple" profiles are either piecewise constant, or else such that the VSE can be integrated analytically. Before considering these, the solution for the simplest profile is now given.

A.2.1. Constant Coefficients

First we evaluate the Green's Function $G(\eta, \eta_o)$ defined by

$$\frac{d^2G}{d\eta^2}(\eta,\eta_o) + \nu^2 G(\eta,\eta_o) = \delta(\eta-\eta_o) \qquad (A.4)$$

$$\frac{dG}{d\eta}(\eta,\eta_o) + \alpha G(\eta,\eta_o) = 0 \qquad (A.5)$$

$$\frac{dG}{d\eta}(\eta,\eta_o) + \gamma G(\eta,\eta_o) = 0 \qquad (A.6)$$

where $\delta(\eta - \eta_o)$ is the delta function, defined by

$$\delta(\eta-\eta_o) = \lim_{\varepsilon\to 0}\begin{cases} \frac{1}{2\varepsilon} & |\eta-\eta_o| \leq \varepsilon \\ 0 & |\eta-\eta_o| > \varepsilon \end{cases}$$

Integrating A.4 gives

$$\left[\frac{dG}{d\eta}(\eta,\eta_0)\right]_{\eta_0-}^{\eta_0+} = 1 \qquad (A.7)$$

$$\left[G(\eta,\eta_0)\right]_{\eta_0-}^{\eta_0+} = 0 \qquad (A.8)$$

where

$$\left[X(\eta)\right]_{\eta_0-}^{\eta_0+} = \lim_{\varepsilon \searrow 0}\left(X(\eta_0+\varepsilon)-X(\eta_0-\varepsilon)\right) \qquad (A.9)$$

The solution to Equations A.5 to A.8 must be sinusoidal in $\nu\eta$ to satisfy A.4 away from $\eta = \eta_0$. It can be shown to be

$$G(\eta,\eta_0) = \begin{cases} \dfrac{\left[\frac{\gamma}{\nu}\sin\nu(\eta_T-\eta_0)+\cos\nu(\eta_T-\eta_0)\right]\left[\nu\cos\nu\eta-\alpha\sin\nu\eta\right]}{\left[\nu(\alpha-\gamma)\cos\nu\eta_T+(\alpha\gamma+\nu^2)\sin\nu\eta_T\right]} & \eta \leqslant \eta_0 \\ \dfrac{\left[\frac{\gamma}{\nu}\sin\nu(\eta_T-\eta_0)+\cos\nu(\eta_T-\eta)\right]\left[\nu\cos\nu\eta_0-\alpha\sin\nu\eta_0\right]}{\left[\nu(\alpha-\gamma)\cos\nu\eta_T+(\alpha\gamma+\nu^2)\sin\nu\eta_T\right]} & \eta \geqslant \eta_0 \end{cases} \qquad (A.10)$$

The Equations to be solved are A.1 to A.3. Using Equations A.4 to A.6 it can be shown that:

$$\xi(\eta) = \int_0^{\eta_T} F(\eta_0)\,G(\eta,\eta_0)\,d\eta_0 + \beta\,G(\eta,0) - \delta\,G(\eta,\eta_T) \qquad (A.11)$$

For both tides and planetary waves with B and X ($\propto u$) independent of height, $\delta = 0$ and $\gamma = i\nu$ and so

$$\xi(0) = \frac{1}{\alpha+i\nu}\left[\beta + \int_0^{\eta_T} F(\eta_0)\,e^{i\nu\eta_0}\,d\eta_0\right] \qquad (A.12)$$

It is this expression that is used to derive Equations 4.55 and 5.10.

The forcing term, F, is a linear function of the heating and also proportional to the square root of density. The latter is a consequence of normalising the dependent variable so that there is no $\frac{d\xi}{d\eta}$ term in the VSE. Before normalisation the forcing is

independent of density, afterwards

$$F(\eta) = A\rho^{1/3}(\eta)\, \mathcal{J}_\eta[J(\eta)] \tag{A.13}$$

where A is a constant and $\mathcal{J}_\eta$ is a linear operator, so

$$\mathcal{J}_\eta[BC(\eta)] = B\,\mathcal{J}_\eta[C(\eta)]$$

What happens if the same amount of energy input with similar vertical variations is centred at a different level? (This can only apply to ozone absorption as tropospheric forcing always extends down to the ground).

Let
$$J(\eta) = \begin{cases} M(h)\,\tilde{J}(\eta - h) & |\eta - h| \leq h_1 \\ 0 & |\eta - h| > h_1 \end{cases} \tag{A.14}$$

where h is the centre of the heating. $\tilde{J}$ is normalised so that $\tilde{J}(0) = 1$ and hence M(h) can be evaluated using the fact that the total energy input $E = \int \rho\, J dz$.

$$M(h) = \rho\,(0)/\rho\,(h) = e^{h/H} \tag{A.15}$$

As $\mathcal{J}_\eta$ is linear this factor can be removed from the integral and using A. 12 to A. 15 it can be shown that

$$\xi(0) = \frac{1}{\alpha + i\nu}\left\{\beta + Ae^{i\nu h}e^{h/2H}\int_{-h_1}^{h_1} \rho_0^{1/2}(0)\, e^{i\nu z}\, \mathcal{J}_z[\tilde{J}(z)]\, dz\right\} \tag{A.16}$$

As only the component forced by ozone absorption is considered, $\beta = 0$ and so, if the heating profile is raised with E fixed, then the amplitude at the ground increases by a factor $e^{h/2H}$. So the effect of changes in UV are doubly felt: first directly by changing the total energy input but also by altering the ozone profile and hence the height of absorption. The latter effect is less than 10% of the former and highly sensitive to how the ozone profile varies. If the ozone varies as given by Penner and Chang (1978) the two

effects have the same sign while the results of Callis and Nealy (1978) give opposite signs (see Table 4.9).

A.2.2. Piecewise Constant Coefficients

This case where there are two or more layers with ν^2 constant in each, is only of interest in the case of planetary waves and cannot occur in any simple model of tides. For planetary waves on a sphere with constant zonal velocity u

$$\nu^2 = \frac{-1}{4H^2} + \frac{gB(z)}{f^2}\left[\frac{2\Omega \sin\theta}{uR} - \frac{(n+2)(n-1)}{R^2}\right] \qquad (A.17)$$

At the tropopause the static stability, B(z), changes very rapidly and can be modelled as a discontinuous change. This implies a discontinuity in $\nu(\eta)$ so a two layer model with ν constant in each layer is considered. To solve this, two boundary conditions at the interface are needed.

Physically these conditions are that pressure is continuous across the interface and that the interface must behave as a material surface. If the interface is

$$h(x,y,t) = \bar{h} + h'(x,y,t)$$

then the conditions are

$$\left.\begin{aligned} [p] &= 0 \\ \frac{D}{Dt}(z - h) &= 0 \end{aligned}\right\} \quad \text{at } z = h \qquad (A.18)$$

(with [ ] as defined in Equation A.9, the change in value at $z = h$) With undisturbed pressure and density continuous across $z = h$ we can replace the first condition by

$$[\delta p] = 0 \qquad \text{at } z = \bar{h} \qquad (A.19)$$

which in the notation of this chapter implies $\xi(\eta)$ continuous at $z = \bar{h}$. The second condition can be expanded, giving

$$\frac{\partial z}{\partial t} = \frac{\partial h'}{\partial t} + \bar{u}\frac{\partial h'}{\partial x} \quad \text{at } z=\bar{h} \tag{A.20}$$

Now $\frac{\partial z}{\partial t} = w$, so if h' independent of t then operating on A.20 with $[\ ]$ gives

$$[w] = \frac{\partial h'}{\partial x}[\bar{u}] = 0 \tag{A.21}$$

substituting for w, using the thermodynamic equation, gives the condition that $\frac{1}{B}\left(\frac{d\bar{s}}{dz} + \frac{\bar{s}}{2H}\right)$ is continuous at z = h.

The upper and lower boundary conditions are as before and given in Section A.1.2. There are two results, one for tropospheric ($\eta_o < h$) and one for stratospheric heating ($\eta_o > h$). The former is denoted by the subscript L and the latter by U, and similarly B_L, ν_L are tropospheric values while B_u, ν_u are stratospheric.

It can be shown that the Green's Functions at the ground ($\eta = 0$) are:

$$G_u(0,\eta_o) = \frac{\nu_L e^{i\nu_u(\eta_o - h)}}{(i\nu_u + \frac{1}{2H})(\nu_L \cos\nu_L h - i\nu_u \sin\nu_L h)} \tag{A.22}$$

$$G_L(0,\eta_o) = \frac{\nu_L(\frac{1}{2H} - i\nu_u)\cos\nu_L(h-\eta_o) - (\nu_L^2 + \frac{i\nu_u}{H})\sin\nu_L(h-\eta_o)}{(\nu_u^2 + \frac{1}{4H^2})(\nu_L \cos\nu_L h - i\nu_u \sin\nu_L h)} \tag{A.23}$$

What effect does the introduction of a tropopause have on the surface amplitude? Assuming $\nu^2 > 0$ for all ν's, then for the three cases of interest, the amplitudes squared are:

(a) No tropopause. $$(A)^2_{a,\nu} = \frac{1}{(\nu^2 + \frac{1}{4H^2})} \tag{A.24}$$

(b) Tropopause, heating above it

$$(A)_b^2 = \frac{\nu_L^2}{\left(\nu_u^2 + \frac{1}{4H^2}\right)\left(\nu_L^2 \cos^2 \nu_L h + \nu_u^2 \sin^2 \nu_L h\right)} \tag{A.25}$$

(c) Tropopause, heating below it

$$(A)_c^2 = \frac{\nu_L^2\left[\left(\nu_u^2+\frac{1}{4H^2}\right)\cos^2\nu_L(h-\eta_0) - \frac{\nu_L}{H}\left(1-\frac{\nu_u^2}{\nu_L^2}\right)\cos\nu_L(h-\eta_0)\sin\nu_L(h-\eta_0) + \left(\nu_L^2+\frac{\nu_u^2}{4H^2\nu_L^2}\right)\sin^2\nu_L(h-\eta_0)\right]}{\left(\nu_u^2+\frac{1}{4H^2}\right)^2\left(\nu_L^2\cos^2\nu_L h + \nu_u^2 \sin^2 \nu_L h\right)} \tag{A.26}$$

As $B_u > B_L$, then $\nu_u^2 > \nu_L^2$ and so for heating above the troposphere

$$(A)_b \leq (A)_{a,\nu_u} < (A)_{a,\nu_L} \tag{A.27}$$

Equality occurs if, and only if, $\sin \nu_L h = 0$. The critical parameter is $\left(\frac{\nu_L h}{2\pi}\right)$, the number of wavelengths the troposphere is above the ground. Typical values when $n = 2$ are $h = \pi/2\nu_L$ and $\nu_L \simeq \frac{3}{4}\nu_u$. These values lead to

$$(A)_b \simeq \frac{3}{4}(A)_{a,\nu_u}$$

In the other case, that of heating in the troposphere, the Equation for the amplitude (A.26) is more complicated. With heating near the ground $h - \eta_0 \simeq h \simeq \pi/2\nu_L$, for the $n = 2$ mode, so

$$(A)_c^2 = \left(\frac{\nu_L^4}{\nu_u^2} + \frac{1}{4H^2}\right) \Big/ \left(\nu_u^2 + \frac{1}{4H^2}\right)^2 \tag{A.28}$$

and so

$$(A)_c < (A)_{a,\nu_u} < (A)_{a,\nu_L} \tag{A.29}$$

Using typical values of $\nu_L \simeq \frac{3}{4}\nu_u \simeq \frac{8}{7H}$, $h \simeq \frac{\pi}{2\nu_L}$ gives the following dependence on η_o

$$(A)_c = \frac{3}{4}\left[1 - \frac{1}{3}\cos\nu_L\eta_o\left(\cos\nu_L\eta_o - \sin\nu_L\eta_o\right)\right]^{1/2}(A)_{a,\nu_u} \quad (A.30)$$

which is 0.6 for heating at the ground rising to 0.9 for heating just below the tropopause.

So the effect of including a tropopause in the model is to reduce the wave amplitude, hence neglecting the tropopause results in an overestimated amplitude, for forcing by stratospheric heating by tropospheric heating and by orography.

A.2.3. ν^2 Being a Simple Function of η

The models considered have been very idealistic, with assumptions made so that the differential equation has constant coefficients. Now more realistic vertical profiles are considered which lead to ν^2 varying with η in such a way that the VSE (Equation A.1) still has analytic solutions. Even so, these analytic solutions involve either Bessel or else Whittaker Functions. Using these methods the solutions are noticeably closer to both observations and computation results than from the constant models.

Two cases are considered, one where ν^2 is a linear function of η and the other where it is a linear function of $1/\eta$.

(a) $\nu^2 = A\eta + B$

This case occurs in tidal models when the temperature is assumed to be a linear function of η, i.e.

$$T = T_o + a\eta$$

then $$\nu^2 = \eta\left\{\frac{a\mathcal{K}}{h_n}\right\} + \left\{\frac{1}{h_n}(\mathcal{K}T_o + a) - \frac{1}{4}\right\} \qquad (A.31)$$

so $$A = \frac{a\mathcal{K}}{h_n} \qquad (A.32a)$$

$$B = \frac{1}{h_n}(\mathcal{K}T_o + a) - \frac{1}{4} \qquad (A.32b)$$

If a is constant, then A and B are also. This model, though, is physically meaningless, for if a is the tropospheric adiabatic lapse rate of -3 K/km then above 100 km the temperature would be below absolute zero. This is, by definition, impossible. However, this parameterisation is useful in multi-layer models of tides, where a is negative in the troposphere and mesosphere, positive in the stratosphere and thermosphere, and zero at the tropopause, stratopause and mesopause. This method was used by Pekeris (1937), but as the thermospheric temperature was not known then he estimated it, at a value much less than it was later found to be. This model is highly accurate as the only height dependent variable in ν^2 is temperature, which is well approximated by a series of straight lines. Indeed the numerical solutions were evaluated using such a profile (see Figure 4.16).

The solutions are Bessel Functions, and so the boundary conditions between two layers are complicated. It may seem surprising that there have not been attempts to repeat Pekeris' work with the now more accurate temperature and heating profiles. The reason why it was not done here is because the algebra is daunting, while the computational solution is simple.

To obtain this form for ν^2 in modelling planetary waves, B would need to be a linear function of η while U was constant. A

much more realistic approximation is constant static stability in uniform wind shear. This leads to the other simple form of ν^2.

(b) $\nu^2 = C/\eta + D$

With uniform wind shear, $u = u_o + e\eta$, then a co-ordinate transformation is needed.

Let $$h = \eta - \frac{u_o}{e} \qquad (A.33)$$

then $$\nu^2 = \frac{1}{h}\left\{\frac{g\beta}{f_0^2}\frac{\beta}{e}\right\} - \left\{\frac{1}{4H^2} + \frac{g\beta}{f^2}(k^2+l^2)\right\} \qquad (A.34)$$

and so $$C = \frac{g\beta}{f_0^2}\frac{\beta}{e} \qquad (A.35a)$$

$$D = -\frac{1}{4H^2} - \frac{g\beta}{f_0^2}(k^2+l^2) \qquad (A.35b)$$

By changing the scaling of h, the D term can be normalised to $-\frac{1}{4}$. Then the VSE becomes

$$\frac{d^2\xi}{dh'^2} + \left[-\frac{1}{4} + \frac{C'}{h'}\right]\xi = F' \qquad (A.36)$$

which is a special form of Whittaker's Equation, the solutions of which are related to Confluent Hypergeometric Functions, (see Shutts, 1978).

This method was used by Shutts, and provided results which compare well with the observations. It is, however, complex and tiresome. Again, the computational solution is the normal means of solving the equation. For, to improve accuracy a multilayer method is needed, with uniform shear and static stability in each layer. This greatly increases the laboriousness of the method.

So while it is possible to solve the VSE analytically, using reasonable approximations to the vertical profile of wind, temperature and static stability, it is normally more efficient to solve it

computationally. The one case in which analytic solutions are useful is when there is a critical layer, where u and therefore vertical wavelength, is 0. When this occurs ν is infinite and the numerical method fails. For this case, Shutts (1978) patched together the computational solution for below the critical layer with the analytic solution within and above the critical layer. However, this problem does not occur here as there is no critical layer at mid-latitudes in winter.

A.3. Computational Solutions of the VSE

The computational solution can be used for any $\nu(\eta)$ and $F(\eta)$ profiles so long as $\nu \neq 0$. The method is both fast and economic. Repeated numerical integrations will indicate how sensitive the solutions are to the vertical structure, as is done in Section 5.3.2. The method used here, first devised by Bruce et al. (1953), is described by Chapman and Lindzen (1970).

First the Vertical Structure Equation, A.1, is converted to its finite difference form using

$$\frac{d\xi}{d\eta} = \frac{\xi_{i+1} - \xi_{i-1}}{2\delta\eta} \tag{A.37}$$

$$\frac{d^2\xi}{d\eta^2} = \frac{\xi_{i+1} - 2\xi_i + \xi_{i-1}}{\delta\eta^2} \tag{A.38}$$

where $\delta\eta$ is the vertical grid length and ξ_i (i = 1 to N) is the value of ξ at the i^{th} level, there being a total of N levels. Substituting A.37 and A.38 into A.1 leads to the finite difference equation:

$$A_i \xi_{i+1} + B_i \xi_i + C_i \xi_{i-1} = D_i \tag{A.39}$$

where

$$\begin{aligned} A_i &= 1.0 \\ B_i &= -2.0 + \delta\eta^2 \nu_i^2 \\ C_i &= 1.0 \\ D_i &= \delta\eta^2 F_i \end{aligned} \tag{A.40}$$

So as to satisfy both top and bottom boundary conditions (bc) simultaneously, two dummy variables, U_i and V_i, are introduced, though they have no physical meaning. They are introduced by defining

$$\xi_i = U_i \xi_{i+1} + V_i \tag{A.41}$$

Now the bottom bc is used to evaluate U_1 and V_1. A slightly modified form of A.37 in A.2 gives

$$\frac{\xi_2 - \xi_1}{\delta\eta} + \alpha \xi_1 = \beta \tag{A.42}$$

which, when rearranged, is

$$\xi_1 = \frac{\xi_2}{(1-\alpha\delta\eta)} - \frac{\beta\delta\eta}{(1-\alpha\delta\eta)} \tag{A.43}$$

Comparing A.41 and A.43:

$$\begin{aligned} U_1 &= \frac{1}{(1-\alpha\delta\eta)} \\ V_1 &= \frac{-\beta\delta\eta}{(1-\alpha\delta\eta)} \end{aligned} \tag{A.44}$$

Substituting A.41 with i replaced by i-1, in A.39 and rearranging

$$\xi_i = -\frac{A_i \xi_{i+1}}{B_i + U_{i-1} C_i} + \frac{D_i - V_{i-1} C_i}{B_i + U_{i-1} C_i} \tag{A.45}$$

Comparing A.41 and A.45

$$U_i = \frac{-A_i}{B_i + U_{i-1} C_i} \quad ; \quad V_i = \frac{D_i - V_{i-1} C_i}{B_i + U_{i-1} C_i} \tag{A.46}$$

So using the coefficients A_i, B_i, C_i and D_i and U_{i-1} and V_{i-1}, U_i and V_i can be evaluated. U_1 and V_1 are known from A.44, so solving A.46 for $i = 2,3....N$ gives U_i and V_i throughout the region of integration.

The top bc is applied to evaluate ξ_N. Substituting A.37 in A.3, evaluated at $i = n - 1$, gives

$$\frac{\xi_N - \xi_{N-2}}{2\delta\eta} = -\gamma \xi_{N-1} + \delta \qquad \text{(A.47)}$$

Using A.41 with $i = N-2$ and $N-1$, ξ_{N-1} and ξ_{N-2} can be eliminated from A.47, so

$$\xi_N = \frac{2\delta\eta\cdot\delta + V_{N-2} + V_{N-1}[U_{N-2} - 2\delta\eta\cdot\gamma]}{1 + U_{N-1}[U_{N-2} - 2\delta\eta\cdot\gamma]} \qquad \text{(A.48)}$$

Finally, having found ξ_N and U_i, V_i for all i, A.41 is solved for $i = N-1, N-2,....2$, hence all the ξ_i's are evaluated.

Using this numerical method, the VSE can be solved for various heating and ν^2 profiles. By varying the heating profile and/or $\nu^2(\eta)$ it can be determined how sensitive the amplitude is to a parameter. In particular, an amplification mechanism may be found in which a change induced by solar variability in one parameter could cause drastic changes in the wave at the ground.

ACKNOWLEDGEMENTS

This work was predominantly carried out at the Atmospheric Physics Group of Imperial College, London, under the enthusiastic supervision of Dr. J. Green. I thank that group, and in particular Dr. Green and Dr. K. Bignell, for their comments, advice and insight. The remainder of the work was done at the Appleton Laboratory, Slough, and discussions there with Dr. J. King were very fruitful. Data was kindly provided by both the Appleton Laboratory and the Meteorological Office Library. I am very grateful to Eileen Wakeman for typing the thesis.

My parents and my brother have helped and encouraged me throughout my researches. I thank God for making it possible for me to do this work and giving me the strength to complete it.

This work was financed by a NERC studentship in collaboration with the Appleton Laboratory.

REFERENCES

Abramowitz M and Stegun I A	1965	"Handbook of Mathematical Functions", New York
Allen C W	1973	"Astrophysical Quantities", The Athlone Press, London
Angell J K and Korshover J	1978	"Recent rocketsonde-derived temperature variations in the Western Hemisphere", J Atmos Sci 35:1758-1764
Angell J K and Korshover J	1979	"Comparison of ozone variations derived from ozonesondes and UMKEHR measurements for the period 1969-1976", Mon. Wea. Rev. 107:599-607
Angione R J, Medeiros E J and Roosen R G	1976	"Stratospheric ozone as viewed by the Chappuis Band", Nature 261:289-290
Bates J R	1977	"The dynamics of ultra-long waves in mid-latitudes", Quart J R Met Soc 103:397-430
Brookes C E P	1934	"The variations of the annual frequencies of thunderstorms in relation to sunspots", Ibid 60:153-162
Bruce G H, Peaceman D W, Rachford H H and Rice JD	1953	Trans Am Inst Min Metall Engnrs 198:97-92
Butler S T and Small K A	1963	"The excitation of atmospheric oscillations", Poc Roy Soc A 274:91-121
Callis L B and Nealy J E	1978	"Solar UV variability and its effect on stratospheric thermal structure and trace constituants", Geo Res Lett 5:249-252
Carrington R C	1858	Mon Not R Astrom Soc 19:1-
Carrington R C	1863	"Observations of the spots on the sun", Williams and Norgate, London
Chapman S and Lindzen R S	1970	"Atmospheric Tides", D Reidel Pub Co, Dordrecht, Holland

Charney J G and Drazin P G 1961 "Propagation of planetary-scale disturbances from the lower into the upper atmosphere", J Geophys Res 66:83-109

Craddock J M 1968 "Statistics in the computer age", English University Press

Dickinson R E 1973 "A method for parameterization of infra-red cooling between altitudes of 30 and 70 km", J Geophys Res 78:4451-4457

Dütch H U 1979 "The search for solar cycle-ozone relationships", J Atmos Terr Phys 41:771-785

Eddy J A 1977 "Historical evidence for the existence of the solar cycle", in "The solar output and its variation", O R White, Ed; Colorado Associated Univ Press, Bolder Colorado

Edmonds H J 1980 "A study of the general circulation over the northern hemisphere during the winters 1976-77 and 1977-78", Mon Wea Rev 108:1538-1553

Ellis J S and Vonder Haar T H 1976 "Zonal average earth radiation budget measurements from satellites for climatic studies", Atmos Sci Paper 240, Dept Atmos Sci, Colorado State Univ

Forbes J M and Garrett H B 1978 "Thermal excitation of atmospheric tides due to insolation absorption by O_3 and H_2O", Geo Res Lett 5:1013-1016

Foukal P V, Mack P and Vernazza J E 1977 "The effect of sunspots and faculae on the solar constant", Astro J 215:952-959

Fracastro M G and Marocchi D 1978 "A sunspot analysis, 1943-77", Solar Phys 60: 171-180

Fraedrich K and Bottger H 1978 "Wave number frequency analysis of the 500 mb geopotential at 50°N", J Atmos Sci 35:745-750

Fröhlich C 1977 "Contemporary measures of the solar constant", in "Solar output and its variations", O R White, Ed: Colorado Associated Univ Press, Bolder, Colorado

Geller M A and Alpert J C	1980	"Planetary wave coupling between the troposphere and the middle atmosphere as a possible sun-weather mechanism", J Atmos Sci 37:1197-1215
Geller M A and Avery S K	1978	"Northern hemisphere distribution of diabatic heating in the troposphere derived from general circulation data", Mon Wea Rev 106:629-636
Giwa F B A	1972	"A note on the diurnal variation of surface temperature and pressure at some Nigerian meteorological stations", Plan Space Sci 20:1941-1948
Green J S A	1965	"Atmospheric tidal oscillations: an analysis of the mechanisms", Proc Roy Soc A 288:564-574
Green J S A	1979	"Possible mechanisms for sun-weather relationships", J Atmos Terr Phys 41:765-770
Hartmann D L and	1979	"A mechanistic model of ozone transport by planetary waves in the stratosphere", J Atmos Sci 36:350-364
Haurwitz B	1956	"The geographical distribution of the solar semi-diurnal pressure oscillation", New York Univ Meteor Papers 5;2:1-36
Haurwitz B	1965	"The diurnal pressure oscillation", Arch Met Geo und Bioklimat A14:361-379
Haurwitz B and Cowley A D	1973	"The diurnal and the semi-diurnal barometric oscillations, global distribution and annual variation", Pure Appl Geophys 102:193-222
Heath D F	1973	"Space observations of the variability of solar irradiance in the near and far Ultra-Violet", J Geophys Res 78:2779-2792
Heath D F and Thekaekara M P	1977	"Measures of the solar spectral irradiance between 1200 and 3000Å", in "The solar output and its variations", O R White, Ed; Colorado Associated Univ Press, Bolder, Colorado

Herman J R and Goldberg R A	1978	"Sun, weather and climate", NASA SP 426, US Government Printing Office, Washington
Hines C O	1974	"A possible mechanism for the production of sun-weather correlations", J Atmos Sci 31:589-591
Holopainen E O	1979	"A diagnostic study of the long term budget of momentum of atmospheric large scale motion over the British Isles", Quart J R Met Soc 105:859-871
Holton J R	1975	"The dynamic meteorology of the stratosphere and mesosphere", Met Monograph 37, Am Met Soc
Hough S S	1898	"On the application of harmonic analysis to the dynamical theory of tides, part 2: On the general integration of Laplace's dynamical Equations", Phil Trans Roy Soc A 191:139-185
Howard R and Harvey J	1970	"Spectroscopic determinations of solar rotation", Solar Phys 12:23-51
Johnson R G and Imhof W L	1975	"Direct satellite observations on bremsstrahlaing radiation as a technique to investigate its role in meteorological processes", Goddard Space Flight Centre, Rep NASA SP 366
King J W, Slater A, Smith P A, Stevens A and Willis D M	1977	"Large amplitude standing planetary waves induced in the troposphere by the sun", J Atmos Terr Phys 39:1357-1367
Klejmenova E P	1967	"On the variation of thunderstorm activity in the solar cycle", Meteor Gidrol 8:64-68
Laplace P S	1799	"Mechanique Celeste", Paris
Leovy C	1964	"Radiative equilibrium of the mesosphere", J Atmos Sci 21:238-248
Lindzen R S	1967	"Thermally driven diurnal tides in the atmosphere", Quart J R Met Soc 93:18-42
Lindzen R S	1968	"The application of classical tidal theory", Proc Roy Soc A303:299-316

Lindzen R S	1978	"Effect of daily variations of cumulonimbus activity on the atmospheric semi-diurnal tide", Mon Wea Rev 106:526-533
Lindzen R S and Hong S-S	1974	"Effects of mean zonal winds and horizontal temperature gradients on solar and lunar semi-diurnal tides in the atmosphere", J Atmos Sci 31:1421-1446
Lindzen R S and Will D I	1973	"An analytic formula for heating due to ozone absorption", Ibid 30:513-515
Livingston W and Duvall T R Jr	1979	"Solar rotation, 1966-1978", Solar Phys 61:219-231
McGuirk J P and Reiter E R	1976	"A vascillation in atmospheric energy parameters", J Atmos Sci 33:2079-2093
Manabe S and Wetherald R T	1967	"Thermal equilibrium of the atmosphere with a given distribution of relative humidity", Ibid 24:241-259
Markson R	1978	"Mechanism for solar control of atmospheric electrification and weather", in collection of extended summaries of contributions presented at Joint Symposium C IAGA/IAMAP Joint Assembly, 1977
Mitchell A C	1930	"Diurnal variation of pressure and temperature at Richmond (Kew Observatory) 1871-1926", Quart J R Met Soc 56:76-78
Nastrom G D and Belmont A D	1980	"Apparent solar cycle influence on long period oscillations in stratospheric zonal wind", Geo Res Lett 7:457-460
Newton H W and Nunn M L	1951	"The sun's rotation as derived from sunspots 1933-1944 and additional results", Mon Not R Astron Soc 111:413-421
Nicolet M	1975	"Stratospheric ozone: An introduction to its study", Rev Geo Space Phys 13:593-636
Parker B N	1976	"Global pressure variation and the 11-year solar cycle", Met Mag 105:33-44

Pekeris C L	1937	"Atmospheric Oscillations", Proc Roy Soc A 158:650-671
Penner J E and Chang J S	1978	"Possible variations in atmospheric ozone related to the eleven year cycle", Geo Res Lett 5:817-820
Pittock A B	1978	"A critical look at long-term sun-weather relationships", Rev Geo Space Phys 16:400-420
Rhodes E, Deubner F-L and Ulrich R K	1979	"A new technique for measuring solar rotation", Astro J 227:629-637
Roberts W O and Olson R H	1973	"New evidence for effects of variable solar corpuscular emission on the weather", Rev Geo Space Phys 11:731-740
Sanker-Rao M	1965	"Continental elevation influence on the stationary harmonics of the atmospheric motion", Pure Appl Geophys 60:141-159
Schoeberl M R and Geller M A	1976	"The structure of stationary planetary waves in winter in relation to the polar night jet intensity", Geo Res Lett 3:177-180
Schoeberl M R and Geller M A	1977	"A calculation of the structure of planetary waves in winter", J Atmos Sci 34:1235-1255
Schoeberl M R and Strobel D F	1978a	"The zonally-averaged circulation of the middle atmosphere", Ibid 35:577-591
Schoeberl M R and Strobel D F	1978b	"The response of the zonally averaged circulation to stratospheric ozone reductions", Ibid 35:1751-1757
Schuurmans C J E and Oort A H	1969	"A statistical study of pressure changes in the troposphere and lower stratosphere after strong solar flares", Pure Appl Geophys 75:233-246
Sekihara K	1979	"The influence of solar sorpuscular radiation on the meteorology of the troposphere", Papers in Met and Geophys 30:141-151
Shutts G J	1978	"Quasi-geostrophic planetary wave forcing", Quart J R Met Soc 104:331-350

Siebert M	1961	"Atmospheric Tides", Advan Geophys 7:105-187
Simon P C	1977	Comment on Heath and Thekaekara's paper in "The solar output and its variations", O R White, Ed; Colorado Assoc Univ Press, Bolder, Colorado
Smith E V P and Gottlieb D M	1974	"Solar flux and its variations", Space Sci Rev 16:771-802
Stagg J M	1931	"Atmospheric pressure and the state of the Earth's magnetism", Nature 127:402
Thomson W	1882	"On the thermodynamic acceleration of the Earth's rotation rate", Proc Roy Soc, Edinburgh 11:396-405
Thomson W	1891	"Harmonic analysis of hourly observations of air and temperature at British observatories", Official Pub No 93
Thrush B A	1980	"The chemistry of the stratosphere", Phil Trans Roy Soc A 296:149-160
Vallis G K	1980	"A zonally averaged general circulation model for climate studies", Ph.D. Thesis, Univ of London
van Loon H, Jenne H and Labitzke K	1973	"Zonal harmonic standing waves", J Geophys Res 78:4463-4471
Van Tend W and Zwaan C	1976	"On differences in differential rotation", in "Basic mechanisms of solar activity", Bumba and Kleczek, Eds
Vitinskij Ju I	1969	"On the problem of active longitudes of sunspots and flares", Solar Phys 7:210-216
Walterscheid R L, De Vore J G and Venkateswaran S V	1980	"Influence of mean zonal motion and meridional temperature gradients on the solar semi-diurnal atmospheric tide: A revised spectral study with improved heating rates", J Atmos Sci 37:455-470

Walterscheid R L and Venkateswaran S V 1979 "Influence of mean zonal motion and meridional temperature gradients on the solar semi-diurnal atmospheric tide: A spectral study. Part II Numerical results", Ibid 36:1636-1662

Williams R G 1979 "Comments on 'Large amplitude standing planetary waves induced in the troposphere by the sun', by J W King et al.", J Atmos Terr Phys 41:643-645

Yallop R D and Hohenkert C Y 1980 "Distribution of sunspots, 1874-1976", Solar Phys 68:303-305